THESIS

BENEFICIAL USE OF OFF-SPECIFICATION FLY ASHES TO INCREASE THE SHEAR STRENGTH AND STIFFNESS OF EXPANSIVE SOIL-RUBBER (ESR) MIXTURES

Submitted by

Ethan Patrick Wiechert

Department of Civil and Environmental Engineering

In partial fulfillment of the requirements

For the Degree of Master of Science

Colorado State University

Fort Collins, Colorado

Spring 2011

Master's Committee:

Advisor: J. Antonio H. Carraro

Angela A. Guggemos
Charles D. Shackelford

ABSTRACT OF THESIS

BENEFICIAL USE OF OFF-SPECIFICATION FLY ASHES TO INCREASE THE SHEAR STRENGTH AND STIFFNESS OF EXPANSIVE SOIL-RUBBER (ESR) MIXTURES

The potential use of off-specification fly ashes to increase the shear strength and stiffness of an expansive soil-rubber (ESR) mixture was investigated systematically in this study. The off-specification fly ashes used included a high sulfur content fly ash and a high carbon content fly ash. A standard Class C fly ash was also used as a control fly ash to develop a basis for comparison of the effects of the off-specification fly ashes. The ESR mixture consisted of high-plasticity clay blended with 20% 6.7-mm granulated rubber (by weight). The fly ash content required to develop pozzolanic reactions was determined based on the concept of lime fixation point and kept constant for all ESR-fly ash mixtures. At this selected fly ash content, ESR-fly ash mixtures were tested at a single relative compaction level and curing times of 7 and 14 days. Unconfined compression testing was performed on compacted specimens to validate the fly ash content selected and the effect of curing time on the development of pozzolanic reactions. The effect of the fly ash type, curing time and mean effective stress was evaluated by performing isotropically consolidated undrained triaxial compression tests on saturated specimens at mean effective stress levels of 50, 100 and 200 kPa. Stiffness changes due to fly ash addition were evaluated during undrained compression. Large-strain stiffness was

measured using conventional external displacement transducers. Very-small strain stiffness was evaluated from shear wave velocity measurements using a bender element apparatus. Results suggest that the shear strength and stiffness improvements imparted by the off-specification fly ashes is similar to or better than the improvements imparted by conventional Class C fly ash.

ACKNOWLEDGEMENTS

Professor Antonio Carraro deserves special acknowledgement for the support and guidance during preparation of the thesis and during coursework during graduate study. Thanks to Professors Charles Schakelford and Angela Guggemos for support on the graduate committee.

The author would like to acknowledge Lester Litton for encouragement for continuing graduate studies and for his guidance and mentoring.

A special acknowledgement to the author's wife Kelly, and sons Branden and Ryan, for their support and encouragement they provided. The author would also like to thank his parents and family for their support.

This report was prepared by funds provided by the United States Department of Transportation to the Mountain-Plains Consortium (MPC). The MPC member universities including North Dakota State University, Colorado State University, University of Wyoming, South Dakota State University and Utah State University.

Supply of fly ash was provided from the Rawhide Energy Station, Laramie River Station and Drake Power Plant through the cooperative efforts the American Coal Ash

Association and Boral Material Technologies. The scrap tire rubber was provided by Caliber Recycled Products Inc. Their material contributions are appreciated.

TABLE OF CONTENTS

LIST OF TABLES

LIST OF FIGURES

LIST OF ACRONYMS

AASHTO .....American Association of State Highway and Transportation Officials
ACAA .....American Coal Ash Association
ASTM ..... American Society for Testing and Materials
CAA ..... Clean Air Act
CAIR ..... Clean Air Interstate Rule
CAMR.....Clean Air Mercury Rule
CBR.....California Bearing Ratio
CCP .....Coal Combustion Product
CD .....Consolidated Drained
CDPHE .....Colorado Department of Public Health and Environment
CH ..... High Plasticity Clay
CIU..... Isotropic-Consolidated Undrained Triaxial Compression
CL .....Low Plasticity Clay
CSL ..... Critical State Line
CSU.....Colorado State University
CU .....Consolidated Undrained
DL .....Drake Laramie River
EPA .....Environmental Protection Agency
ESR ..... Expansive Soil-Rubber
FAC..... Fly Ash Content
FBC ..... Fluidized Bed Combustion
FESEM..... Field Emission Scanning Electron Microscope
FGD..... Flue Gas Desulfurization
L ..... Laramie River
LOI.....Loss of Ignition
LPT .....Linear Potentiometric Transducer
MPC ..... Mountain Plains Consortium
NC .....Normally Consolidated
OCR ..... Overconsolidation Ratio
R..... Rawhide
RC .....Rubber Content
RMA .....Rubber Manufacturers Association
SEM ..... Scanning Electron Microscope

STR ..... Scrap Tire Rubber
USCS..... Unified Soil Classification System

CHAPTER 1: INTRODUCTION

1.1. Problem Statement

Approximately 4.6 million tons of scrap tires were generated in the United States in 2007 (Rubber Manufacturers Association 2009). In that same year, about 89% of the generated scrap tires went to end use markets. However, in states such as Colorado, about 55 million scrap tires remain in storage at designated scrap tire facilities (Colorado Department of Public Health and Environment 2009). There is an obvious advantage in discovering and implementing alternative uses to expand the end use markets for scrap tire rubber (STR) and reduce the exorbitant numbers of scrap tires remaining in the landfills in Colorado.

Currently, approximately 12% of the STR generated in the United States is beneficially used in end use markets in civil engineering projects (Rubber Manufacturers Association 2009). Beneficial use of STR in civil engineering applications is desirable, not only from a sustainable point of view, but also since STR is a relatively light-weight material, which makes it an ideal candidate for use in embankment fills and retaining wall backfills. STR has been investigated early on as an alternative to conventional geomaterials in civil engineering applications (Humphrey et al. 1993). Later studies investigated the use of sand-rubber mixtures (Ahmed & Lovell 1993; Lee et al. 1999; Youwai & Bergado 2003; Lee et al. 2007; Kim & Santamarina 2008), while other studies have investigated the use

of clay-rubber mixtures (Ozkul & Baykal 2001; Cetin et al. 2006) in civil engineering applications. With expansive soils being a major cause of damages to structures each year, additional mitigation techniques are advantageous to reduce costly damages caused by heaving of expansive soil. While several studies have been published on the use of soil-rubber mixtures, most of these previous studies have not focused on the more specific case of expansive soil-rubber (ESR) mixtures.

A recent study that focused on the swell potential of an ESR mixture has shown that STR addition reduced both the swell percent and the swell pressure of an expansive soil from Colorado (Seda et al. 2007). STR addition to expansive soil has shown to increase the shear strength, defined by the slope of the critical state line (CSL) of specimens compacted to similar soil states (Dunham-Friel 2009). However, that same study indicated a significant reduction in stiffness takes place due to STR addition to the soil.

The beneficial use of STR mixed with expansive soils is of interest to civil engineering applications since the swell percent and the swell pressure can be potentially reduced with no deleterious effect to the shear strength of the mixture (Seda et al. 2007, Dunham-Friel 2009). However, for applications whose design and analysis rely upon the stiffness characteristics of the materials used (e.g. roadways and foundations); more stringent stiffness requirements may be in order. Consequently, the focus of this study was to investigate the feasibility of using off-specification fly ashes to increase the stiffness of ESR mixtures so that the final mixture can have acceptable shear strength, stiffness and

swell potential characteristics, and, at the same time, be developed entirely using alternative, sustainable materials.

1.2. Research Objectives

The first objective of this research was to determine if a conventional Class C fly ash could be used to improve the stiffness and shear strength of an ESR mixture. Secondly, determine if off-specification fly ashes could be used in lieu of conventional Class C fly ash. Thirdly, to determine a fly ash content (*FAC*) necessary to promote pozzolanic development in the ESR-fly ash specimens and to assess the impact of various types of fly ashes on the soil's index properties (liquid limit and plastic limit).

The shear strength and stiffness of the ESR-fly ash mixtures were evaluated by a systematic experimental laboratory testing program. Results obtained for the ESR-fly ash mixtures tested were then compared with results obtained for an ESR mixture (Dunham-Friel 2009) to determine the effects imparted by the addition of various types of fly ashes.

The shear strength and stiffness was evaluated on specimens where the effect of the fly ash type and cure time was systematically evaluated using undrained axi-symmetric triaxial compression testing at three levels of mean effective stress (50, 100 and 200 kPa). The very small-strain stiffness was evaluated using bender elements.

1.3. Research Scope

This study was carried out using a single source of soil and rubber, and three different types of fly ash. The fly ash consisted of a conventional Class C and two off-specification fly ashes.

The rubber content (*RC*), which was defined as the ratio of dry mass of rubber to the dry mass of rubber and soil (or dry mass of rubber, soil and fly ash for mixtures stabilized with fly ash), was kept constant and equal to 20% for all specimens. For the ESR mixtures stabilized with fly ash, the *FAC*, which was defined as the ratio of dry mass of fly ash to the dry mass of fly ash and soil, was determined and kept equal to 14%, as it will be discussed in Section 6.1.

Specimens used in the stiffness and strength tests were prepared by statically compacting predetermined amounts of soil, rubber and/or fly ash (depending upon whether specimens of ESR or ESR-fly ash mixtures were prepared, respectively) according to the AASHTO T 307 method. Specimens were compacted to a single target level of relative compaction (C_R) of 95% of the standard Proctor maximum dry density and at standard Proctor optimum water content (w_{opt}) determined for each of the mixtures tested according to ASTM D 698. ESR specimens were subjected to further laboratory testing immediately after compaction. Specimens containing fly ash were compacted 2 h after fly ash addition to simulate typical field compaction conditions and then allowed to cure inside the split compaction mold for 7 or 14 days at approximately 22±1.5 ˚C. Specimens prepared as described above were then subjected to:

- Unconfined compression testing to assess whether the fly ash, at the selected *FAC*, induced pozzolanic reactions in the mixtures.
- Undrained axi-symmetric (triaxial) compression on isotropically consolidated specimens to evaluate swell potential, consolidation (λ, N, c_v, m_v), critical-state shear strength (ϕ_c), and stiffness (G) parameters. Triaxial testing was completed at three levels of mean effective stress (p') (50, 100 and 200 kPa).
- Stiffness at large strains was evaluated using external transducers during triaxial compression.
- Stiffness at very small strains was evaluated using bender elements mounted in the triaxial platens.

1.4. Manuscript Organization

The manuscript is organized into eight chapters that outline, present and analyze the experimental laboratory testing program followed to complete the research objectives. More concisely, the chapters are organized as follows.

Chapter 1 provides an introduction to the problems associated with scrap tire accumulation in the United States. Since many civil engineering applications may necessitate the need for a stiff material, it is hypothesized that off-specification fly ash could be used to increase the shear strength and stiffness of an ESR mixture. The background necessary for this hypothesis is discussed in Chapter 2. Chapter 3 summarizes the conceptual framework used to analyze and present the data obtained from the laboratory investigation. Chapter 4, 5 and 6 are devoted to presenting the methods,

results, and analysis of the laboratory investigation, respectively. Chapter 7 summarizes the findings of this study and provides suggestions for future work. Chapter 8 provides a summary of references.

CHAPTER 2: LITERATURE REVIEW

2.1. Scrap Tire Rubber

In 2007, about 89% of the 4.6 million tons of scrap tires generated in the United States went to end-use markets (Rubber Manufacturers Association 2009). Those markets include tire derived fuel (52.8%), ground rubber (16.8%), civil engineering projects (11.9%), reclamation projects (2.8%), exported tires (2.2%) and other miscellaneous items (1%) (Rubber Manufacturers Association 2009). Even with about 89% of the STR going to end-use markets, the Rubber Manufacturers Association estimates that approximately 128 million scrap tires remained in stockpiles in 2007. A distribution of scrap tires in the United States in 2007 is shown in Figure 2.1. About 55 million scrap tires remain in storage at designated scrap tire facilities in Colorado (Colorado Department of Public Health and Environment 2009).

Stockpiles of scrap tires can occupy large volumes of space in landfills and raise environmental concerns and health risks. Scrap tire stockpiles provide breading grounds for mosquitoes and rodents, which can spread and transmit threatening diseases such as dengue fever, encephalitis and West Nile virus and are at risk for stockpile fires (U.S. EPA 2006). The potential deleterious effects of STR on the environment and on human and environmental health have prompted research for additional end use markets.

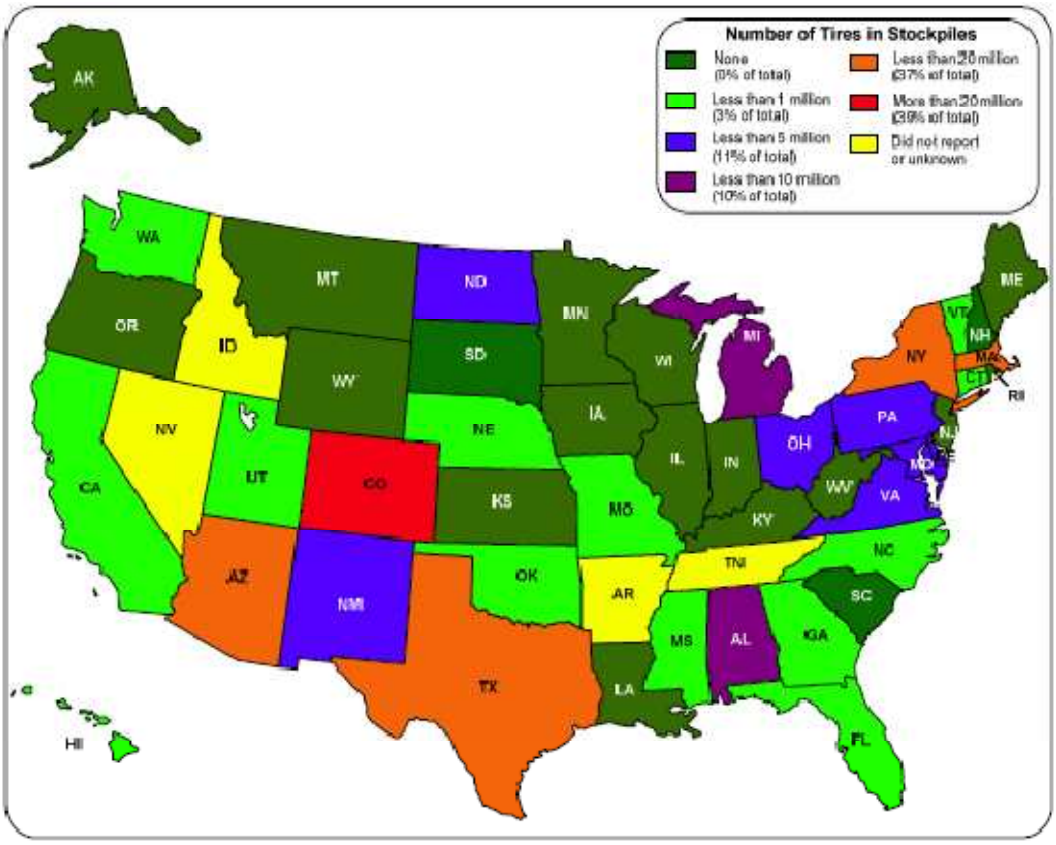

Figure 2.1 Distribution of scrap tires remaining in stockpiles in the United States (RMA 2009)

2.2. Sand-Rubber Mixtures

Early studies (Humphrey et al. 1993, Ahmed & Lovell 1993) investigated the use of STR as an alternative to conventional geomaterials in civil engineering applications. Since STR is a relatively light material, its use in civil engineering applications, such as in embankment fills and retaining walls is desirable. However, STR exhibits high compressibility (Ahmed & Lovell 1993) which, in some applications, may limit its use as a geomaterial. Investigations performed on sand-rubber mixtures (Ahmed & Lovell 1993) indicate that mixtures exhibited increased compressibility with addition of rubber tire chips, concluding that the compressibility of the mixtures is due to rearrangement,

bending, flattening or elastic deformations of rubber particles. Other studies have investigated the shear strength, compressibility and mechanical response of sand-rubber mixtures.

Lee et al. (2007) studied sand-rubber mixtures with ground rubber (rubber particles smaller than the sand particles) to investigate the small-strain stiffness and shear strength of mixtures at various *RC*. The mean particle size of the rubber (D_{50}=0.09 mm) was about 4 times smaller than the mean sand particle (D_{50}=0.35 mm) size. Testing completed on the sand-rubber mixtures was completed using standard triaxial and consolidometer apparatuses. Triaxial testing completed using consolidated drained protocol concluded that friction angles steadily decreased with the addition of rubber. A maximum reduction of 37% was observed with a mixture containing 100% rubber from a mixture containing 100% sand. Results indicate that stiffness decreased with increased rubber fraction, approximately by 95% and 80% at very small- and large-strains, respectively. Compressibility of mixtures was shown as a plot of vertical strain versus vertical effective stress. The compressibility of the mixtures was observed by the slope of the strain-stress plot. A mixture with 100% rubber exhibited a normally consolidated compression slope of approximately 0.16 (vertical strain to vertical stress) compared to the sand which exhibited 0.008.

Kim & Santamarina (2008) tested with sand-rubber mixtures to evaluate the effect of large rubber particles in sand mixtures. In their study, the rubber consisted of granulated rubber (D_{50}= 3.5 mm) which was approximately 10 times larger than the mean sand

particle size (D_{50}= 0.35 mm). Experimental testing was completed in a consolidometer apparatus fitted with bender elements to measure shear wave velocities. Their experimental program results suggest an optimum rubber content can be determined to provide maximum shear wave velocity (very small-strain stiffness). The volumetric fraction of rubber and size of rubber inclusions dictated the mechanical response of sand-rubber mixtures tested.

2.3. Clay-Rubber Mixtures

Previous studies investigated the use of sand-rubber mixtures in civil engineering applications. However, it is apparent that clay-rubber mixture could potentially be used as well. In general, results from previous studies suggest mixtures of clay with rubber can increase the shear strength of the clay soil but may reduce stiffness of clay alone (Ozkul & Baykal 2001; Cetin et al. 2006; Dunham-Friel 2009). Studies on expansive soil rubber (ESR) mixtures also suggest that rubber may increase the compressibility and reduce the swell potential and swell pressure of the expansive clay (Seda et al. 2007; Dunham-Friel 2009). Those studies are discussed below in further detail.

The mechanical response of clay-rubber mixtures was investigated (Ozkul & Baykal, 2007) using small sized tire buffings, acting as a fiber inclusions and kaolin clay (CL). The tire buffings used in their study were between 0.3 mm to 3.6 mm in diameter, and approximately 2 to 25 mm in length. Laboratory testing was carried out using a triaxial apparatus using consolidated undrained and consolidated drained testing protocols. The mixtures were tested at a *RC* of approximately 9%, compacted with either the standard or

modified Proctor effort at water contents 1 to 2% above the respective Proctor optimum water contents. Results of the drained triaxial testing indicate a general increase in shear strength of specimens containing rubber, more so at confining stresses at 200 kPa or less. Critical state friction angle was not indicated for drained or undrained tests. During drained triaxial testing, none of the samples appeared to reach critical state, defined by constant volume during shearing. As such, definite conclusions on any improvement of the critical state friction angle by the addition of rubber, is somewhat unclear. Stiffness of the mixtures was not directly commented on by the authors. However, observation of the slope of the principal stress difference verses axial strain plots for drained and undrained shearing conditions (Young's secant modulus of elasticity) provide some insight of the stiffness for each of the mixtures. Tests completed for confining stress of 50, 100, 200 and 300 kPa indicated specimens containing rubber exhibited a lower stiffness than the soil alone.

The mechanical response of kaolin clay (CL) and mixtures of clay with either coarse or fine size rubber were investigated by Cetin et al. (2006). The course size rubber consisted of particles approximately 2 to 5 mm while the fine rubber was approximately 0.07 to 0.5 mm. Shear strength testing was completed using a direct shear apparatus using consolidated undrained testing protocol. Normal stresses used during testing were 54, 109, 163 and 327 kPa. The initial soil state (i.e. water content and dry densities, soil fabric) of each specimen tested was not provided by the authors. The authors of the investigation concluded that the shear strength of the clay was improved with additions of up to 20% coarse or up to 30% fine sized rubber.

Seda et al. (2007) investigated expansive clay (CH) and expansive clay mixed at a *RC* of 20% (rubber was 2.0 to 6.7-mm sized). Swell and consolidation was evaluated on specimens prepared near 100% of standard Proctor maximum dry density and near optimum water content, using one-dimensional swell-consolidation apparatus. Specimens were inundated with water under a vertical stress of 6.1 kPa. Results indicate the addition of rubber reduced the swell potential and swell pressure of the expansive soil by approximately 49% and 75%, respectively. The additional of rubber increased the compression index by 24% and the recompression index by 57%. Thus, the study concludes the addition of rubber reduces swell and swell pressure of expansive soil, but inadvertently increases compressibility.

A recent study investigated the shear strength and stiffness of expansive clay soil and rubber mixtures in undrained triaxial compression (Dunham-Friel 2009). The rubber particles used in the study included 6.7-mm (maximum size) with a majority of the particles between 2 to 6 mm. Specimens were prepared for isotropic swell testing and consolidated undrained triaxial tests, by statically compacting specimens in accordance with AASHTO T 307. For the isotropic swell testing, a mixture including 20% rubber content (*RC*) (defined as the mass of dry rubber to the mass of dry rubber and dry soil) was compared with the expansive soil at a similar soil state. The soil state was approximately 95% of the standard Proctor maximum dry density and at approximately standard Proctor optimum water content. Results indicated the expansive soil exhibited an isotropic swell of 6.5% while the soil-rubber mixture exhibited a swell of 2.3%. The swell of the soil-rubber mixture was approximately 35% of the swell experienced by the

soil alone. These results collaborate with earlier conclusions on the reduced swell potential of ESR mixtures (Seda et al. 2007). For undrained triaxial compression testing, mixtures of clay-rubber were prepared at *RCs* of 0, 10 and 20%. Undrained triaxial testing was completed on specimens prepared at a single relative compaction equal to 95% of standard Proctor maximum dry density at water contents of approximately 2% above, 2% below and near standard Proctor optimum water content. Specimens for triaxial testing were prepared according to AASHTO T 307 using a static compaction procedure. Large-strain stiffness was measured using external transducers while the very small-strain stiffness was measured using bender elements mounted in the triaxial apparatus. Measurements of the small-strain stiffness were obtained at the end of each of the consolidation phases at 30, 50, 100 and 200 kPa. The study concluded that the critical state friction angle increased with increasing *RC*. ESR mixtures with a *RC* of 10 and 20% showed the critical state friction angle increase by approximately 3 and 11%, respectively. Additions of rubber lowered the very small-strain and large-strain stiffness from the soil alone. The large-strain stiffness was lowered more with higher *RC*s and mean effective stresses. For mixtures with *RC* of 10%, the stiffness at 0.4% axial strain was lowered to approximately 45, 55 and 60% of the stiffness of the expansive soil at mean effective stresses of 50, 100 and 200 kPa, respectively. At the same axial strain and respective mean effective stresses, mixtures with a *RC* of 20% reduced the stiffness to approximately 65, 80 and 85% of the soil alone. At very small strains, the stiffness of mixtures with a *RC* of 10 and 20% were approximately 45 to 60% and 62 to 75% of the soil alone, respectively.

2.4. Coal Combustion Products

Coal combustion products (CCPs) are materials produced in power plants as a result of combustion of coal. CCP's consist of numerous materials including fly ash, bottom ash, boiler slag, flue gas desulfurization (FGD) material and fluidized bed combustion (FBC) ash (U.S. Environmental Protection Agency, 2005). Generally, heavier and larger particles that fall to the bottom of the boiler are referred to bottom ash and the lighter ash particles that are carried upward through the flue gas is considered fly ash. Boiler slag is produced in wet boiler while FGD material is a result of emission scrubbing in which sulfur is removed from the flue gas emission. The general process can be observed in Figure 2.2.

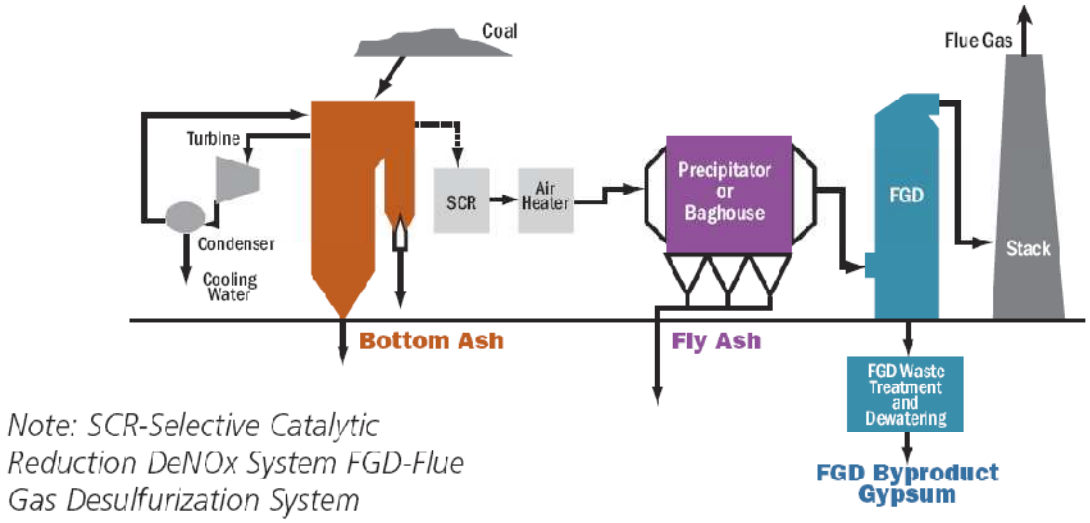

Figure 2.2 Typical steam generating system (U.S. Environmental Protection Agency 2005)

Fly ash is known for beneficial uses, primarily resulting from its pozzolanic capacity. End use markets for use of CCP's are shown below in Figure 2.3. More specifically, in 2008, approximately 136 million tons of CCP's were produced in the United States and

approximately 61 million tons of the produced fly ash was beneficially used in markets (U.S. Environmental Protection Agency 2010).

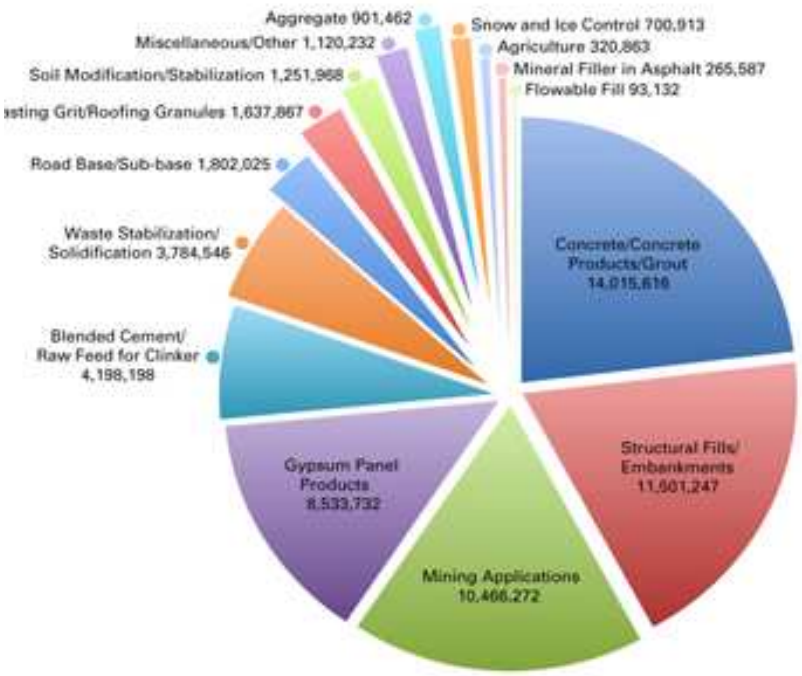

Figure 2.3 CCP Applications (U.S. Environmental Protection Agency 2010)

2.5. Fly Ash

Fly ash is a CCP that is collected from the flue-gas at coal burning power plants. The chemical constituents of the fly ash are largely governed by the type of coal used in the combustion process. Two main types of coal combusted include anthracite or bituminous coal and lignite or subituminous coal. The combustion of bituminous coal usually produces a fly ash low in free lime while combustion of subituminous coals produces fly ashes that typically have higher amounts of free lime. The major chemical constituents of the fly ash include silicon, aluminum and calcium. Minor chemical constituents include iron, magnesium, sulfur, sodium, and potassium.

According to ASTM C 618, fly ash can be categorized based on chemical constituents. The three classes of fly ash include Class N, Class F, or Class C. Class F fly ashes are typically produced from bituminous coals were Class C fly ashes are typically produced from subituminous coals. Class F ash usually has a free lime content of 2 to 6% whereas Class C fly ash commonly contains between 15 and 35% free lime (U.S. Environmental Protection Agency 2005). The chemical requirements for fly ash classification are summarized below in Table 2.1.

Table 2.1 Chemical Requirements of Fly Ash per ASTM C 618

	Class		
	N	**F**	**C**
Sum of Silicon Dioxide (SiO_2, Aluminum Oxide (AL_3O_3), Iron Oxide (Fe_2O_3)	70.0 Min.	70.0 Min.	50.0 Min.
Sulfur Trioxide, SO_3 (%)	4.0 Max.	5.0 Max	5.0 Max.
Loss on Ignition, LOI (%)	10.0 Max.	6.0 Max.	6.0 Max.

Many subituminous coal ashes, in the presence of water can exhibit "self-cementing" behavior. The bituminous coal fly ash often requires an additional free lime source to develop pozzolanic reactions. In the presence of water, the general pozzolanic development of the self cementing fly ash is illustrated below where R is either Ca^{2+} or Mg^{2+}. Similarly, the alumina oxides and silica oxides may also exist in clay soil.

$$R(OH)_2 + SiO_2 + H_2O \rightarrow (x)RO(y)SiO_2(z)H_2O$$

$$R(OH)_2 + Al_2O_2 + H_2O \rightarrow (x)RO(y)Al_2O_2(z)H_2O$$

$$R(OH)_2 + Al_2O_2 + SiO_2 + H_2O \rightarrow (x)RO(y)Al_2O_2(z)SiO_2(w)H_2O$$

Fly ash materials that do not conform to the requirements established by ASTM C 618 are referred to herein as off-specification fly ash. Typical off-specification characteristics of fly ash include high SO_3 content or high loss on ignition (LOI). Off-specification fly ashes are more often disposed of since use in concrete is not recommended (ASTM C 618), development of pozzolanic reactions necessary for soil stabilization may be insufficient, and there may be time delays or other undesirable chemical reactions (e.g. ettringite and thaumasite crystal development).

According to the American Coal Association (2008), The Clean Air Act (CAA), the Clean Air Interstate Rule (CAIR) and the Clean Air Mercury Rule (CAMR) have resulted in more stringent control of emissions by generating facilities. One such emission is the reduction of sulfur dioxide (SO_2) emission. Some coal-burning power plants reduce SO_2 emissions by scrubbing the flue-gas utilizing FBC or FGD systems. The FBC or FGD

material obtained during the scrubbing process can be collected, separated or reintroduced into the fly ash collected in the bag house. The FBC process removes the SO_2 during the combustion process by using lime in a fluidized bed. The FGD system removes the SO_2 from the flue-gas after combustion by introducing lime to form calcium sulfate. If the FDG material is separated from the fly ash, the FDG can be used is the development of gypsum wallboard, Portland cement, and also as a soil amendment for agricultural purposes. If the FDG material is reintroduced into the fly-ash, the additional SO_x may develop an otherwise standard fly ash to be off-specification. With increases in SO_x content in the fly ash, formation of highly expansive ettringite and thaumasite crystals are an increased possibility and may require special evaluation.

According to the U.S. Environmental Protection Agency (2008), increasing limits on NO_x emission have led to widespread use of low NO_x coal burners. The low NO_x burners are often inefficient at combusting all the coal. As such, the fly ash is often produced with higher carbon content. Higher carbon in the fly ash can result in problems with air entrainment and durability in Portland cement concrete (American Coal Ash Association, 2003).

2.6. Soil Stabilization

Stabilization is the permanent improvement of engineering performance. Various methods exist to stabilize soil including chemical stabilization, mechanical stabilization, biological and thermal. Desired engineering characteristic usually include increasing the soil shear strength and/or stiffness, reducing the soil compressibility and/or swell

potential. Mechanical stabilization methods can include soil state modifications (such as static or dynamic compaction), consolidation (e.g. preloading, surcharging) and admixing of other geomaterials. Chemical stabilization might be accomplished by admixing of compounds such as lime, Portland cement, bitumen and CCPs. For the purpose of this study, emphasis will be on stabilization of fine grained soils using fly ash.

2.7. Stabilization of Fine Grain Soils with Fly Ash

As discussed in Section 2.5, Class C fly ash has chemical constituents that enable pozzolanic reactions within a soil matrix and the development cementitious bonds. Self-cementing, Class C fly ash, has been documented by many authorities as a method of soil stabilization (American Coal Ash Association Educational Foundation 2008, Center for Transportation Research and Education 2005, and U.S. Environmental Protection Agency 2005). Class C fly ash can be used to stabilize coarse grain soils (such as aggregate base) or fine grain soils (such as silt and clay) because of its unique ability of self-cementing characteristics. Improvements attained by the introduction of Class C fly ash to soil include significant drying; reduction in plastic limit, plasticity index and shrink-swell; and increases in shear strength (American Coal Ash Association Educational Foundation 2008). Some affects of Class C fly ash on soil density, optimum water content, plasticity, compaction delay, shrink-swell potential, stiffness and shear strength are outlined below. Other specific studies on stabilization of clay soils are further investigated.

Proctor Maximum Dry Weight: Class C fly ash addition tends to increase the maximum standard and modified Proctor dry density and reduces the optimum water

content of soil alone when compacted with no compaction delay (Center for Transportation Research and Education 2005).

Compaction Delay: The maximum Proctor dry density tends to decrease while the optimum water content tends to increase with compaction delay (Misra 1998; American Coal Ash Association Educational Foundation 2008). The unconfined compressive strength of fly ash stabilized soil tends to be reduced with increases in compaction delay (American Coal Ash Association Educational Foundation 2008; Center for Transportation Research and Education, 2005), primarily due to the development of tricalcium aluminate prior to compaction which allows less pozzolanic bonds to develop when soil is compacted. Density is lowered since more compaction energy is required to overcome the tricalcium aluminate formations (American Coal Ash Association, 2003).

Cure Time: Unconfined compression strength tends to increase with curing time (Misra 1998; Center for Transportation Research and Education, 2005).

Shrink-Swell: Shrink-swell is reduced by development of physical cementitious particle bonding which reduce/restrict movement within the soil matrix (American Coal Ash Association, 2003).

Stiffness: Stiffness of clay soils stabilized with fly ash tends to increase with additions of Class C fly ash (Misra 1998).

In an investigation completed by Misra (1998), soil consisting of blends of kaolinite, bentonite and natural lean clay soils were evaluated in the laboratory to determine the effect of compaction delay, water content and cure time on the unconfined compressive strength of prepared specimens. The blended soils (kaolinite and bentonite) all classified

as high plasticity clay (CH) while the natural clay soils classified as either CH or lean clay (CL). Specimens were evaluated at with various fly ash contents, water contents and compaction delays. The author reports specimens compacted without compaction delay exhibited slightly lower optimum water content and higher maximum dry density. Delaying compaction time increased the optimum water content of the mixtures and lowered the maximum dry density. Unconfined compressive strength testing was completed on specimens, containing different fly ash and water contents, were compacted and cured for 7 days. Results indicate highest unconfined compressive strengths were obtained with the lowest compaction delay and at higher fly ash contents. Strain monitoring during compression was completed on specimens at single fly ash content at various water contents and compaction delays. The author reports an increase stiffness of specimens with fly ash addition.

A laboratory investigation was completed by Cokca (2001) to determine the effectiveness of stabilizing expansive clay with the addition of high calcium fly ash, low calcium fly ash, lime and cement. For this study, expansive clay consisting of a blend of 85% kaolinite and 15% bentonite was used. The high calcium fly ash in the study was blended with the soil at 0, 3, 5, 8, 10, 15, 20, and 25% by dry weight. The mixtures were evaluated for plasticity and swell potential. Mixtures were compacted (assumed with no compaction delay) statically at a single water content and dry density. With additions of fly ash, experimental testing shows a general reduction of the liquid limit, an increase in the plastic limit, a reduction in the plasticity index, and a reduction in the swell potential. Further reductions in the swell potential are observed after 7 days and again at 28 days of

curing time at 22 °C. Changes between plasticity and swell are limited between 20 and 25% fly ash.

A study completed by Edil et al. (2006), investigated the California bearing ratio (CBR) and resilient modulus (M_r) of soft fine-grained soils stabilized with fly ash. The soil used in this study consisted of seven soils including CL, CH and OH. The fly ashes used in this study included two Class C fly ashes and two off-specification fly ashes. Classification of off-specification was due to either high SO_3 or high LOI. Evaluation of the CBR and M_r were evaluated on specimens consisting of soil mixed with different fly ash and fly ash contents. Specimens subjected to CBR testing were prepared by compacting soil and fly ash blends, after a 2 h compaction delay, with standard Proctor effort. Specimens were compacted at the soil's standard Proctor optimum water content and 7% wet of the soil's optimum water content. CBR testing was carried out after curing the specimens at 25 °C for 7 days. The specimens prepared for M_r testing were prepared similar to the CBR specimens, but at water contents between standard Proctor optimum water content and 18% above optimum water content. M_r testing was carried out after curing the specimens at 25 °C for 14 to 56 days prior to testing. Results indicate that specimens with fly ash, compacted 7% wet of optimum water content, exhibited a CBR that was on average 400% to 800% of the CBR of the soil, for fly ash contents of 10% and 18%, respectively. Mixtures with off-specification fly ashes showed similar or more improvement to the CBR than mixtures with the Class C fly ash. Specimens of soil, compacted at optimum water content, generally exhibited higher M_r than specimens containing 10% fly ash which were compacted 7% above optimum water content. For

similar water contents conditions, specimens with 18% fly ash content exhibited M_r of 80 to 250% of the M_r of the soil. Similar to the CBR tests, the mixtures with off-specification fly ashes exhibited similar or higher M_r than mixtures with Class C fly ash.

2.8. Summary

Section 2.1 through 2.7 present the detailed findings of the reviewed literature that pertains to scope of this study. The topics of the literature review include STR, sand-rubber mixtures, clay-rubber mixtures, coal combustion products, fly ash, soil stabilization, and stabilization of fine grain soils with fly ash. A summary of the reviewed literature is below which substantiated, in part, the hypothesis of this study.

The reviewed literature indicates a large quantity of scrap tires remain in stockpiles throughout the United States; Colorado having among the largest scrap tire stockpiles (RMA 2009). End-use markets have been developed to use scrap tires and reduce stockpiles; however, the existing end use markets are not expending the exorbitant numbers of scrap tire remaining. The need to develop additional end-use market is evident. Civil engineering applications have potential for the use of high quantity of scrap tires (i.e. roadway development and embankment).

Previous studies recognized the potential for STR in civil engineering applications, in part because it's a relatively light material, and began investigating the use of STR as an alternative to conventional geomaterials (Humphrey et al. 1993; Ahmed & Lovell 1993). However, those findings suggest that STR exhibits high compressibility (Ahmed &

Lovell 1993) which potentially limits its use in civil engineering applications. Studies were expanded to invetigate STR mixed with sand or clay.

Studies investigating sand-rubber mixtures found additions of rubber to the sand tends to increase the mixture's compressibility (Ahmed & Lovell 1993, Lee et al. 2007) and decrease the friction angle (rubber particles smaller than the sand particles) (Lee et al. 2007). The large-strain and very-small strain stiffness was also reduced with the addtion of rubber (Lee et al. 2007).

Further studies investigated clay-rubber mixtures concluded additions of rubber increased the friction angle of the host clay (Ozkul & Baykal 2007, Cetin et al. 2006, Dunham-Friel 2009) and reduced the stiffness at large strains (Ozkul & Baykal 2007, Dunham-Friel 2009) and at very small strains (Dunham-Friel 2009). Investigations completed with expansive soil showed the addition of rubber reduce the swell (Seda et al. 2007, Dunham-Friel 2009) and the swell pressure (Seda et al. 2007).

In expansive clay soil, the increase in shear strength and reduction of swell and swell pressure with the addition of STR is highly advantageous in civil engineering applications; however, the reduced stiffness may limit the use of clay-rubber mixtures. By increasing the stiffness of clay-rubber mixtures, more end-use applications may be available. Conventional Class C fly ash has been documented by many authorities as one method to stabilize soil (American Coal Ash Association Educational Foundation 2008, Center for Transportation Research and Education 2005, and U.S. Evironmental

Protection Agency 2005). The addition of conventional Class C fly ash to clay soil tends to reduce the plasticity index and shrink-swell (American Coal Ash Association Educational Foundation 2008), increase the unconfined compressive strength (Misra 1998; Center for Transportation Research and Education, 2005), increase the stiffness (Misra 1998), increase the CBR and M_r (Edil et al. 2006).

However, according to the American Coal Association (2008), recent legislation has resulted in more stringent control of emissions by power generating facilities. As a result, scrubbers and plant altercations have resulted in additional chemicals being comingling with otherwise conventional Class C fly ash, resulting in fly ash that is off-specification. End use markets for off-specification fly ashes are very limited and consequently often land filled or stockpiled. Since emission controls are probably only to become more stringent in the future, it's likely more off-specification fly ash will take the place of conventional Class C fly ash.

Few studies have investigated the use of off-specification fly ash for soil stabilization. However, a particular study concluded that clay soil stabilized with off-specification fly ash increased the CBR and M_r of the soil greater than that same clay stabilized with conventional Class C fly ashes (Edil et al. 2006).

Based on the literature review of STR, sand-rubber and clay-rubber mixtures, it appears that additional end use markets for STR could be developed if soil-rubber mixtures were stiffer and could develop higher shear strength. It is hypothesized that the stiffness and

shear strength of an ESR mixture could be increased by conventional Class C fly ash and also by off-specification fly ashes.

CHAPTER 3: CONCEPTUAL FRAMEWORK

3.1. Critical State Framework

The framework for critical state soil mechanics is based on a failure envelope (critical state line or CSL) such as the one shown in *p´*, *q*, *e* (or *v*) space (Figure 3.1).

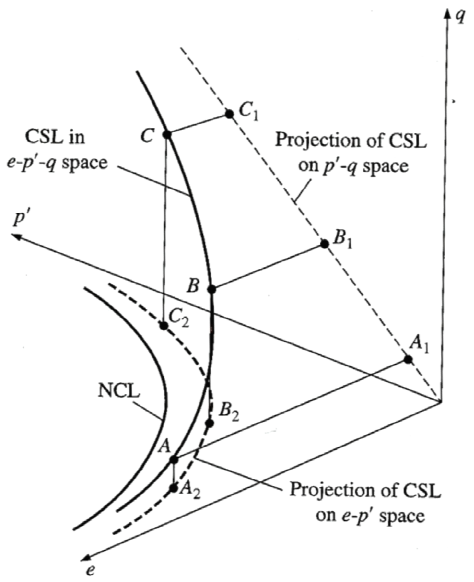

Figure 3.1 Critical-state line in *e-p´-q* space (Salgado 2008)

The critical state framework is based on the idea that, as soil strains, the particles will eventually reach a point that shear resistance is governed by the intrinsic frictional resistance developed between the soil particles. Critical state is defined when the soil is in equilibrium with the applied stresses. Under drained shearing conditions, critical state is

mobilized when no further changes in volume occur (constant volume). Critical state occurs in undrained shearing conditions when the excess pore water pressures mobilized during shearing of the soil are constant. The main parameters defining the CSL are shown below in Equation 1 and Equation 2 (Schoefield & Wroth 1968)

$$q = Mp' \qquad \text{(Equation 1)}$$

$$\Gamma = v + \lambda \ln p' \qquad \text{(Equation 2)}$$

where v is the specific volume (=1+e). For axi-symmetric conditions, $q = (\sigma_1 - \sigma_3)$ is the deviatoric stress, and $p' = \frac{\sigma_1' + \sigma_2' + \sigma_3'}{3}$ is the mean effective stress. The CSL defines the states under which the soil is in equilibrium with the applied stresses. However, under low mean effective stress, the soil can exist at points above the CSL due to dilatency in the case of uncemented soils. The critical state friction angle (ϕ_c) is related to the critical state parameter M by Equation 3 (Atkinson 1993). The state of the soil prior to shear will affect the stress path followed by the soil during shearing.

$$\sin \phi_c = \frac{3M}{6 + M} \qquad \text{(Equation 3)}$$

For loose soil states, contraction will occur in drained conditions, whereas positive pore water pressure generation will develop in undrained conditions. This behavior would be typical of normally consolidated clay or loose sand.

For dense soil states, the particles will tend to dilate, especially under relatively low mean effective stresses. Soil dilatency is primarily due to volume changes whereby soil

particles roll over one another and shift within the soil matrix. This behavior would be typical of overconsolidated clay or dense sand.

Under drained conditions, dilation is associated with an increase in volume of the specimen with applied strains (Figure 3.2(a)) which may or may not be preceded by initial contraction. During undrained conditions, negative excess pore water pressure will develop as the soil attempts to dilate. For clays the negative excess pore pressures can be observed as a function of the overconsolidation ratio (OCR) (Henkel 1956) which would be a similar behavior for dense sand. The idealized behavior of clay during undrained conditions is shown in Figure 3.2(b).

Soil exhibiting dilatency displays a “peak” in its stress path for temporary states lying above the CSL. The shear strength mobilized at any point above the CSL is defined by the peak friction angle (ϕ_p).

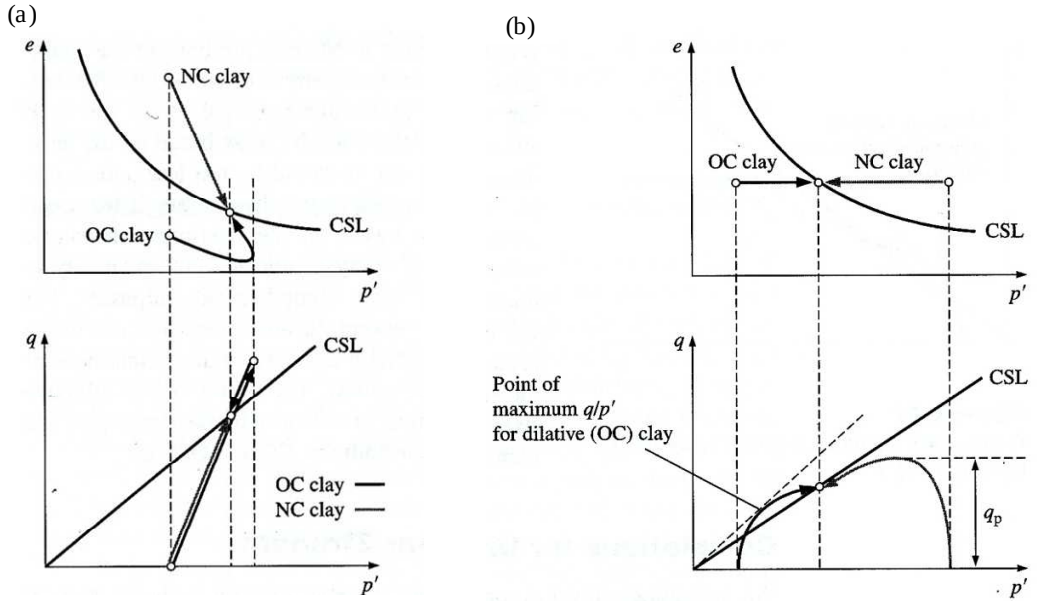

Figure 3.2 (a) NC and OC clay in drained conditions, (b) NC and OC clay in undrained conditions (Salgado 2008)

3.2. Axi-symmetric Compression

Many applications in geotechnical engineering depend on the accurate prediction of soil shear strength and mechanical response. Such applications include bearing capacity of foundations, prediction of lateral earth pressures for retaining walls, shear strength for slope stability analysis, stability of embankments, etc. Accurate and precise prediction of soil behavior, in combination with high-quality modeling, can provide geotechnical designs that are safe and cost effective.

Prediction of soil shear strength for geotechnical design is often based on characterizing the soil through experimental laboratory testing. The critical-state shear strength of soil is affected by different intrinsic characteristics which include soil mineralogy, grain size distribution and particle angularity (Salgado 2008). State variables of the soil affecting

its shear strength include void ratio (or relative density), water content, soil fabric, cementation and effective confining stress (discussed further in Section 3.3).

The triaxial test is widely used to evaluate the shear strength of soil experimentally. In a standard triaxial test, the cell pressure or radial stress (σ_r) applied to the specimen is a principal stress. In a typical axi-symmetric test, the other applied stress is the axial stress (σ_a) which is determined as the sum of the deviatoric stress and the radial stress. The applied normal stresses can be measured with pressure transducers and axial force transducers. In axi-symmetric compression, $\sigma_a=\sigma_1$ and $\sigma_r=\sigma_2=\sigma_3$. In this study, triaxial testing will imply axi-symmetric conditions.

When assessing the soil shear strength, it is essential to measure the stresses in terms of effective stress. The effective stress is the actual stress carried by the soil skeleton and represents what the soil actually "feels." The effective stress concept states that when a stress is applied to a unit volume of soil, the soil supports the total stress by two components which include the pore pressure (u) and the effective stress (σ').

$$\sigma' = \sigma - u \qquad \text{(Equation 4)}$$

In consolidated drained (CD) triaxial testing, the effective stress can be fully mobilized by completely allowing the soil to drain during shearing (i.e. by allowing pore water pressures to dissipate completely). Alternatively, consolidated undrained (CU) triaxial tests are carried out by measuring the excess pore water pressures generated during

shearing. In this study, CU tests were used, and, as such, will be discussed further in the following section.

3.3. Consolidated Undrained Triaxial Compression

In the critical state framework, the shear strength of soil is dependent on the void ratio (e) or specific volume (v) among other variable such as (p', ϕ_c, etc.). It is often desirable to determine the shear strength of soil at various specific volumes to determine the stress path to CSL. The consolidated isotropically undrained triaxial test is typically conducted in phases: isotropic consolidation and shearing.

In the isotropic consolidation phase, σ_r is increased to a desired level (e.g. 50, 100 or 200 kPa) under undrained conditions. This increase in mean effective stress will cause an instantaneous increase in pore water pressures in the specimen. Then the drainage lines are opened and the pore water pressures are allowed to dissipate as the specimen contracts and water drains out of the specimen. The drainage of pore water during consolidation leads to a decrease in the specimen's specific volume.

During undrained shearing, the specimen is sheared with all drainage lines closed. Therefore, a change in the deviatoric stress ($\Delta q=\Delta\sigma_a$) will immediately cause a change in pore water pressure (Δu).

The radial stress does not change during the shearing phase ($\Delta\sigma_r=0$). As a result, changes in mean stress (Δp) are related to axial stress changes ($\Delta\sigma_a$) through Equation 5.

$$\Delta p = \frac{\Delta \sigma_a}{3} \qquad \text{(Equation 5)}$$

Accordingly, changes in mean effective stress ($\Delta p'$) are related to axial stress changes ($\Delta \sigma_a$) and changes in pore water pressure (Δu) through Equation 6.

$$\Delta p' = \frac{\Delta \sigma_a}{3} - \Delta u \qquad \text{(Equation 6)}$$

Plotting q versus p' is the most rigorous way to express the stress path for triaxial compression. For undrained response the total stress path has a 3:1 slope. The effective stress paths will vary depending on the soil state and Δu generated during shearing. Effective stress paths for undrained loading can be observed in Figure 3.3 for ESR rubber mixtures (Dunham-Friel 2009) similar to the ones used in the present study.

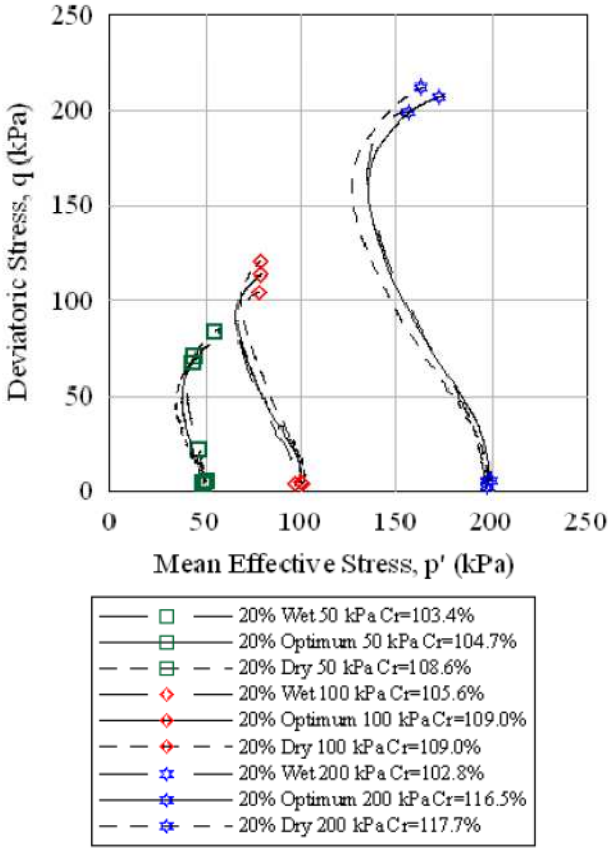

Figure 3.3 CU triaxial stress path of ESR mixtures (Dunham-Friel 2009)

3.4. Large-Strain Stiffness

Soil stiffness is non linear and decays with strain (Atkinson 2000). As a result, it is useful to represent soil stiffness as a function of strain. Soil stiffness can be measured in the laboratory during routine triaxial testing and may be commonly expressed as the Young's modulus of elasticity (E) through a convenient selection of reference axes. Tangent stiffness (E_t) can be deduced from the initial stages of the axial strain (ε_a) versus deviatoric stress (q) curve as the slope of a line tangent to any point on the ε_a vs. q curve. In its secant form (E_s), stiffness might be alternatively expressed as the slope of the secant line from the origin through the same point on the ε_a vs. q curve. Alternatively, it might be convenient to express soil stiffness from undrained triaxial compression tests in terms of the shear modulus (G) of the material, which can also be deduced from the initial stages of the ε_a vs. q curve as:

$$G = \frac{\delta q}{3\delta\varepsilon_a} = \frac{E}{2(1+\nu)} = \frac{E}{3} \qquad \text{(Equation 7)}$$

where δq and $\delta\varepsilon_a$ are the deviatoric stress and axial strain increments, respectively, and ν is the Poisson's ratio of the material (equals 0.5, for incompressible materials). From the Mohr circle of strains, the maximum shear strain increment ($\delta\gamma$) in the material can be deduced through:

$$\delta\gamma = \varepsilon_a(1+\nu) = 1.5\varepsilon_a \qquad \text{(Equation 8)}$$

Equations 7 and 8 assume an elastic treatment for the incremental response of the materials may be adopted even though their overall stress-strain response may be far from linearly elastic (Muir-Wood 2004).

Accurate soil stiffness evaluation relies upon precise measurements of the applied stresses and soil deformations. External displacement transducers provide accurate data for axial strains larger than 0.1% (Atkinson 2000). Limitations of external transducer measurements may be due to piston friction (if an external load cell is used), deformation of equipment components, and seating errors, among other sources (Baldi et al. 1988). Axial strain measurements between 0.001 and 0.1% would necessitate the use of local displacement transducers (Jardine et al. 1984). Dynamic methods based on shear wave velocity (V_s) measurements can also be used to evaluate stiffness in the very small axial strain range (Atkinson 2000) by resolving axial strains to values smaller than 0.001% (Dyvik & Madshus 1985). An idealized representation of soil shear stiffness with shear strain is shown in Figure 3.4.

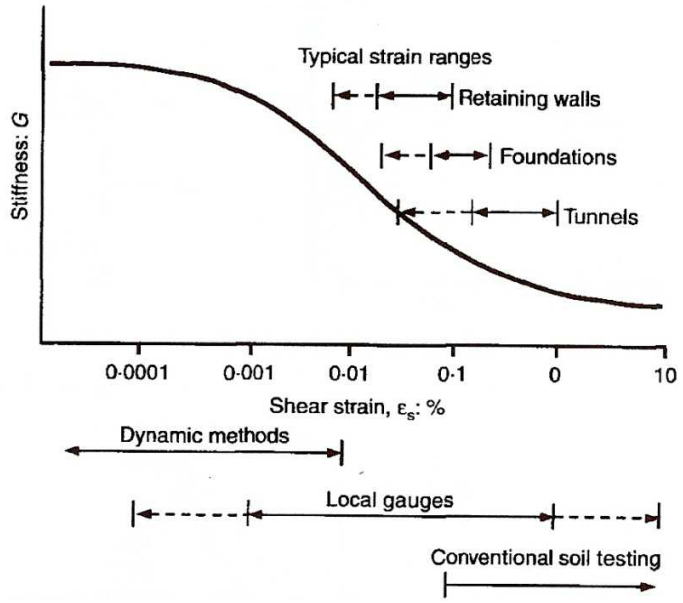

Figure 3.4 Shear strain degradation curve (Atkinson 2000)

3.5. Very Small-Strain Stiffness

Soil stiffness at axial strains between 0.0001 and 0.001% is referred to as very small-strain stiffness (Atkinson 2000). At very small strains, the accuracy of stiffness measurements can be significantly improved by using V_s-based methods, as discussed above. Soil stiffness in the very small-strain range (also referred to as G_{max} or G_0) can be deduced from simple one-dimensional wave propagation analysis as:

$$G_{max} = \rho V_s^2 \qquad \text{(Equation 9)}$$

where ρ is the total density of the material.

CHAPTER 4: EXPERIMENTAL PROGRAM

4.1. Materials

4.1.1. Soil

The soil used in this study was obtained from the Colorado State University (CSU) expansive soil test site (Dunham-Friel 2009). The site is located at the CSU Engineering Research Center, approximately 1.1 km west of Overland Trail and 0.3 km south of Laporte Avenue in Fort Collins, Larimer County, Colorado (Figure 4.1). The soil obtained from the expansive soil test site is identified by the Department of the Interior U.S. Geological Survey, Geologic Map of the Horsetooth Reservoir Quadrangle, as belonging to the Pierre Shale formation (Figure 4.1). A more detailed diagram of the sampling area used to collect the samples is shown in Figure 4.2.

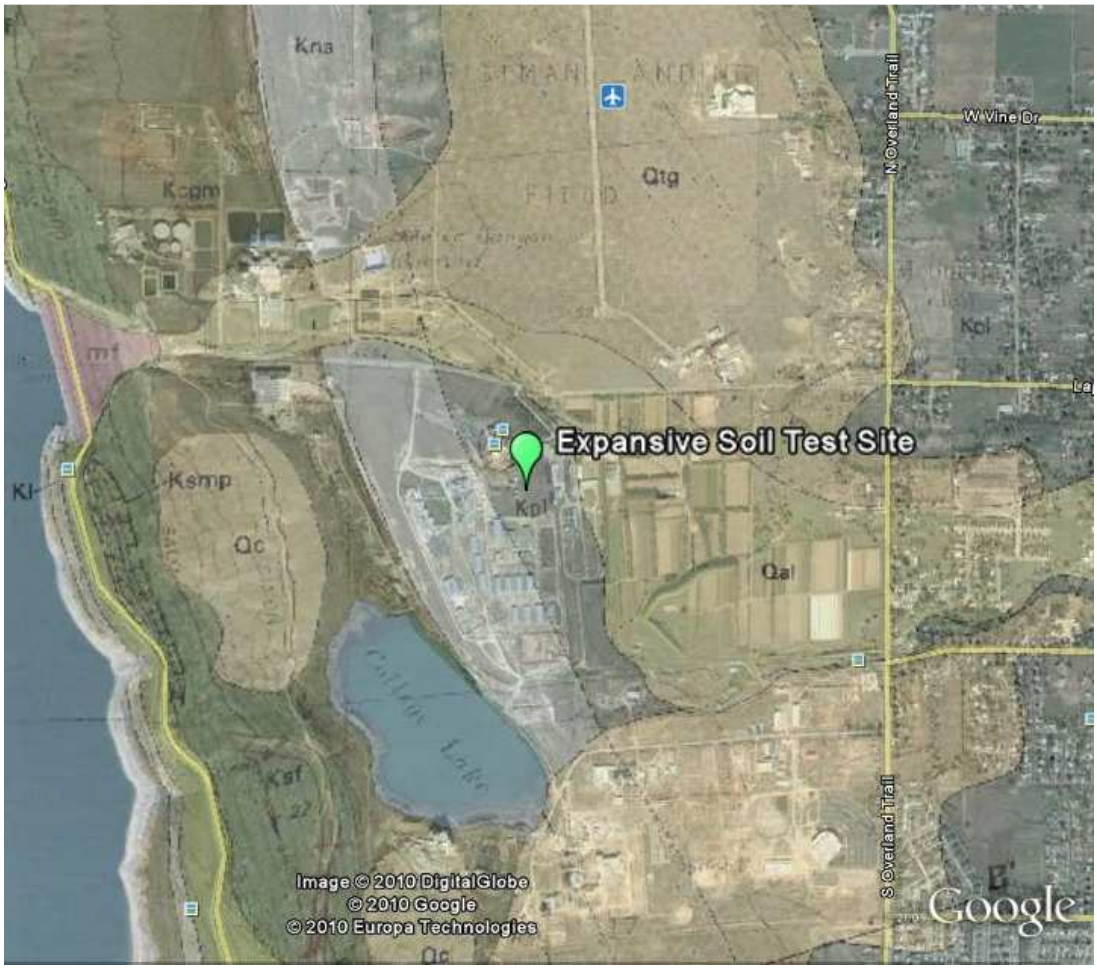

Figure 4.1 Expansive Soil Test Site at the Engineering Research Center of Colorado State University (Fort Collins, Colorado)

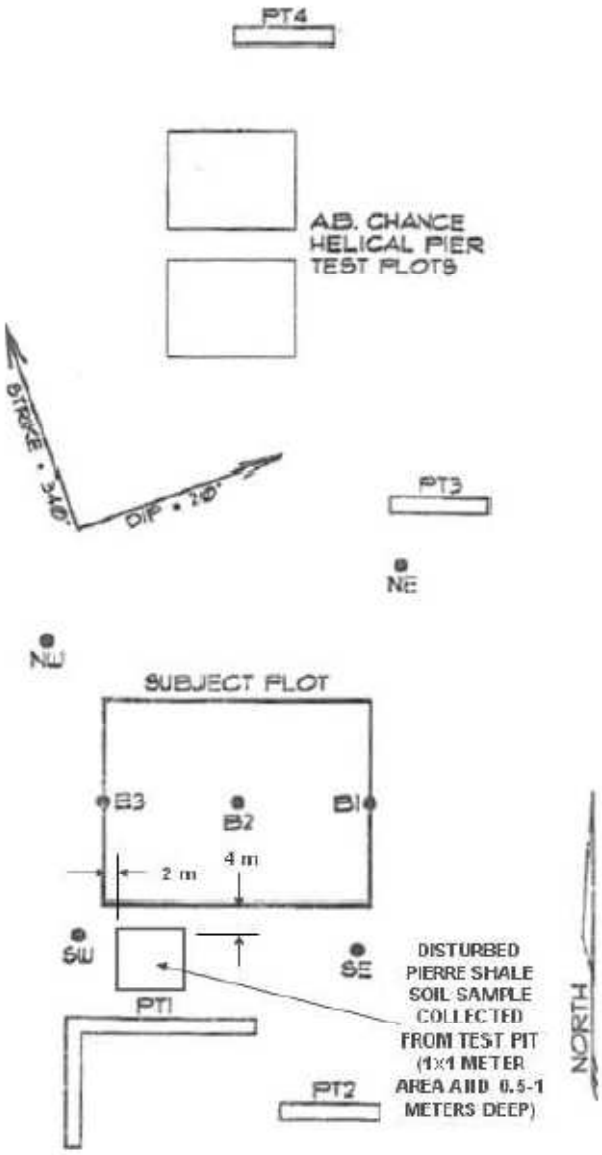

Figure 4.2 Detailed site diagram of expansive soil test site showing sampling location (Dunham-Friel 2009, Modified after Abshire 2002)

Atterberg limits (ASTM D 4318), sieve analysis (ASTM C 117 and C 136) and specific gravity (ASTM D 422) tests (Dunham-Friel, 2009) completed on the expansive soil are summarized in Table 4.1. Based on the results of the index properties, the soil classifies

as high plasticity clay (CH) in accordance with the Unified Soil Classification System (USCS). The particle size distribution of the expansive soil is shown in Figure 4.3.

Table 4.1 Soil index properties

Liquid Limit, w_L	Plasticity Index, I_P	Specific Gravity, G_s	% Finer No. 4	% Finer No. 200	USCS
54%	33%	2.72	100	93.1	CH

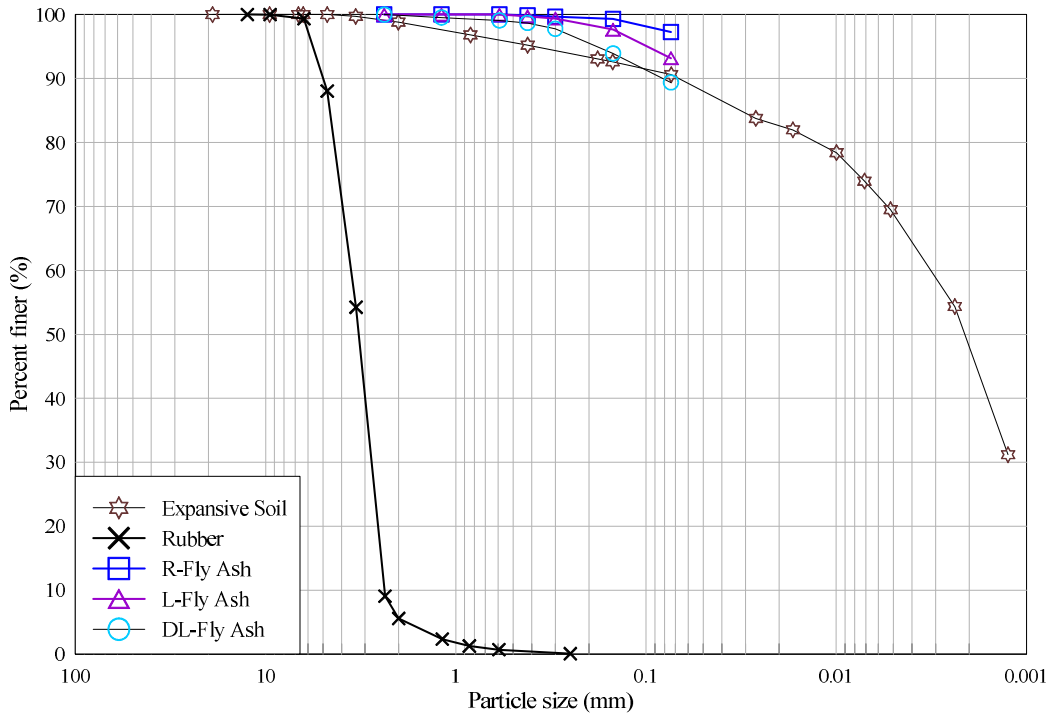

Figure 4.3 Particle size distribution of expansive soil, rubber (Dunham-Friel 2009), R-fly ash, L-fly ash, and DL-fly ash.

4.1.2. Rubber

The STR material used in this study was manufactured by Caliber Recycled Products Inc. Commerce City, Colorado, and consists of granulated rubber with nominal maximum particle size of 6.7-mm and specific gravity equal to 1.16 (Dunham-Friel 2009). Particle size distribution of the STR used in this study is shown in Figure 4.3.

4.1.3. Fly Ashes

The fly ashes used in this study were obtained from three different sources. The standard Class C fly ash was produced at the Laramie River Station in Wheatland, Wyoming. The off-specification fly ashes were produced at the Rawhide Energy Station, which is located north of Fort Collins, Colorado, and at the Martin Drake Power Plant in Colorado Springs, Colorado. The approximate locations of the coal combustion power plants along with other coal combustion power plants in Colorado and shown in Figure 4.4.

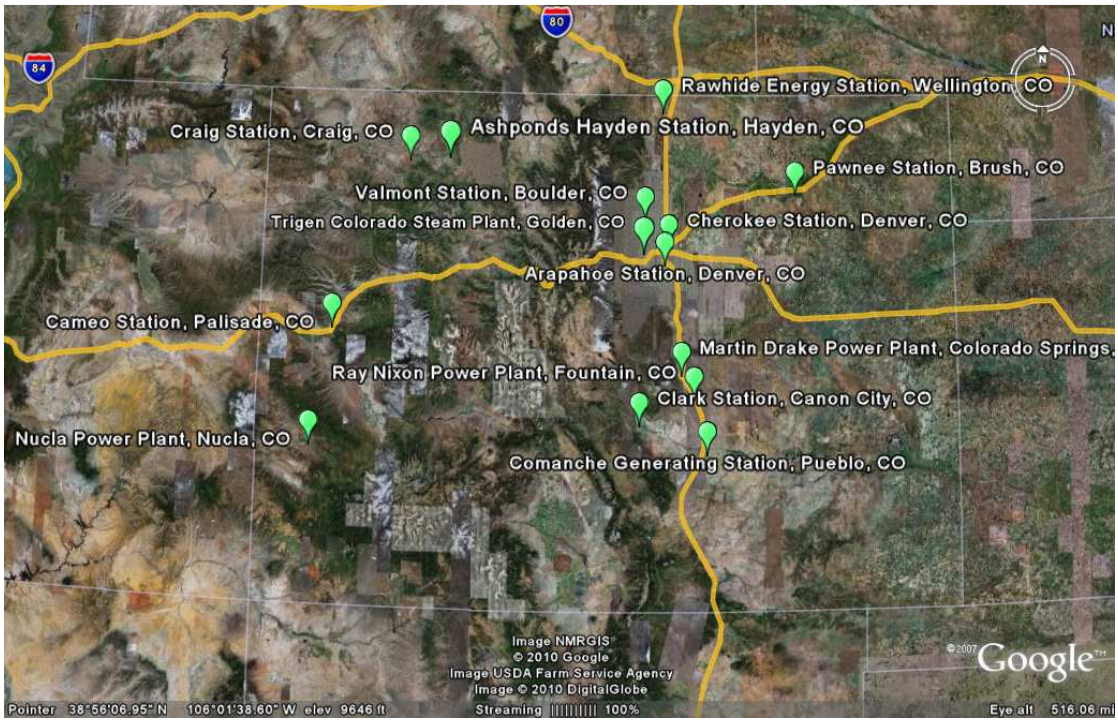

Figure 4.4 Coal combustion power plants in Colorado (created using information provided by sourcewatch.org)

The chemical composition, loss on ignition and specific gravity of each fly ash tested is shown in Table 4.2. The Laramie River Station ash is a Class C fly ash. The Drake 5 fly ash is an off-specification due to its high LOI. The Rawhide fly ash is an off-specification

ash based on its high sulfur trioxide (SO_3) content and relatively low amount of pozzolanic materials (<50%). For this study, the 20% 6.7-mm ESR mixture (Dunham-Friel 2009) was blended with the Laramie River Station fly ash, with the Rawhide Energy Station fly ash, or with a mixture of 40% Drake 5 and 60% Laramie River Station ashes. Hereafter, the Laramie River Station fly ash, the Rawhide Energy Station fly ash and the Drake 5-Laramie River fly ash blend will be referred to as L, R and DL-fly ashes, respectively. Particle size distributions of the fly ashes tested are shown in Figure 4.3.

Table 4.2 Chemical composition and ASTM classification of the fly ashes tested.

Chemical Constituent	**ASTM C 618 Requirements**	**Laramie River Ash (L)**	**Rawhide Ash (R)**	**Drake 5 Ash**	**40% Drake 5 / 60% Laramie River Blend (DL)**
Silicon Dioxide (SiO_2), %		33.7	26.6	35.1	34.3
Aluminum Oxide (Al_2O_3), %		18.6	12.8	17.5	18.1
Iron Oxide (Fe_2O_3), %		5.7	5.4	3.4	4.8
Sum of SiO_2, Al_2O_3, Fe_2O_3, %	50.0 Min.	58.0	44.8	56.0	57.2
Calcium Oxide (CaO), %		27.9	29.7	12.3	21.7
Magnesium Oxide (MgO), %		6.1	5.5	3.2	4.9
Sulfur Trioxide (SO_3), %	5.0 Max.	1.8	12.4	1.4	1.7
Sodium Oxide (Na_2O), %		2.0	1.6	1.2	1.7
Potassium Oxide (K_2O), %		0.4	0.4	0.6	0.5
Loss on Ignition, %	6.0 Max.	0.2	2.5	22.8	9.3
Specific Gravity		2.60	2.41	1.76	2.18
ASTM Classification	Class C	Class C	Off-Spec	Off-Spec	Off-Spec

4.2. Scanning Electron Microscope

A scanning electron microscope (SEM) was used to observe the micro-fabric (approximately 10 to 50 μm) and mini-fabric (approximately 100 to 500 μm) of the L, R and D-fly ashes (the blended DL was not observed in the SEM). The SEM used was a JSM-6500F Field Emission Scanning Electron Microscope (FESEM), managed by the Department of Chemistry in the Central Instruments Facility at CSU in Fort Collins, Colorado. The SEM provides a relatively large depth of field (magnification to less than

10 Å) but requires oven-dry specimens, an evacuated chamber, and specimen coating (for maximum viewing detail).

For this study, the fly ash samples were oven dried at approximately 110 ˚C for 24 h. Then, the fly ashes were placed on the SEM specimens and the surface of the fly ashes was coated ("painted") with gold. Following coating, the specimens were placed on the specimen holder and loaded into the SEM chamber and the chamber was evacuated to less than $2x10^{-7}$ kPa. Photographs were captured for each of the fly ashes at x250, x500 and x2000 magnifications.

4.2.1. Laramie River Fly Ash

The SEM photographs of the L-fly ash are shown below in Figure 4.5. Photograph (a), (b) and (c) were obtained at magnification levels of x250, x500 and x2000, respectively. Observation of the L-fly ash particles indicates the particles are amorphous, spherically shaped, with a glassy appearance. The particles appear to range from a maximum particle size of approximately 20 μm.

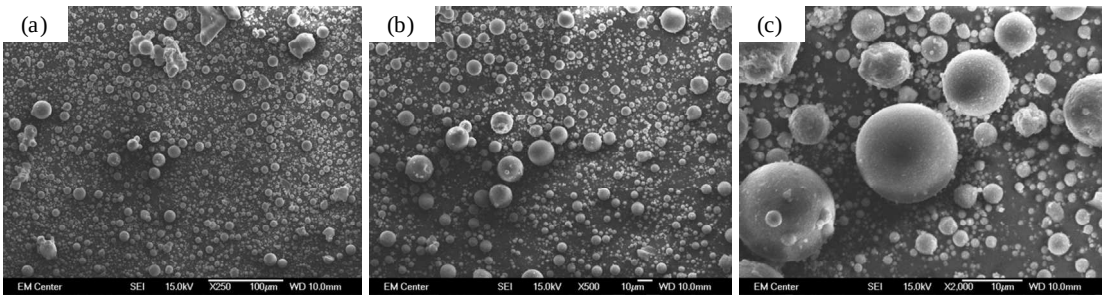

Figure 4.5 SEM photographs of L-fly ash: (a) x250, (b) x500, (c) x2000

4.2.2. Rawhide Fly Ash

SEM photographs of the R-fly ash are shown below in Figure 4.6. Photographs (d), (e) and (f) were obtained at the same magnification levels as the L-fly ash, respectively. Observation of the R-fly ash particles indicate the particle size and shape is similar to that the L-fly ash; however, the R-fly ash particles appear more rough with a less glassy appearance. The particles appear to be bonded with another material.

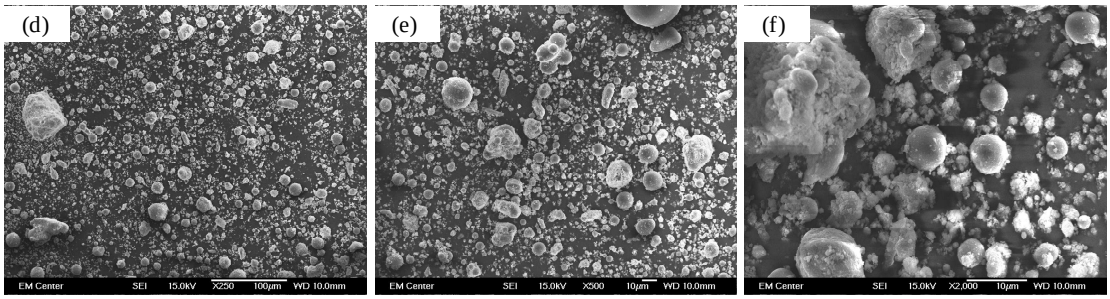

Figure 4.6 SEM photographs of R-fly ash: (a) x250, (b) x500, (c) x2000

4.2.3. Drake Fly Ash

Photographs (g), (h) and (i) of the D-fly ash are shown below in Figure 4.7. The D-fly ash has a significantly different appearance than the L or R-fly ashes. The D-fly ash particles appear rough and more frictional. The particles also appear relatively porous. Particles sizes vary with a maximum particle size of approximately 100 μm.

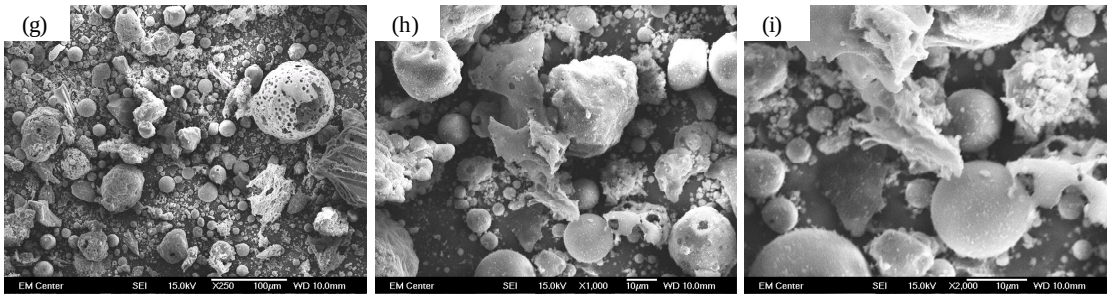

Figure 4.7 SEM photographs of D-fly ash: (a) x250, (b) x500, (c) x2000

4.3. Mixture Design

The amount of fly ash required to develop pozzolanic reactions with the soil was estimated by the lime fixation point method (Hilt & Davidson 1960). The lime fixation point method was used in this study to systematically estimate the *FAC* to be added to the ESR mixture. R, L and DL-fly ashes contain approximately 25 to 35% of (MgO + CaO), as shown in Table 4.2. The amount of lime for fixation depends on the chemical interactions that occur between the soil and the lime. When Ca^{2+} and/or Mg^{2+} are introduced to soil, the soil initially undergoes a preferential sequence of cation exchange in the form of heavier multivalent cations displacing monovalent cations ($Mg^{2+} > Ca^{2+} > Na^{+} > K^{+}$) (Transportation Research Board 1987). The crowding of multivalent cations on the surface of the clay particles changes the particles' electrical charge so that the clay particles become attracted to one another. The electrical attraction causes the clay particles to flocculate and aggregate and also reduces soil plasticity (Hilt & Davidson, 1960).

Hilt & Davidson (1960) measured the unconfined compressive strength of specimens containing various amounts of lime. The specimens prepared in their study were 2 inches in diameter and 2 inches tall. The specimens were molded with standard Proctor effort at a water contents that maximized the unconfined compressive strength after 7 days of curing at approximately 70 ˚F. Specimens containing 0, 1, 2, 3, 4, 5, 6, 8 and 12% lime by dry weight of soil were subjected to unconfined compression (without saturating) after 7 or 28 days of curing. Their results show that the unconfined compressive strength of

clay remains relatively constant when addition of lime causes increases in the soil-lime plastic limit. When the plastic limit remains constant with further lime addition, the unconfined compressive strength of the soil-lime mixtures tended to increase. Therefore, Hilt & Davidson (1960) suggested that the plastic limit would be indicative of the quantity of lime required to "fix" the soil (satisfy the initial cation exchange and allow further development of pozzolanic reactions). In this study, it was hypothesized that the ESR-fly ash mixtures would develop similar plasticity change characteristics as a result of additions of lime to the ESR mixtures.

Laboratory testing was conducted to determine the plasticity characteristics of the soil-fly ash blends by determining the liquid limit (w_L) the plastic limit (w_P) and the plasticity index (I_P) in accordance with ASTM D 4318. Laboratory soil-fly ash blends were prepared as follows.

After dry preparation of the soil (ASTM 4318), de-ionized water was added to the samples to obtain a water content that was visually estimated to be slightly below the w_L. The soil samples were then sealed in glass containers and allowed to soak for at least 16 h. After soaking, a predetermined mass of fly ash was added to the samples. Prior to further laboratory testing, the soil-fly ash mixtures were allowed to age, at approximately 21 ˚C, for up to 24 h for mixtures containing L-fly ash or up to 7 days for mixtures with R-fly ash. In each of the Atterberg limit tests performed at this stage, the liquid limit was performed first, followed by the plastic limit test. The *FAC* is defined as:

$$FAC\,(\%) = \frac{M_{\,fly\,ash}}{M_{\,soil} + M_{\,fly\,ash}} \times 100\% \qquad \text{(Equation 10)}$$

where M_{soil} and $M_{fly\ ash}$ are the dry mass of soil and fly ash, respectively.

4.4. Compaction

Water content versus dry unit weight relationships were established for the 20% 6.7-mm ESR (Dunham-Friel 2009) and its mixtures with fly ashes of a constant *FAC* equal to 14%. This selected *FAC* will be discussed in the chapter when the lime fixation point results are presented. The *RC* may be redefined as follows for the ESR-fly ash mixtures:

$$RC\,(\%) = \frac{M_{\,rubber}}{M_{\,rubber} + M_{\,soil} + M_{\,fly\,ash}} \times 100\% \qquad \text{(Equation 11)}$$

where M_{rubber} is the dry mass of the rubber.

Representative samples of the expansive soil and rubber were obtained and processed through a No. 4 sieve according to ASTM D 698 and ASTM D 1557. A predetermined mass of dry soil finer than the No. 4 sieve was combined with granulated rubber and de-ionized water and allowed to soak for a period of at least 16 h. After this initial period, fly ash was added and blended to the mixture. The mixture was then sealed and aged for 2 h at about 21 ˚C. After aging, standard Proctor (ASTM D 698) and modified Proctor (ASTM D 1557) tests were performed.

4.5. Unconfined Compression

Unconfined compression (ASTM Specification D 2166) testing of ESR and ESR-fly ash mixtures was performed as part of the experimental program. It should be pointed out

here that the only purpose of these unconfined compression tests was to confirm that the *FAC* selected was sufficient to promote pozzolanic reactions within the ESR mixtures stabilized with fly ash. The development of pozzolanic reactions in the ESR-fly ash mixtures was assessed by comparison of the peak axial stress measured in unconfined compression for all of the ESR and ESR-fly ash mixtures tested. Unconfined compression testing results were neither used nor intended to assess the shear strength parameters (i.e. ϕ_c or s_u) of the materials tested. This is because the unconfined compression specimens were not saturated prior to shearing and both the initial soil suction in the specimens and the pore pressures during unconfined compression were not measured. Without an accurate measurement of the initial stress state of the specimens (induced by soil suction), it would be conceptually wrong to expect unconfined compression test results can correlate to the actual shear strength parameters of the materials tested. Any discussion on the actual shear strength parameters of the materials tested in this study is carried out at a later section based on the results of triaxial tests performed on fully-saturated specimens subjected to well known states of stress and density. Unconfined compression testing was completed on ESR, ESR-R, ESR-L and ESR-DL mixtures (same mixtures used in the standard and modified compaction tests). All mixtures consisted of expansive soil with a *RC* of 20% and a *FAC* of 14%.

Mixtures of ESR and ESR-fly ash were prepared as outlined previously for the compaction tests. Like the compaction testing, mixtures containing fly ash were aged for 2 h prior to compaction. Specimens were compacted for unconfined compression testing in accordance with AASHTO T 307. Specimen compaction was carried out by statically

compacting a series of five lifts, each scarified prior to addition of the next lift, in a rigid split mold. The split mold was lubricated with either high vacuum grease or petroleum grease applied to the interior of the mold to minimize side friction during specimen extrusion. The energy required to extrude specimens was lowest when the high vacuum grease was used. Specimens were compacted to a target soil state corresponding to approximately 95% of the standard Proctor maximum dry density and optimum water content determined for each of the mixtures tested.

ESR specimens were subjected to further laboratory testing immediately after compaction. Specimens containing fly ash were allowed to cure inside the split compaction mold for 7 or 14 days at approximately 22±1.5 ˚C. During curing, the mold was kept inside three impermeable flexible polyethylene plastic bags to minimize water content changes. Water content changes (Δw) during curing were lower than ±0.07% using this method.

After curing, specimens containing fly ash were removed from the split compaction mold by initially applying an axial load on one end of the specimen to overcome any bonding that may have developed between the specimen and the mold. Once the specimen was relatively free within the mold, the split mold lateral restraints were removed. Then the specimen was removed from the split mold by sliding the opposing halves of the split mold in opposite directions (removing the specimen in this fashion minimized sample disturbance and lateral strains). Finally, unconfined compression testing was carried out

using a constant rate of strain of 1%/min. A description of the equipment used during compression testing is shown in Table 4.3.

Table 4.3 Details of equipment used to carry out unconfined compression testing.

Equipment	Manufacturer	Range	Accuracy	Resolution
Compression Machine	Geotest Instrument Corp., Evanston IL	--	--	--
Data Acquisition	Trautwein Soil Testing Equip. Co., Houston, TX	--	--	--
Displacement Transducer	Novotechnik, Southborough, MA	0 - 152 mm	0.27	.0025 mm
Force Transducer	Artech Industries Inc., Riverside, CA	0 - 8900 N	0.14	0.5 N

4.6. Undrained Triaxial Testing

Triaxial compression testing was performed on ESR and ESR-fly ash specimens prepared at a single target relative compaction (C_R) of 95% of standard Proctor maximum dry density and at optimum water content. ESR-fly ash specimens were stabilized with R, L and DL-fly ashes (same as those used in unconfined compression testing) prepared and cured for 7 or 14 days. Triaxial testing was performed to evaluate the effect of fly ash type, curing time and mean effective stress (p') on the triaxial response of saturated ESR-fly ash specimens so that it could be compared to the responses of the expansive soil and ESR mixtures (Dunham-Friel 2009). The mechanical response of the ESR-fly ash specimens was investigated through isotropic swell, isotropic consolidation and undrained triaxial compression. Undrained triaxial compression was completed at mean effective stress levels of 50, 100 and 200 kPa. Through the measurements of displacement during shearing using external transducers, the large-strain stiffness was determined. Very small-strain stiffness was evaluated using bender elements.

4.6.1. Triaxial Equipment

Triaxial compression was accomplished using an automated (GEOJAC) triaxial load frame and (GEOTAC) data acquisition and software manufactured by Trautwein Soil Testing Equipment Co. (Houston, Texas). An S-type load cell, mounted on the GEOJAC piston, was used for measurement of force. Pressure measurements were obtained with two individual pressure transducers (one installed on the cell pressure line and another one on the back/pore pressure line). Vertical displacements of the triaxial specimen during shearing were obtained using an external LPT. The triaxial chamber used in this study consisted of a top and base, separated by a transparent reinforced plexi-glass chamber. The 70-mm diameter triaxial specimen top and base used were also made of plexi-glass fitted with two drain lines each. Filter paper and rigid filter stones were used at the top and base of each specimen. Detailed information of the equipment used to carry out triaxial testing is summarized in Table 4.4.

Table 4.4 Details of equipment used to carry out triaxial testing.

Equipment	Manufacturer	Range/Dim.	Accuracy (%)	Resolution
Panel Board	Trautwein Soil Testing Equip. Co., Houston, TX	--	--	--
Pipettes Volumes	Trautwein Soil Testing Equip. Co., Houston, TX	--	--	0.25 mL
Data Acquisition	Trautwein Soil Testing Equip. Co., Houston, TX	--	--	--
Cell Pressure Transducer*	ELE International, Ltd., USA	0 - 1000 kPa	0.23	0.07 kPa
Pore Pressure Transducer*	ELE International, Ltd., USA	0 - 1000 kPa	0.12	0.04 kPa
Displacement Transducer	Novotechnik, Southborough, MA	0 - 254 mm	0.09	0.0025 mm
Force Transducer*	Artech Industries Inc., Riverside, CA	0 - 8900 N	0.84	0.45 N
Triaxial Cell	Trautwein Soil Testing Equip. Co., Houston, TX	D=127 mm H=273 mm	--	--
Qualitative Filter Paper	Ahlstrom Mt. Holly Springs, PA	D=70 mm	--	--
Filter Stones	--	D=70 mm t=6.35 mm	--	--
Rubber Membranes	Humboldt Manufacturing Co. Schiller Park, IL	D=70 mm t=0.30 mm	--	--

* Indicates accuracy and precision from Dunham-Friel 2009

4.6.2. Triaxial Specimen Preparation

Specimens for triaxial testing were prepared/cured using the same protocol/curing time as outlined for the specimens prepared for unconfined compression (Section 4.5). Once the triaxial specimen was extracted from the split mold, its initial mass, height and diameter were measured to determine state properties of the specimen "as compacted." The specimen was placed on the triaxial platens inside the rubber membrane in accordance with ASTM D 4767. The triaxial cell was then filled with de-aired, de-ionized water and an initial cell pressure, σ_r, of 30 kPa was applied. Changes in the piston location and cell and back pressure volumes were recorded before and after each stage throughout the test to determine changes in the state properties of the specimen. During triaxial testing, a

stringent timeline was adhered to for each stage of testing to minimize the differences between specimens that could potentially be developed due to pozzolanic reaction development with time. The time schedule for each stage of triaxial testing are outlined below in Table 4.5. Further testing protocols are discussed individually in the following sections.

Table 4.5 Duration of triaxial compression testing.

Stage of Testing	Duration
Curing in Mold	7 d or 14 d
Flushing	2 d
Back Pressure Saturating	2 d
Consolidating	1 d
Shearing	1 d
Total Approximate Duration	13 d or 20 d

4.6.3. Isotropic Swell

After an initial σ_r of 30 kPa was applied, the specimen was flushed with de-aired, de-ionized water from bottom to top. Volumetric changes and height changes during flushing were monitored with final measurements recorded prior to back pressure saturation and after the specimen was consolidated to 30 kPa. Volumetric changes during the flushing and back pressure saturation periods were used to determine the amount isotropic swell experienced by the specimens.

4.6.4. Back Pressure Saturation

Back pressure saturation of specimens was completed based on the protocol outlined by ASTM D 4767. Back pressure saturation of specimens was completed, such that no radial or back pressure stress increment exceeded 50 kPa, the minimum mean effective stress level used in the study. The level of saturation was indirectly evaluated by

measuring the Skempton's pore pressure parameter *B* (Skempton 1954) as shown in Equation 12. All specimens were deemed saturated when a $B \geq 0.99$ was achieved:

$$B = \frac{\Delta u}{\Delta \sigma_r} \qquad \text{(Equation 12)}$$

where Δu is the change in pore pressure and $\Delta \sigma_r$ is the change in radial stress.

4.6.5. Isotropic Consolidation

Prior to undrained triaxial compression, specimens were isotropically consolidated to mean effective stress levels of 30, 50, 100 and 200 kPa. Specimens subjected to $p' = 100$ and 200 kPa were consolidated in steps (e.g. 50 kPa to 100 kPa to 200 kPa). During each consolidation step, the data acquisition system was utilized to monitor changes of the excess pore water pressure (Δu) with time. During each consolidation step, the percent of excess pore water pressure dissipated was plotted versus time as defined by Equation 13:

$$U_z(\%) = 100 \times (1 - \frac{u_e}{u_o}) \qquad \text{(Equation 13)}$$

where u_e is the excess pore water pressure at any time *t* and u_o is the excess pore pressure at $t = 0$.

The time to dissipate 50% (t_{50}) and 100% (t_{100}) of the excess pore water pressure was used to determine the strain rate to be used during undrained shearing (Head 1986). A strain rate of 1.25% per hour, which was conservatively determined for a specimen stabilized with L-fly ash (Class C) cured for 14 days, was used for all specimens.

The t_{50} obtained at each consolidation step was also used to estimate the hydraulic conductivity, *k*, as a function of mean effective stress. Hydraulic conductivity was estimated using the procedure outlined by Head (1985) which is summarized as follows.

The boundary conditions included a single-drained specimen with vertical drainage only. The coefficient of consolidation, c_{vi}, and coefficient of volume compressibility, m_{vi}, both determined for isotropic conditions by Equations 14 and 15, respectively:

$$c_{vi} = \frac{T_v H^2}{t_{50}} \qquad \text{(Equation 14)}$$

$$m_{vi} = \frac{\Delta e}{\Delta p'} \times \frac{1000}{1 + e_1} \qquad \text{(Equation 15)}$$

where T_v is the coefficient of pore water pressure dissipation, H is the mean height of the specimen before and after consolidation, e_1 is the void ratio at the beginning of the consolidation stage, and Δe and $\Delta p'$ are the changes in void ratio and mean effective stress during consolidation, respectively. The approximate relationship between isotropic consolidation and one-dimensional consolidation (K_o) are given by Equations 16, 17 and 18:

$$c_v = c_{vi} f_{cv} \qquad \text{(Equation 16)}$$

$$f_{cv} = \frac{1}{1 - B(1 - A)(1 - K_o)} \qquad \text{(Equation 17)}$$

$$m_v = \frac{2}{3} m_{vi} \qquad \text{(Equation 18)}$$

where c_v is the K_o the coefficient of consolidation, m_v is the K_o coefficient of volume change, and A and B are Skempton's pore pressure parameters (Skempton 1954). The

pore pressure parameter *A* was obtained at the maximum strain carried out during testing. The pore pressure parameter *B* was determined after back pressure saturation or prior to consolidation and was always equal to or greater than 0.99 for all specimens.

K_o was not determined experimentally but rather estimated using the following relationships outlined below. K_o could be estimated by Equation 19 (Jaky 1944) for normally consolidated soils and then by Equation 20 for overconsolidated soils:

$$K_{o(normally\ consolidated)} = 1 - \sin\phi \qquad \text{(Equation 19)}$$

$$K_{o(overconsolidated)} = K_{o(normally\ consolidated)}\sqrt{OCR} \qquad \text{(Equation 20)}$$

where *OCR* is the overconsolidation ratio. Given a friction angle of the ESR equal to 31° (Dunham-Friel 2009) Equations 19 and 20 indicate K_o should be above 0.5. Therefore, K_o equal to 0.7 was used as suggested for remolded clay, Head (1986). The hydraulic conductivity, *k*, was estimated using Equation 21.

$$k = c_v m_v \qquad \text{(Equation 21)}$$

The consolidation response can also be characterized by changes in the specific volume (*v*) as a function of mean effective stress changes. However, in order to determine *v*, it is necessary to determine the specific gravity of each specimen. Since the specific gravity could be affected by the development of pozzolanic reactions occurring during the triaxial testing, the specific gravity was determined (ASTM D 854) on specimens prepared as outlined in Section 4.5, with the exception that the specimens were oven dried to constant mass at approximately 60 ˚C prior to specific gravity testing. Results of the specific gravity testing are shown below in Table 4.6.

Table 4.6 Specific gravity of ESR-fly ash mixtures cured for 7 and 14 days.

Material	Specific Gravity, G_s		
	Curing Time (day)		Average
	0	14	
ESR-R	2.154	2.127	2.140
ESR-L	2.135	2.113	2.124
ESR-DL	2.118	2.110	2.114

Results of the specific gravity testing indicated a slight reduction for specimens tested at 14 days. This reduction, which may be due to the development of pozzolanic reactions, may lower the water absorption capacity of the specimens, and, as a result, lower their specific gravity. The specific gravity was used for specific volume calculations. The specific gravity determined at 14 days was used for specimens cured for 14 days. The average specific gravity was used for specimens cured for 7 days.

Before and after each isotropic consolidation stage, the triaxial apparatus piston, cell and drainage volume burettes were measured. Measurements obtained were used to estimate the soil state at each level of consolidation and update the specific volume of the specimens at any stage of the test.

4.6.6. Undrained Compression

During compression, all pore water lines were closed to effectively impose undrained conditions to the specimens. During compression, pore water pressure measurements were obtained using the GEOTAC data acquisition system. The specimens were sheared to the maximum piston displacement possible to be mobilized with the system, which corresponds to approximately 27 to 28% axial strains. The specimens were removed from the triaxial apparatus for water content and dry mass determination.

4.6.1. Large-Strain Stiffness Testing

The soil stiffness at large strains was measured during the triaxial tests while the specimens were subjected to undrained compression. In the present study, stiffness is represented as the shear modulus, *G*, through Equation 7, where the Young's modulus of elasticity was taken as the as the secant modulus of elasticity, E_s. Since the soil stiffness is non-linear and decays with strain (Atkinson 2000), the stiffness was determined as a function of strain, which was represented as shear strains through Equation 8.

Axial strains (ε_a) during undrained compression were measured using an external displacement transducer. The deviatoric stress (q) was measured using an external force transducer mounted on the triaxial piston. Measurements of ε_a and q were collected using the GEOTAC data acquisition system.

4.6.1. Small-Strain Stiffness Testing

Shear wave velocity (V_s) was measured experimentally in this study using bender elements (Shirley & Hampton 1977). The bender elements were manufactured by GDS Instruments Limited (Hook, Hampshire, United Kingdom) was used to evaluate the V_s of triaxial specimens under mean effective stress levels equal to 30, 50, 100 and 200 kPa. As previously indicated, V_s depends on the time required for the shear wave to propagate through the specimen. The travel time of the shear wave may be determined as the difference between the time when the input wave is applied and the arrival time associated with the first major reversal of the received signal (Viggiani & Atkinson 1995,

Jovicic et al. 1996). The distance of propagation of the shear wave was taken as the distance between the tips of the bender elements (Viggiani & Atkinson 1995). Both square and sinusoidal input shear waves were used with 14-V input signal amplitude and periods of 0.3 to 0.5 mV. Acquisition of the received wave was obtained using a sampling frequency of 2,000 kamp/s and a sampling interval of 1 ms which were empirically selected to provide a received signal with optimal resolution.

The V_s of the ESR and ESR-fly ash specimens were obtained during triaxial testing after the specimens were saturated and isotropically consolidated to a target mean effective stress level. After V_s was measured, the very small-strain stiffness was determined according to Equation 9.

CHAPTER 5: RESULTS

5.1. Mixture Design

The variation of the liquid and plastic limits of mixtures of the expansive soil with the R-fly ash aged for 1 h as a function of the *FAC* in the mixture is presented in Figure 5.1. A second horizontal axis is also shown in Figure 5.1 to illustrate the same response as a function of the actual (CaO+MgO) content in the mixture. The actual (CaO+MgO) content of the mixture was determined by amount of (CaO) and (MgO) determined for the fly ash as shown in Table 4.2, by Equation 22.

$$(CaO+MgO)(\%)_{content\ in\ mixture} = FAC(\%) \times \frac{(CaO+MgO)(\%)_{content\ in\ fly\ ash}}{100\%} \quad \text{(Equation 22)}$$

Figure 5.2 shows the variation of liquid limit and plastic limit as a function of aging time for specimens of expansive soil and 10.7% R-fly ash.

Finally Figure 5.3 shows the variation of the liquid and plastic limits of mixtures of the expansive soil with the L-fly ash aged for 1 h and 24 h as a function of the *FAC* in the mixture. A second horizontal axis is also shown in Figure 5.3 to illustrate the same variation as a function of the actual (CaO+MgO) content in the mixture.

Testing the liquid limit and plastic limits was carried out to determine the minimum *FAC* required to develop pozzolanic bonds within the ESR mixtures. The mix design methodology is outlined in detail in Section 4.3.

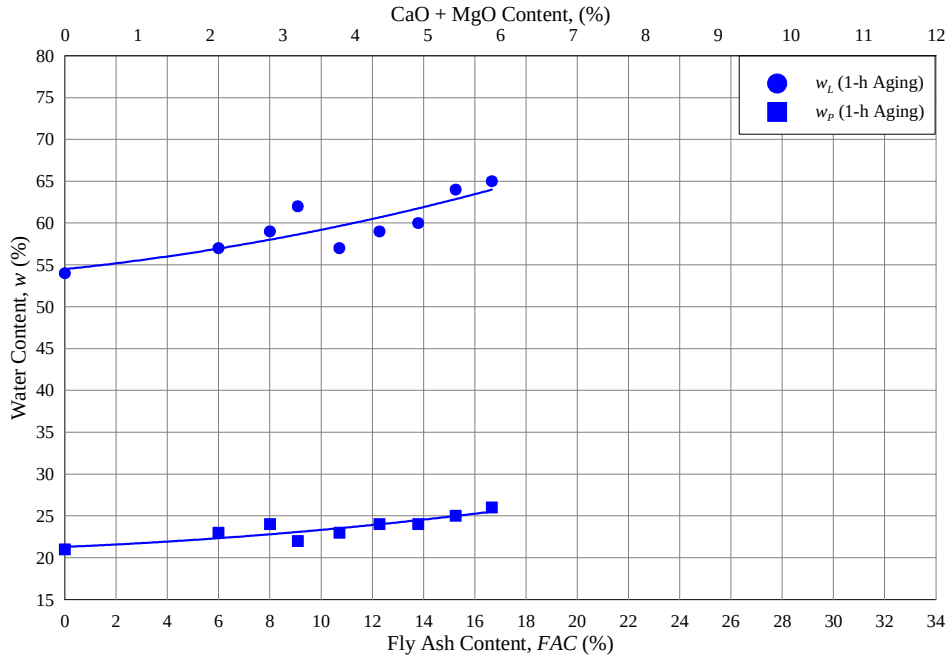

Figure 5.1 Variation of the liquid and plastic limits of expansive soil and R-fly ash mixtures aged for 1 h as a function of the *FAC* and (CaO+MgO) content of the mixture.

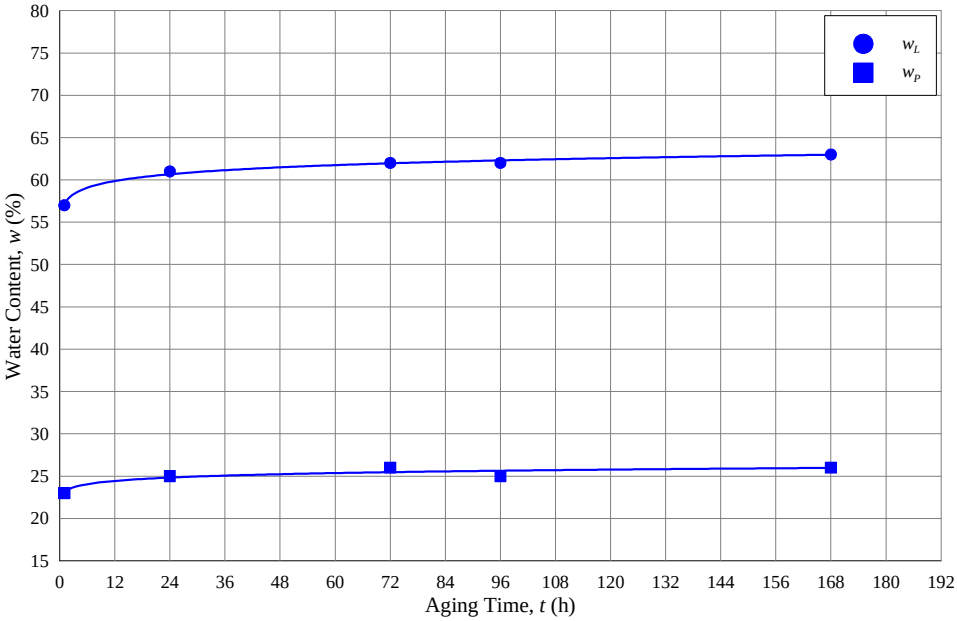

Figure 5.2 Variation of the liquid and plastic limits of expansive soil and 10.7% R-fly ash aged for various times.

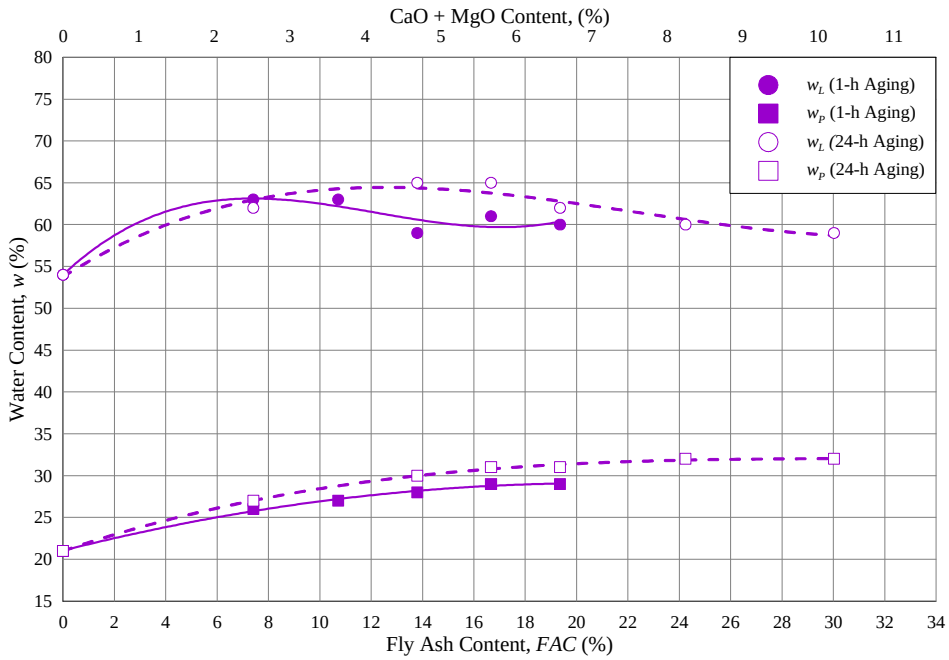

Figure 5.3 Variation of the liquid and plastic limits of expansive soil and L-fly ash mixtures aged for 1 h and 24 h as a function of the *FAC* and (CaO+MgO) content.

5.2. Compaction

Standard and modified compaction tests (ASTM D 698 and ASTM D 1557) were performed on ESR-R, ESR-L and ESR-DL mixtures to determine the maximum dry unit weight and optimum water content for each mixture. The results of the compaction tests carried out using the standard effort were used in subsequent laboratory testing to determine the relative compaction (C_R) of the specimens tested. The standard and modified Proctor results are summarized in Table 5.1. Standard Proctor test results are shown in Figure 5.4. Modified Proctor test results are shown in Figure 5.5. Figure 5.4 and Figure 5.5 also show expansive soil alone and the 20% 6.7-mm ESR mixture determined by Dunham-Friel (2009).

Table 5.1 Compaction parameters for expansive soil, ESR and ESR-fly ash mixtures.

Material	Standard Proctor (ASTM D 698)		Modified Proctor (ASTM D 1557)	
	Maximum Dry Unit Weight, γ_d	Optimum Water Content, w_{opt}	Maximum Dry Unit Weight, γ_d	Optimum Water Content, w_{opt}
	(kN/m^3)	(%)	(kN/m^3)	(%)
Expansive Soil	15.7	23.0	17.9	14.9
ESR	13.8	21.6	14.7	18.5
ESR-R	13.7	20.9	14.8	16.8
ESR-L	13.5	21.5	14.7	16.9
ESR-DL	13.4	22.0	14.5	16.5

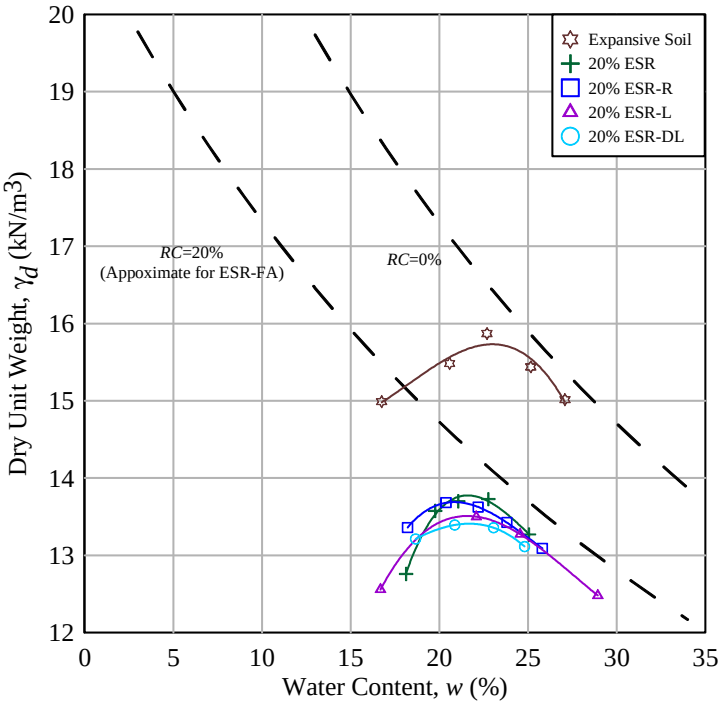

Figure 5.4 Water content versus dry unit weight relationships determined using the Standard compaction effort (ASTM D 698) for the materials tested.

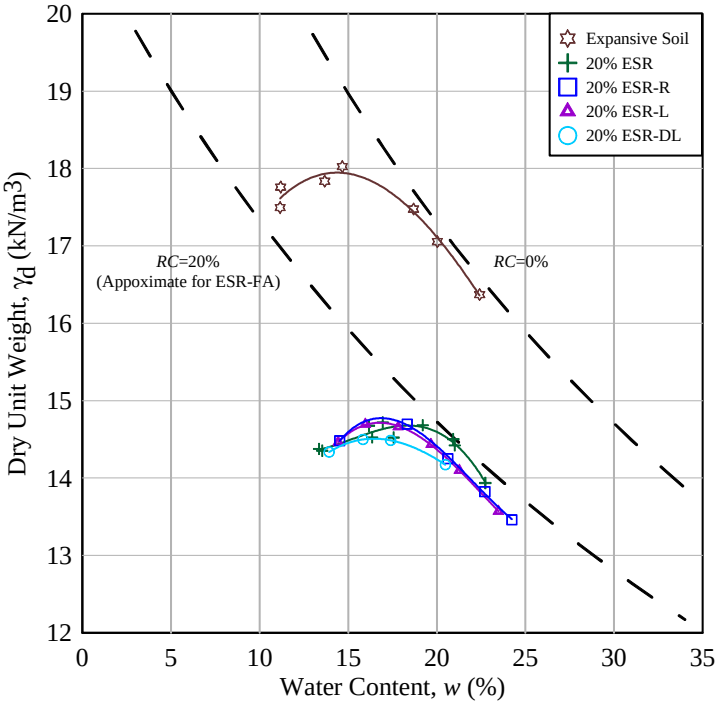

Figure 5.5 Water content versus dry unit weight relationships determined using the Modified compaction effort (ASTM D 1557) for the materials tested.

5.3. Unconfined Compression

5.3.1. Effect of Fly Ash

Specimens of ESR, ESR-R, ESR-L and ESR-DL were compacted (according to the protocol outlined in Section 4.5). Specimens containing fly ash were cured in compaction molds for a period of 7 or 14 days. After curing and extruding from the compaction mold, the specimen height, diameter and wet mass was measured. The specimen dry mass was determined immediately after the unconfined compression test was completed. The measured specimen height, diameter, wet mass and dry mass were used to determine the state of the specimens prior to unconfined compression. The state parameters of all specimens, as well as their peak axial stress, peak axial strain, and coefficient of variances are summarized in Table 5.2. Results of specimens cured for 7 and 14 days are shown in Figure 5.6 and Figure 5.7, respectively.

Table 5.2 Summary of unconfined compression tests for ESR specimens and ESR-fly ash specimens cured for 7 and 14 days.

Material	Curing Time (day)	Dry Unit Weight, γ_d (kN/m^3)	Water Content, w (%)	Relative Compaction, C_R (%)	Deviation from Standard Proctor Optimum Water Content, w-w_{opt} (%)	Peak Axial Stress, σ_{ap} (kPa)	Peak Axial Strain, ε_{ap} (%)	Average Peak Axial Stress (kPa)	Average Peak Axial Strain (%)	Coefficient of Variation (Peak Axial Stress) (%)	Coefficient of Variation (Peak Axial Strain) (%)
ESR		13.0	21.4	94.1	-0.1	73	8.2	70.2	8.1	7.5	2.1
ESR		13.0	21.2	94.6	-0.3	76	7.8				
ESR		13.1	21.5	94.7	0.0	72	8.2				
ESR		13.1	22.0	94.8	0.5	64	8.1				
ESR		13.1	22.0	95.2	0.5	63	7.9				
ESR		13.2	22.3	95.7	0.8	74	8.2				
ESR-R	7	13.0	20.5	94.5	-0.4	134	10.4	134.0	9.6	3.2	7.8
ESR-R	7	13.0	21.2	94.9	0.3	130	9.3				
ESR-R	7	13.1	21.3	95.3	0.4	138	9.0				
ESR-R	14	13.1	20.7	95.9	-0.2	167	7.5	175.2	7.1	4.6	5.5
ESR-R	14	13.2	20.8	96.1	-0.1	183	6.7				
ESR-R	14	13.2	20.9	96.3	0.0	175	7.2				
ESR-L	7	12.9	21.5	95.6	0.0	128	9.3	134.3	8.9	6.1	4.7
ESR-L	7	12.9	21.7	95.8	0.2	132	8.4				
ESR-L	7	13.0	21.6	95.9	0.1	143	9.0				
ESR-L	14	12.9	21.1	95.8	-0.4	158	8.5	166.4	8.2	4.3	4.3
ESR-L	14	13.0	21.2	95.9	-0.3	172	8.2				
ESR-L	14	12.9	21.4	96.1	-0.1	169	7.8				
ESR-DL	7	12.8	21.5	95.4	-0.5	146	9.5	157.4	8.5	6.6	10.1
ESR-DL	7	12.8	21.6	95.5	-0.4	166	7.9				
ESR-DL	7	12.9	21.8	96.1	-0.2	160	8.1				
ESR-DL	14	12.9	21.4	96.3	-0.6	171	8.0	166.6	8.1	7.7	1.5
ESR-DL	14	12.9	21.4	95.9	-0.6	177	8.0				
ESR-DL	14	12.9	21.0	96.0	-1.0	152	8.2				

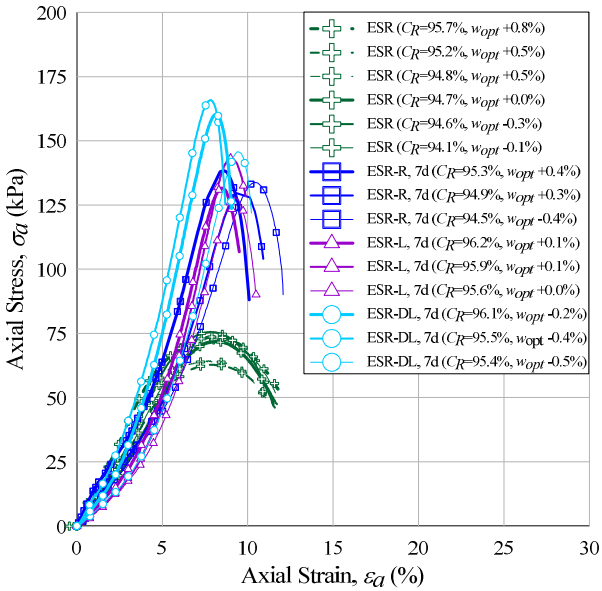

Figure 5.6 Unconfined compression of ESR and ESR-fly ash specimens cured for 7 days.

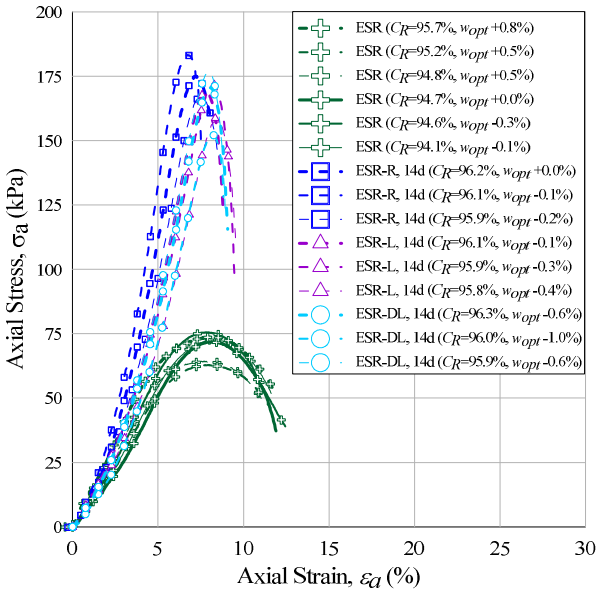

Figure 5.7 Unconfined compression of ESR and ESR-fly ash specimens cured for 14 days.

5.3.2. Effect of Curing Time

To determine the effect of curing time on development pozzolanic reactions, ESR-R, ESR-L and ESR-DL specimens were subjected to unconfined compression testing at 7 and 14 days. Results of the ESR-R, ESR-L and ESR-DL are shown below in Figure 5.8, Figure 5.9, and Figure 5.10, respectively. The variation of the peak unconfined axial stress versus curing time is shown in Figure 5.11. An average linear trend line for each mixture was used to illustrate the effect of curing time. State properties are summarized in Table 5.2.

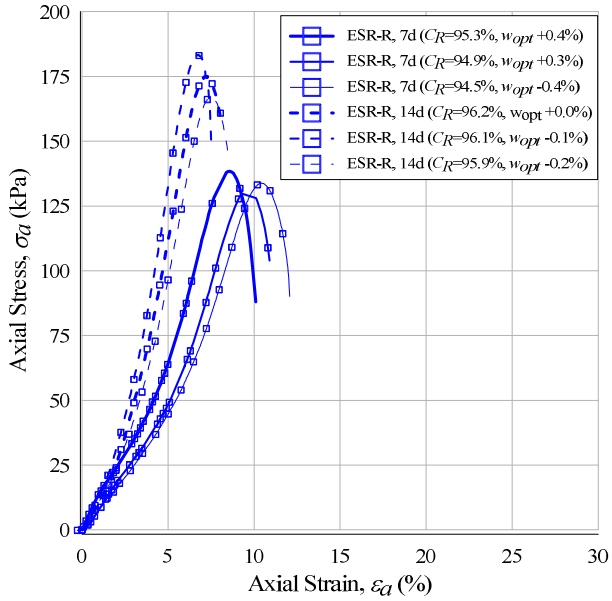

Figure 5.8 Unconfined compression of ESR-R specimens cured for 7 and 14 days.

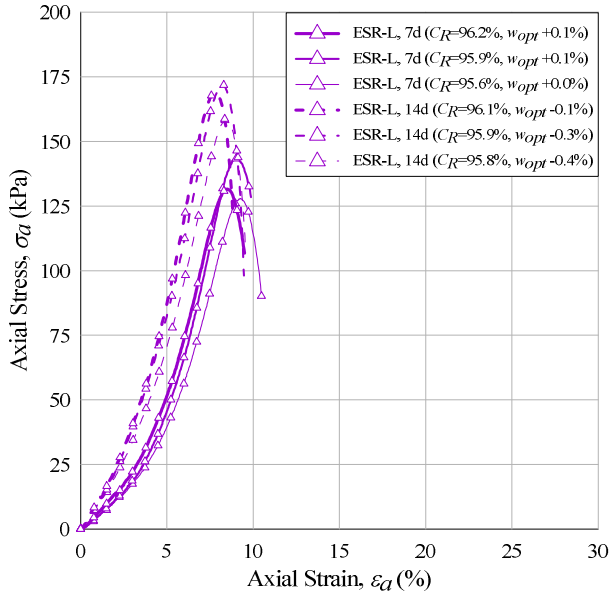

Figure 5.9 Unconfined compression of ESR-L specimens cured for 7 and 14 days.

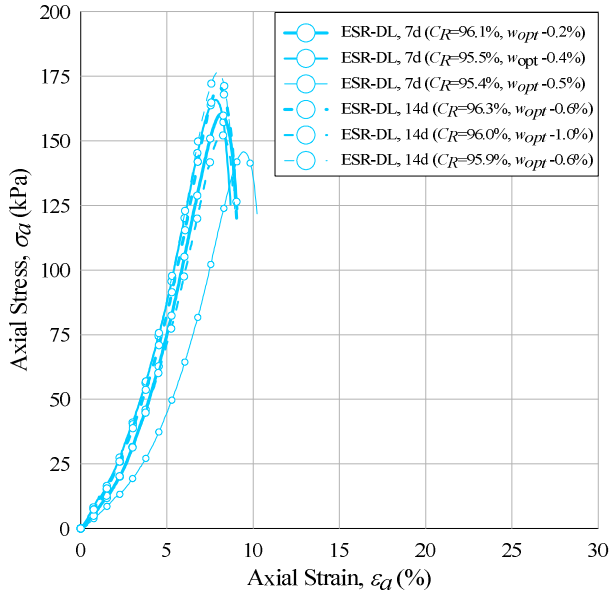

Figure 5.10 Unconfined compression of ESR-DL specimens cured for 7 and 14 days.

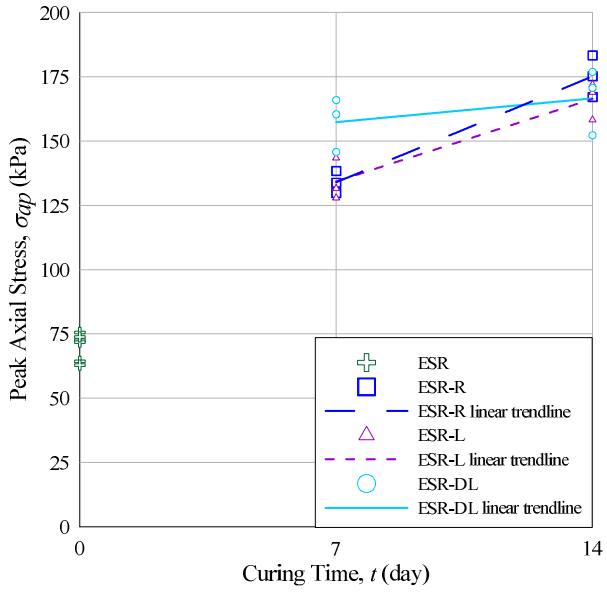

Figure 5.11 Variation of peak unconfined axial stress of ESR and ESR-fly ash specimens with curing time.

5.4. Triaxial Specimens

Specimens of ESR-R, ESR-L and ESR-DL were prepared in accordance with the procedures outlined in Section 4.6.2 and cured for a period of 7 or 14 days. Following the curing period, the specimens were removed from the compaction mold and immediately their wet mass was measured. Before the membrane was placed over the specimens, at least six measurements of the specimen height and diameter were obtained at random locations to develop an average height and diameter. The specimen's wet mass, average height and diameter were used to determine the specimen's initial wet unit weight. The initial dry unit weight was determined based on the water content, obtained from the measurement of the dry mass of the specimen after completion of the test. Table 5.3 summarizes the initial state parameters of the triaxial specimens.

Table 5.3 Initial soil state and isotropic swell parameters of triaxial specimens.

Material	Curing Time (day)	Mean Effective Stress, p' (kPa)	Dry Unit Weight,[1] γ_d (kN/m^3)	Water Content,[1] w (%)	Relative Compaction,[1] C_R (%)	Deviation from Standard Proctor Optimum Water Content, w-w_{opt} (%)	Swell (%)
ESR-R	7	50	13.1	21.3	95.8	0.4	-0.8
ESR-R	7	100	13.1	20.8	95.7	-0.1	-2.6
ESR-R	7	200	13.2	21.1	96.7	0.2	-1.7
ESR-R	14	50	13.2	20.8	96.5	-0.1	-1.7
ESR-R	14	100	13.1	21.3	95.7	0.4	-0.7
ESR-R	14	200	13.2	21.2	96.2	0.3	-0.5
ESR-L	7	50	12.9	21.9	95.5	0.4	0.0
ESR-L	7	50	13.0	21.7	96.2	0.2	-0.3
ESR-L	7	100	12.9	21.6	95.4	0.1	-2.7
ESR-L	7	200	12.9	21.5	95.1	0.0	-3.8
ESR-L	14	50	12.9	21.4	95.6	-0.1	-0.2
ESR-L	14	100	12.9	21.7	95.8	0.2	-0.7
ESR-L	14	200	12.9	21.5	95.7	0.0	-0.6
ESR-L	14	200	13.0	21.5	96.0	0.0	-3.0
ESR-DL	7	50	12.9	21.7	96.3	-0.3	0.0
ESR-DL	7	100	12.8	21.6	95.6	-0.4	-0.5
ESR-DL	7	200	12.8	21.4	95.1	-0.6	-1.1
ESR-DL	14	50	12.9	21.4	96.3	-0.6	-0.1
ESR-DL	14	100	12.9	21.3	96.0	-0.7	-0.3
ESR-DL	14	200	12.9	21.7	96.3	-0.3	-0.4

[1]Determined immediately after curing and removal of specimens from compaction mold.

5.5. Isotropic Swell

Each specimen subjected to triaxial testing was monitored for isotropic swell during the initial flushing period. The swell measured at the end of the isotropic swell testing stage is summarized in Table 5.3.

5.6. Isotropic Consolidation

5.6.1. Effect of Fly Ash

Following back pressure saturation ($B \geq 0.99$), the triaxial specimens were isotropically consolidated to levels of mean effective stress equal to 50, 100 or 200 kPa. Volume change measurements during each of the consolidation stages were used to determine the

specific volume of the specimens at various consolidation stages. The variation of specific volume as a function of the mean effective stress along with other isotropic consolidation parameters are summarized in Table 5.4 for expansive soil and ESR specimens (Dunham-Friel 2009) and in Table 5.5 for ESR-fly ash specimens cured for 7 and 14 days. The variation of specific volume as a function of mean effective stress is shown in Figure 5.12 and Figure 5.13. In Figure 5.12 and Figure 5.13, an average trendline was used for each material to determine the consolidation parameters listed below in Table 5.5.

The isotropic coefficient of consolidation and coefficient of compression were determined during each isotropic consolidation stage from measurements of the pore water pressure dissipation with time. Coefficients of consolidation and compression are summarized in Table 5.6 for isotropic conditions and in Table 5.7 for K_o conditions which were derived as outlined as indicated in Section 4.6.5.

Table 5.4 Specific volume and isotropic consolidation parameters of expansive soil and ESR specimens (Dunham-Friel 2009).

Material	Curing Time (day)	Mean Effective Stress, p' (kPa)	Relative Compaction,[1] C_R (%)				Specific Volume,[2] v				N	λ
			30 kPa	50 kPa	100 kPa	200 kPa	30 kPa	50 kPa	100 kPa	200 kPa		
Exp Soil		50	97.9	98.2				1.73			2.230	0.127
Exp Soil		100	102.2		103.3				1.65			
Exp Soil		200	99.7			109.5				1.55		
ESR		50	102.8	104.7				1.45			1.878	0.107
ESR		100	97.9		109.0				1.40			
ESR		200	103.9			116.5				1.31		

[1]Determined at the end of each consolidation stage as shown in the table.

Table 5.5 Specific volume and consolidation parameters of ESR-fly ash specimens cured for 7 and 14 days.

Material	Curing Time (day)	Mean Effective Stress, p' (kPa)	Relative Compaction,[1] C_R (%)				Specific Volume,[1] v				V_k	K
			30 kPa	50 kPa	100 kPa	200 kPa	30 kPa	50 kPa	100 kPa	200 kPa		
ESR-R	7	50	101.0	101.7			1.52	1.51			1.654	0.043
ESR-R	7	100	102.2	102.8	104.7		1.50	1.49	1.46			
ESR-R	7	200	102.7	103.3	105.2	107.1	1.48	1.47	1.45	1.42		
ESR-R	14	50	100.7	101.5			1.51	1.50			1.658	0.038
ESR-R	14	100	99.3	100.0	101.6		1.55	1.54	1.51			
ESR-R	14	200	100.2	100.8	102.4	104.3	1.52	1.51	1.49	1.46		
ESR-L	7	50	103.4	104.3			1.49	1.48			1.668	0.049
ESR-L	7	50	101.6	102.6			1.52	1.50				
ESR-L	7	100	102.8	103.5	105.6		1.50	1.49	1.46			
ESR-L	7	200	104.5	105.5	107.8	110.3	1.48	1.46	1.43	1.40		
ESR-L	14	50	100.8	101.8			1.52	1.51			1.630	0.035
ESR-L	14	100	102.4	103.3	105.5		1.50	1.48	1.45			
ESR-L	14	200	101.0	102.0	103.8	105.7	1.52	1.50	1.48	1.45		
ESR-L	14	200	103.3	103.9	106.1	108.3	1.52	1.49	1.48	1.45		
ESR-DL	7	50	101.0	101.8			1.53	1.52			1.684	0.046
ESR-DL	7	100	100.6	101.4	103.3		1.53	1.52	1.49			
ESR-DL	7	200	102.2	103.2	105.4	107.8	1.51	1.50	1.46	1.43		
ESR-DL	14	50	100.8	101.7			1.53	1.51			1.656	0.037
ESR-DL	14	100	100.4	101.1	103.0		1.54	1.52	1.50			
ESR-DL	14	200	101.5	102.3	104.0	106.0	1.52	1.51	1.48	1.45		

[1]Determined at the end of each consolidation stage as shown in the table.

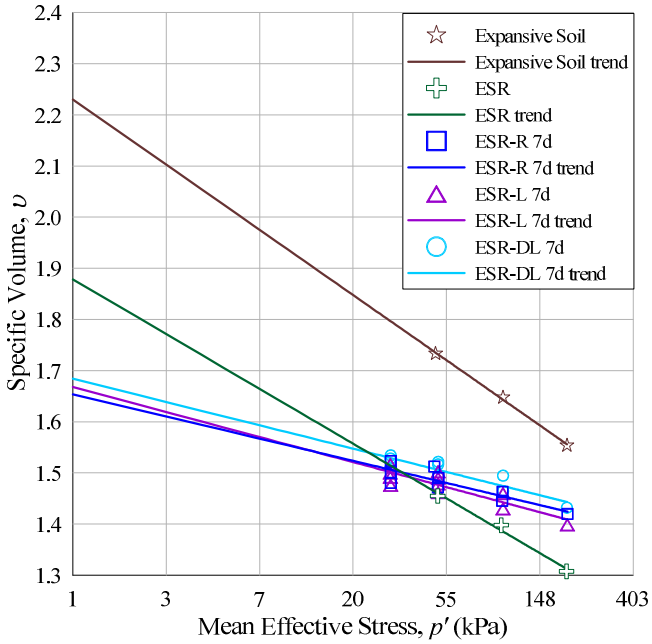

Figure 5.12 Isotropic consolidation response in specific volume versus mean effective stress (p'-v space) of expansive soil, ESR and ESR-fly ash specimens cured for 7 days.

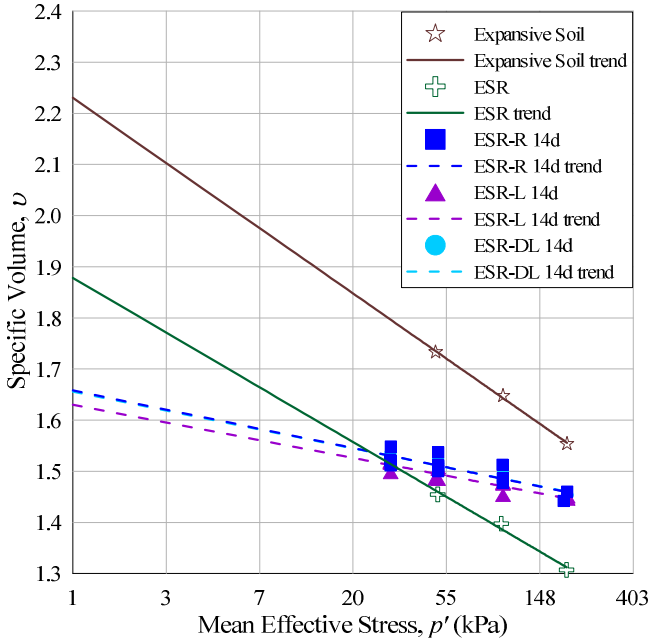

Figure 5.13 Isotropic consolidation response in specific volume versus mean effective stress (p'-v space) of expansive soil, ESR and ESR-fly ash specimens cured for 14 days.

Table 5.6 Isotropic consolidation parameters of ESR-fly ash specimens cured for 7 and 14 days.

Material	Curing Time (day)	Mean Effective Stress, p' (kPa)	Coefficient of Consolidation,[1] c_{vi} m^2/yr			Coefficient of Compression,[1] m_{vi} m^2/MN		
			30-50 kPa	50-100 kPa	100-200 kPa	30-50 kPa	50-100 kPa	100-200 kPa
ESR-R	7	50	22447			0.35		
ESR-R	7	100	33941	11142		0.33	0.36	
ESR-R	7	200	20199	7112	2598	0.31	0.35	0.18
ESR-R	14	50	25027			0.37		
ESR-R	14	100	28910	14246		0.37	0.31	
ESR-R	14	200	18522	8734	4575	0.32	0.32	0.18
ESR-L	7	50	14410			0.43		
ESR-L	7	50	21750			0.47		
ESR-L	7	100	26362	7760		0.33	0.40	
ESR-L	7	200	21640	5779	1766	0.48	0.44	0.22
ESR-L	14	50	25126			0.46		
ESR-L	14	100	26686	5046		0.45	0.42	
ESR-L	14	200	15558	6204	2581	0.47	0.36	0.18
ESR-L	14	200	15222	3882	1073	0.33	0.40	0.21
ESR-DL	7	50	16120			0.37		
ESR-DL	7	100	15750	5762		0.42	0.35	
ESR-DL	7	200	25490	9981	4039	0.47	0.42	0.22
ESR-DL	14	50	22309			0.42		
ESR-DL	14	100	25614	8736		0.37	0.37	
ESR-DL	14	200	16302	6157	3481	0.37	0.34	0.18

[1]Determined during consolidation between mean effective stress shown in table.

Table 5.7 Estimation of K_o consolidation parameters and hydraulic conductivity of ESR-fly ash specimens cured for 7 and 14 days.

Material	Curing Time (day)	Mean Effective Stress, p' (kPa)	Coefficient of Consolidation,[1] c_v m²/yr			Coefficient of Compression,[1] m_v m²/MN			Hydraulic Conductivity,[1] k m/s		
			30-50 kPa	50-100 kPa	100-200 kPa	30-50 kPa	50-100 kPa	100-200 kPa	30-50 kPa	50-100 kPa	100-200 kPa
ESR-R	7	50	33118			0.23			1.6E-06		
ESR-R	7	100	46625	15306		0.22	0.24		2.1E-06	7.6E-07	
ESR-R	7	200	26057	9175	3351	0.21	0.24	0.12	1.1E-06	4.5E-07	8.3E-08
ESR-R	14	50	37192			0.25			1.9E-06		
ESR-R	14	100	40331	19873		0.24	0.21		2.0E-06	8.6E-07	
ESR-R	14	200	24135	11380	5961	0.22	0.21	0.12	1.1E-06	5.0E-07	1.5E-07
ESR-L	7	50	22083			0.29			1.3E-06		
ESR-L	7	50	32978			0.31			2.1E-06		
ESR-L	7	100	38732	11401		0.22	0.27		1.8E-06	6.3E-07	
ESR-L	7	200	29587	7901	2414	0.32	0.29	0.15	2.0E-06	4.8E-07	7.3E-08
ESR-L	14	50	37796			0.31			2.4E-06		
ESR-L	14	100	39464	7462		0.30	0.28		2.4E-06	4.3E-07	
ESR-L	14	200	21473	8563	3562	0.31	0.24	0.18	1.4E-06	4.2E-07	8.9E-08
ESR-L	14	200	20951	3882	1073	0.22	0.27	0.14	9.6E-07	3.0E-07	4.2E-08
ESR-DL	7	50	24383			0.25			1.2E-06		
ESR-DL	7	100	23020	8421		0.28	0.24		1.3E-06	4.1E-07	
ESR-DL	7	200	35038	13720	5553	0.31	0.28	0.15	2.3E-06	7.9E-07	1.7E-07
ESR-DL	14	50	33900			0.28			1.9E-06		
ESR-DL	14	100	37774	12884		0.24	0.25		1.9E-06	6.6E-07	
ESR-DL	14	200	22868	8637	4883	0.25	0.23	0.12	1.2E-06	4.0E-07	1.2E-07

[1]Determined during consolidation between mean effective stress shown in table.

5.6.2. Effect of Curing Time

Similar to plots shown in Section 5.6.1, Figure 5.14 shows the consolidation response of ESR-R, ESR-L and ESR-DL specimens subjected to isotropic consolidation. Figure 5.14 is provided to illustrate the differences between curing specimens for 7 days and 14 days.

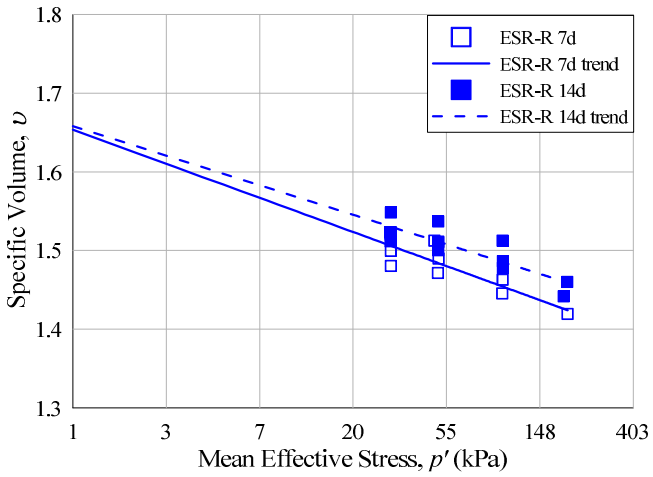

(a)

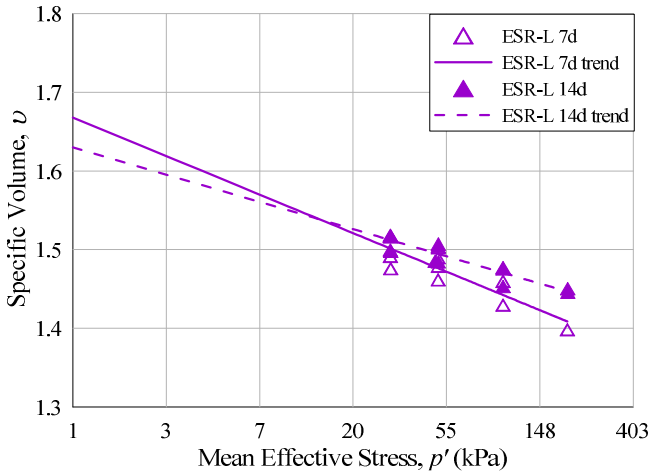

(b)

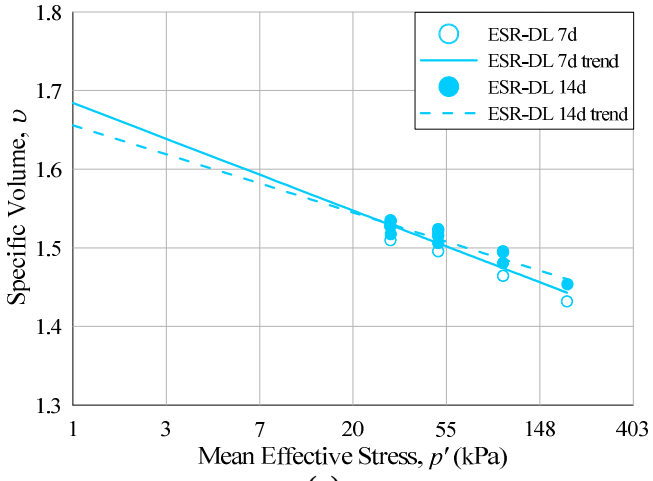

(c)

Figure 5.14 Isotropic consolidation response in specific volume versus mean effective stress (p'-v space) of: (a) ESR-R, (b) ESR-L, and (c) ESR-DL specimens cured for 7 and 14 days.

5.7. Triaxial Compression

5.7.1. Effect of Fly Ash

Specimens of ESR stabilized with fly ash were subjected to isotropic-consolidated undrained triaxial compression (CIU) testing to characterize the shear strength and stiffness characteristics of specimens cured for 7 and 14 days. Results of the triaxial compression tests, based on the critical state framework presented in Section 3.1 are summarized in Table 5.8. The variation of the deviatoric stress, excess pore water pressure and the Skempton's pore pressure parameter *A* with axial strain are shown in Figures 5.15 through 5.17 for specimens cured for 7 days for mean effective stresses equal to 50, 100 and 200 kPa, respectively. Likewise, Figures 5.18 through 5.20 show the results for specimens cured for 14 days. Stress paths are shown in Figures 5.21 through 5.23 for specimens cured for 7 days and in Figures 5.24 through 5.26 for specimens cured for 14 days. Figure 5.27 and Figure 5.28 show the CSL, in p'-q space and p'-v space, of expansive soil, ESR (Dunham-Friel 2009) and ESR-fly ash specimens cured for 7 and 14 days, respectively.

Table 5.8 Summary of CIU testing of ESR-fly ash specimens cured for 7 and 14 days.

Material	Curing Time (day)	Mean Effective Stress, p' (kPa)	Relative Compaction,[1] C_R (%)	Critical State Friction Angle,[2] ϕ_c (°)	Critical State Friction Constant,[3] M	Critical State Friction Angle,[3] ϕ_c (°)
Exp Soil		50	98.2	32.2	1.18	29.5
Exp Soil		100	103.3	32.3		
Exp Soil		200	109.5	28.5		
ESR		50	104.7	36.3	1.24	31.0
ESR		100	109.0	35.3		
ESR		200	116.5	29.6		
ESR-R	7	50	101.7	34.0	1.28	31.9
ESR-R	7	100	104.7	32.1		
ESR-R	7	200	107.1	31.1		
ESR-R	14	50	101.5	33.8	1.27	31.6
ESR-R	14	100	101.6	32.2		
ESR-R	14	200	104.3	30.5		
ESR-L	7	50	104.3	34.7	1.31	32.4
ESR-L	7	50	102.6	34.2		
ESR-L	7	100	105.6	32.5		
ESR-L	7	200	110.3	30.9		
ESR-L	14	50	101.8	35.1	1.28	31.9
ESR-L	14	100	105.5	32.4		
ESR-L	14	200	105.7	30.8		
ESR-L	14	200	108.3	31.6		
ESR-DL	7	50	101.8	34.1	1.30	32.3
ESR-DL	7	100	103.3	32.8		
ESR-DL	7	200	107.8	31.4		
ESR-DL	14	50	101.7	34.3	1.28	31.9
ESR-DL	14	100	103.0	32.2		
ESR-DL	14	200	106.0	31.0		

[1]Determined prior to shearing.

[2]Determined for single mean effective stress.

[3]Determined for multiple mean effective stresses.

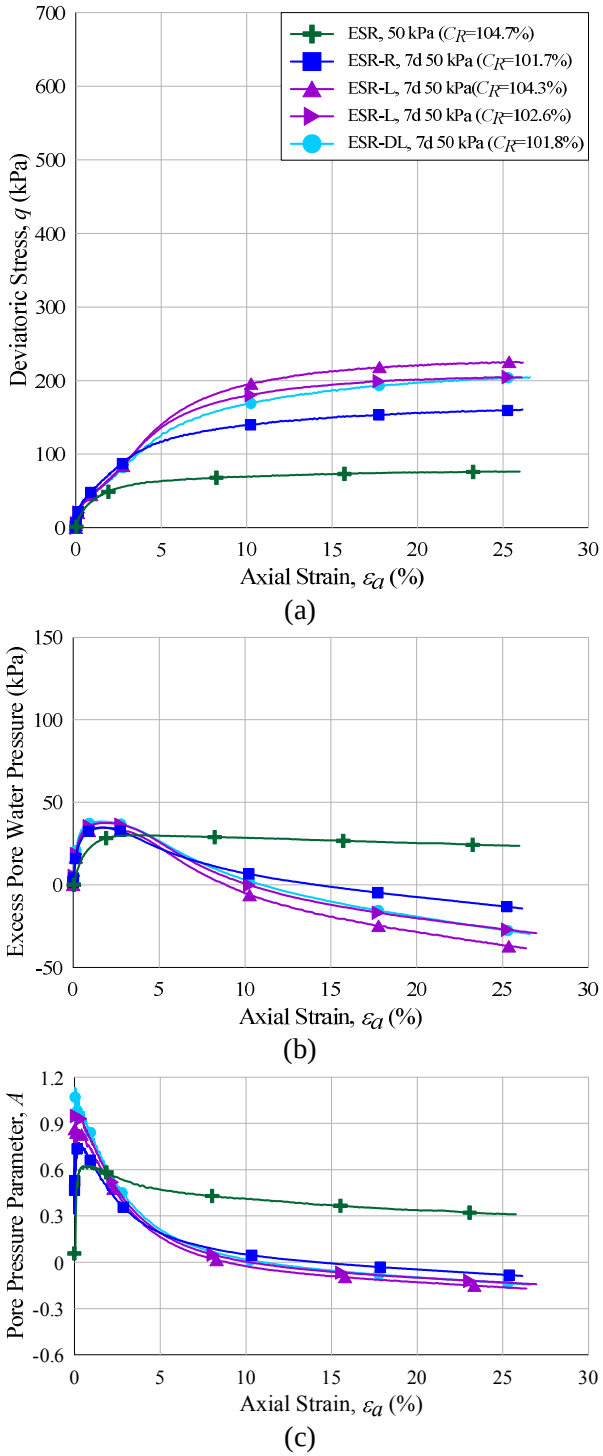

Figure 5.15 CIU response at a mean effective stress of 50 kPa of ESR (Dunham-Friel 2009) and ESR-fly ash specimens cured for 7 days: (a) deviatoric stress, (b) excess pore water pressure, and (c) pore water pressure parameter *A* versus axial strain.

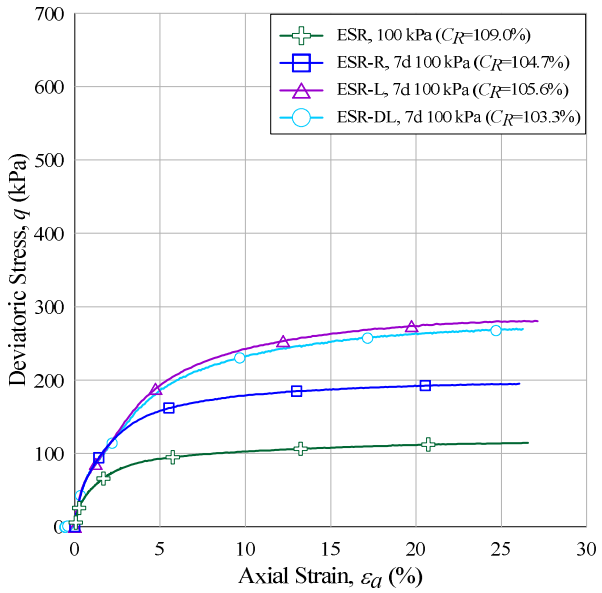

(a)

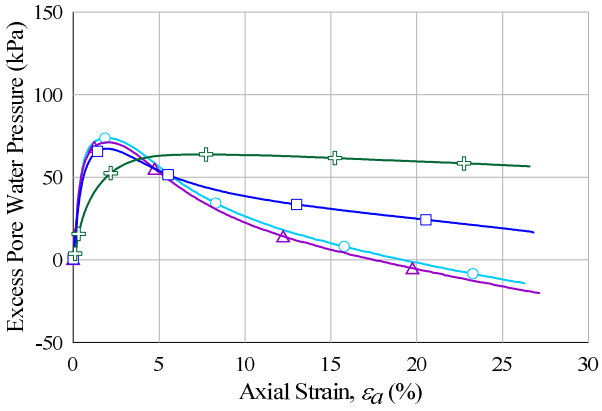

(b)

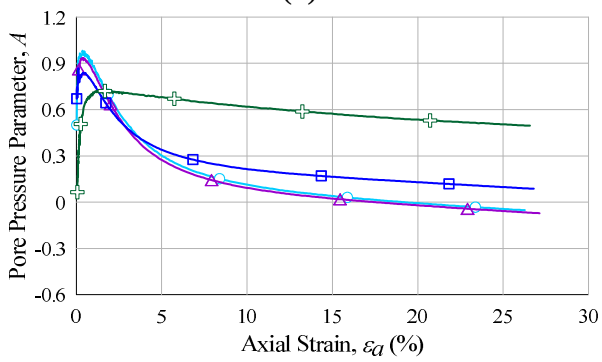

(c)

Figure 5.16 CIU response at a mean effective stress of 100 kPa of ESR (Dunham-Friel 2009) and ESR-fly ash specimens cured for 7 days: (a) deviatoric stress, (b) excess pore water pressure, and (c) pore water pressure parameter *A* versus axial strain.

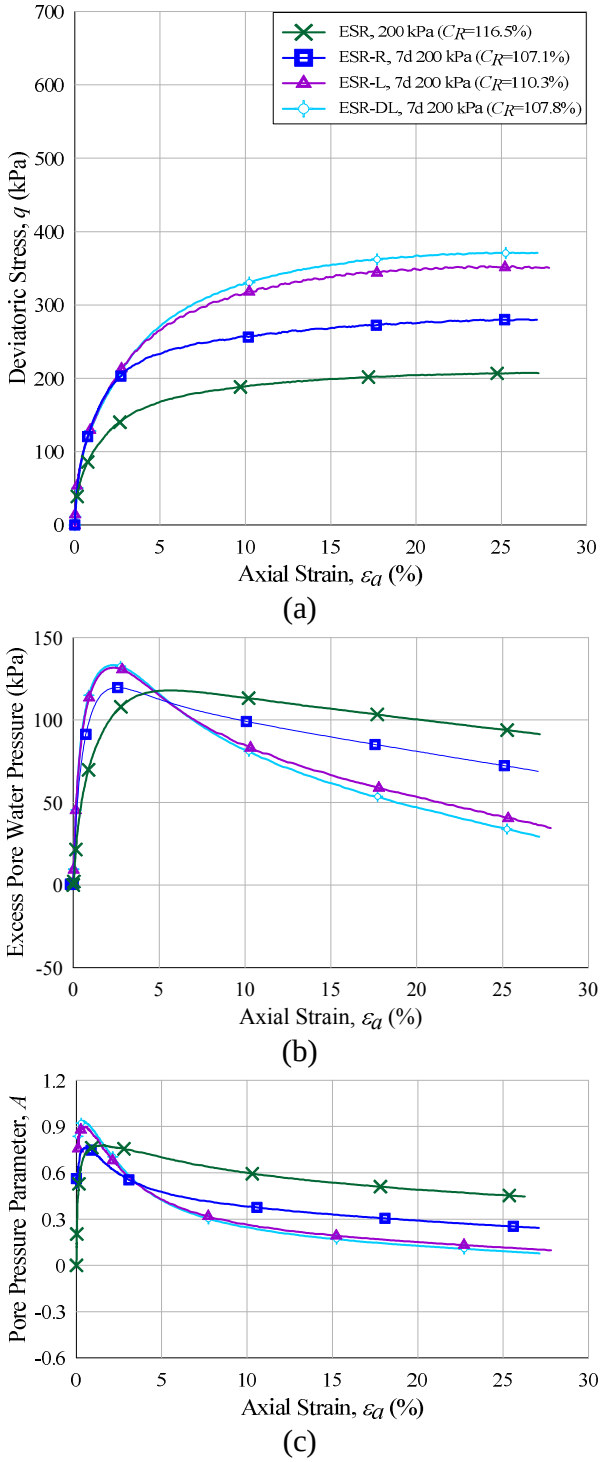

Figure 5.17 CIU response at a mean effective stress of 200 kPa of ESR (Dunham-Friel 2009) and ESR-fly ash specimens cured for 7 days: (a) deviatoric stress, (b) excess pore water pressure, and (c) pore water pressure parameter *A* versus axial strain.

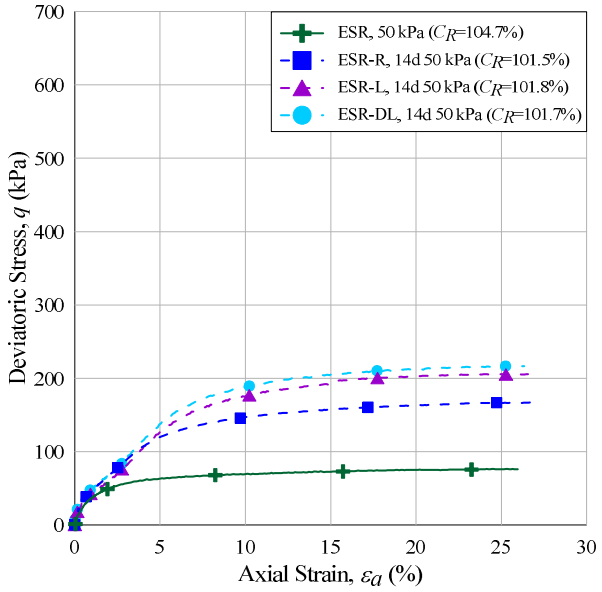

(a)

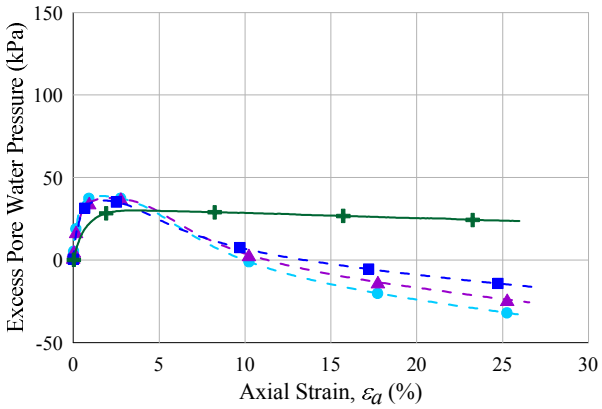

(b)

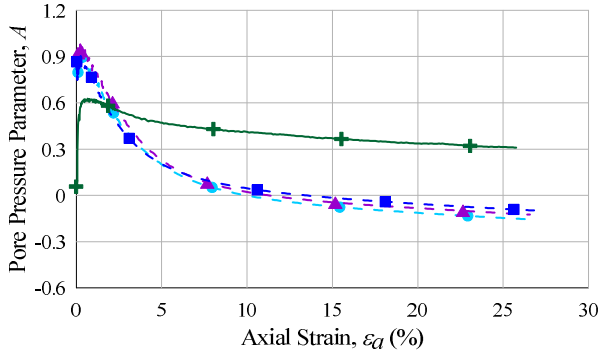

(c)

Figure 5.18 CIU response at a mean effective stress of 50 kPa of ESR (Dunham-Friel 2009) and ESR-fly ash specimens cured for 14 days: (a) deviatoric stress, (b) excess pore water pressure, and (c) pore water pressure parameter *A* versus axial strain.

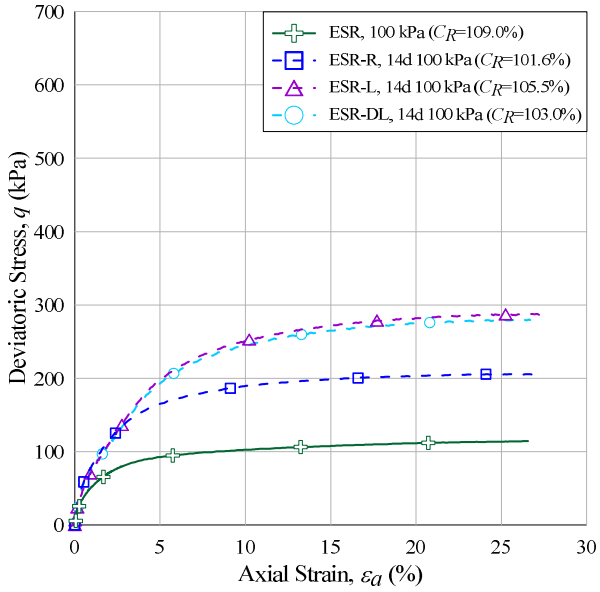

(a)

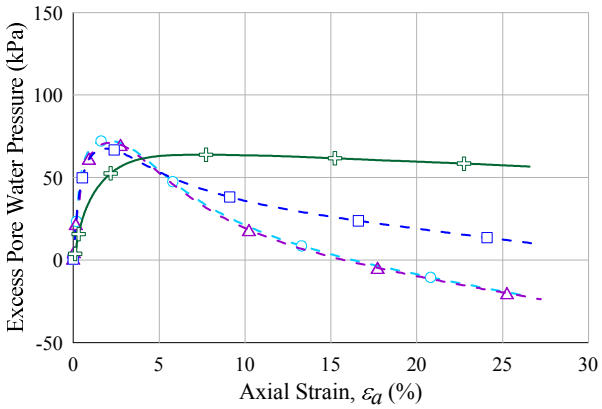

(b)

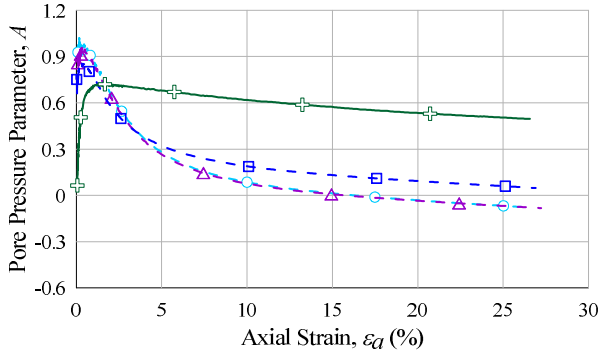

(c)

Figure 5.19 CIU response at a mean effective stress of 100 kPa of ESR (Dunham-Friel 2009) and ESR-fly ash specimens cured for 14 days: (a) deviatoric stress, (b) excess pore water pressure, and (c) pore water pressure parameter *A* versus axial strain.

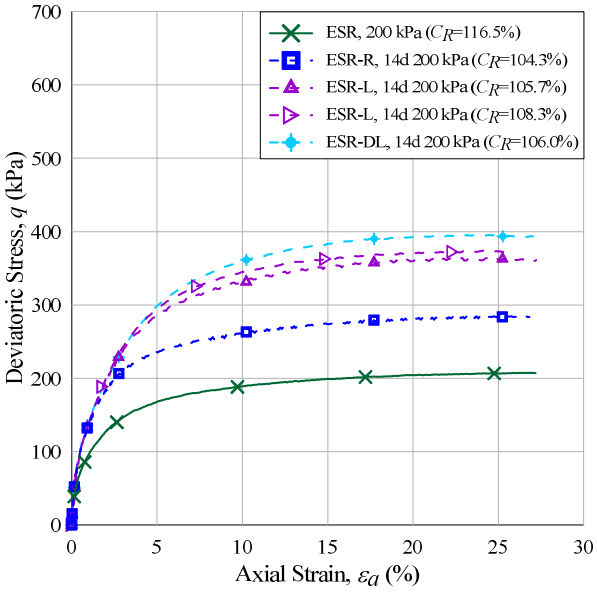

(a)

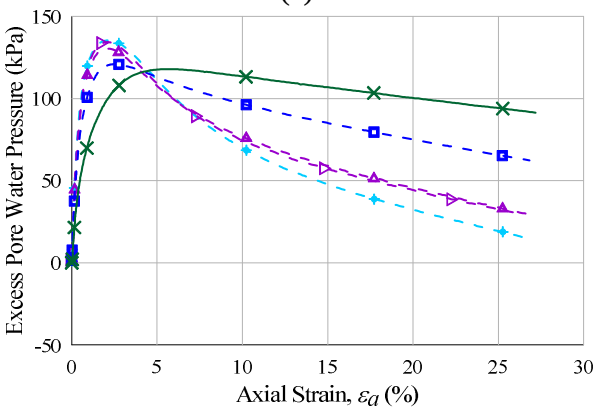

(b)

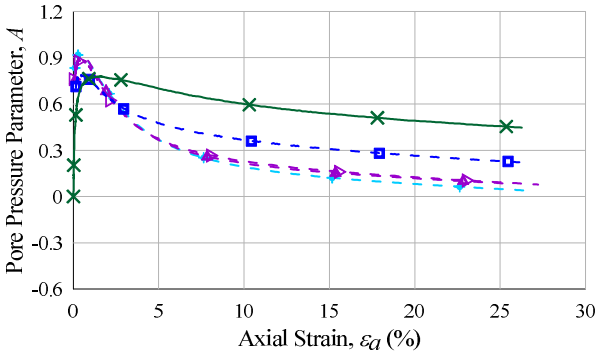

(c)

Figure 5.20 CIU response at a mean effective stress of 200 kPa of ESR (Dunham-Friel 2009) and ESR-fly ash specimens cured for 14 days: (a) deviatoric stress, (b) excess pore water pressure, and (c) pore water pressure parameter *A* versus axial strain.

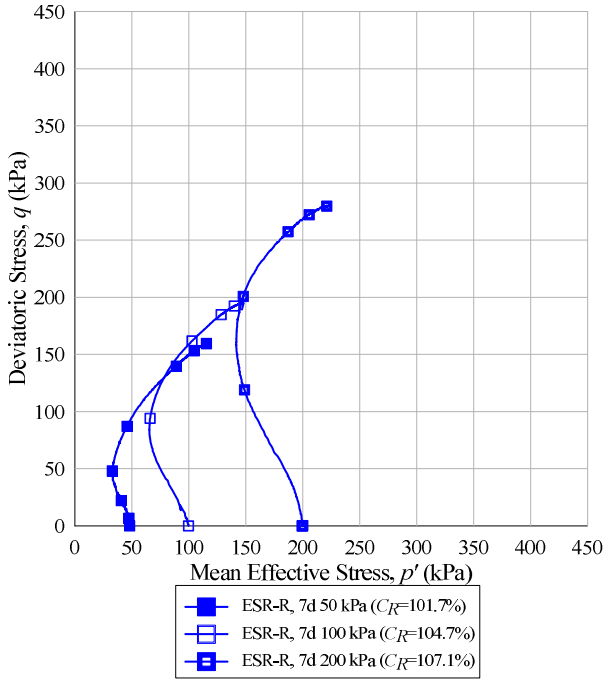

Figure 5.21 Stress path (p'-q space) of ESR-R specimens cured for 7 days.

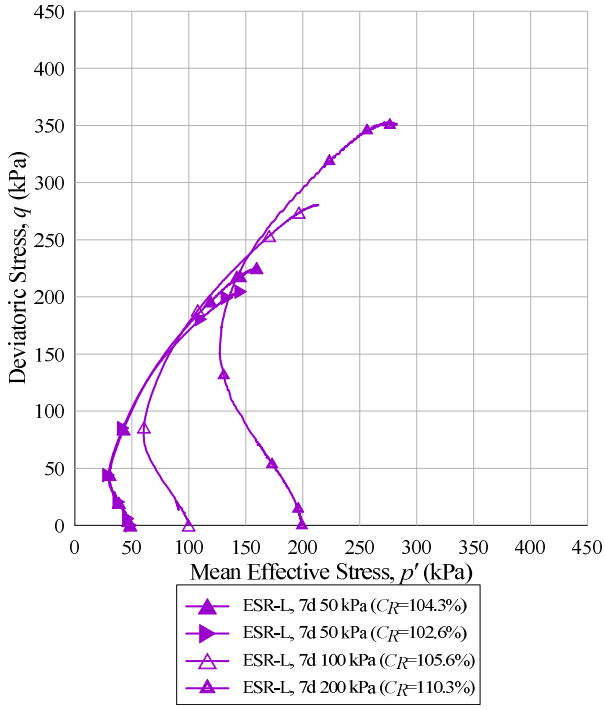

Figure 5.22 Stress path (p'-q space) of ESR-L specimens cured for 7 days.

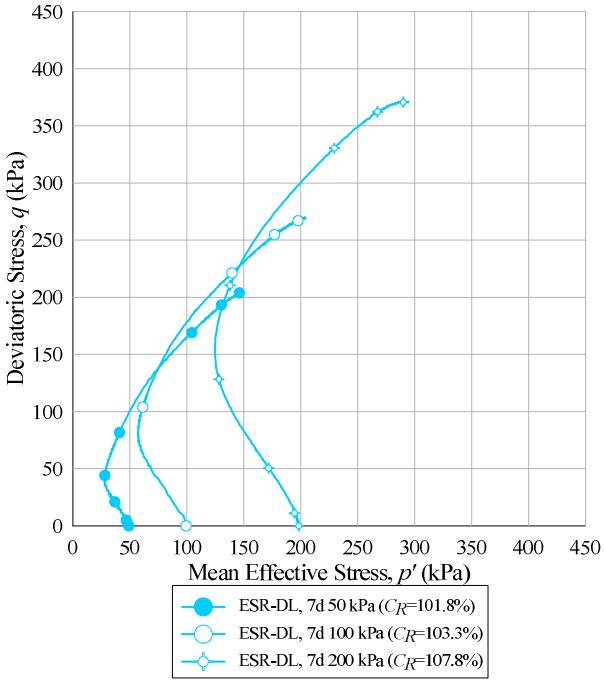

Figure 5.23 Stress path (p'-q space) of ESR-DL specimens cured for 7 days.

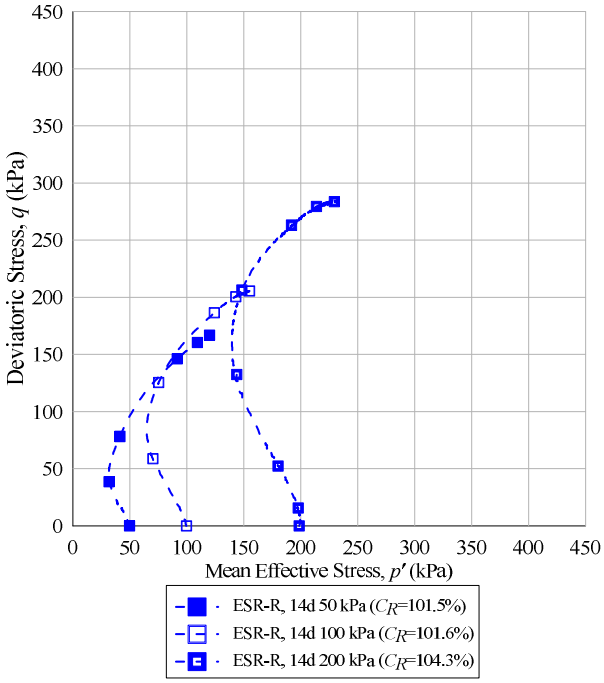

Figure 5.24 Stress path (p'-q space) of ESR-R specimens cured for 14 days.

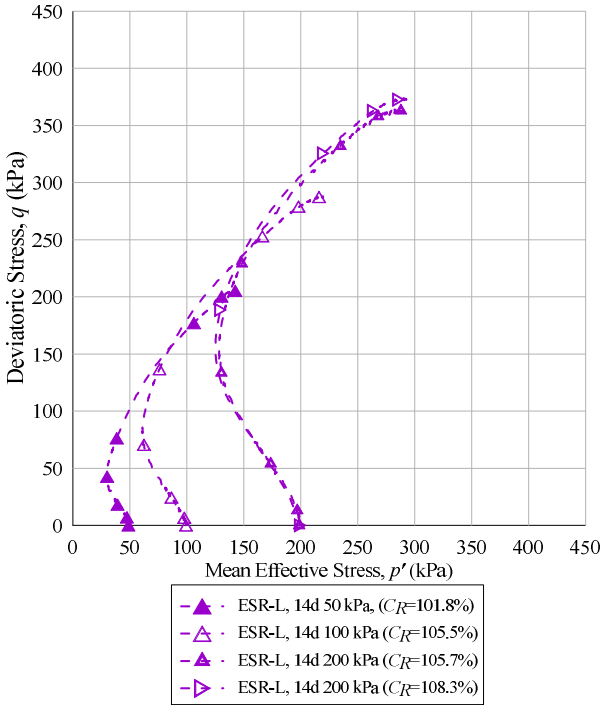

Figure 5.25 Stress path (p'-q space) of ESR-L specimens cured for 14 days.

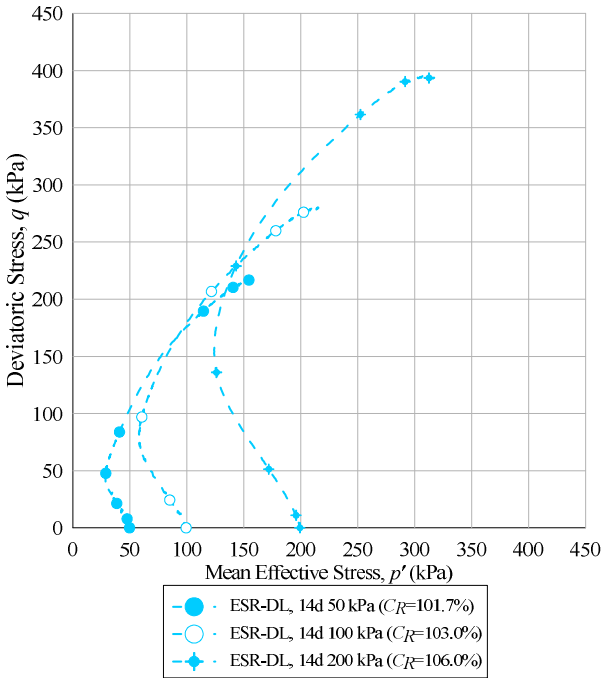

Figure 5.26 Stress path (p'-q space) of ESR-DL specimens cured for 14 days.

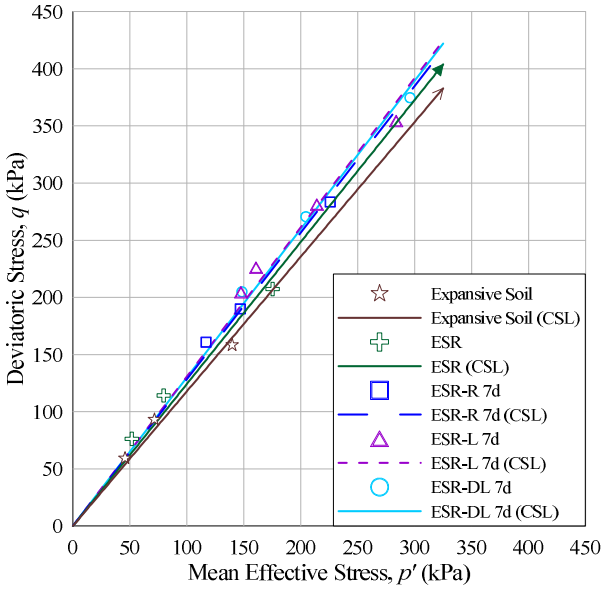

(a)

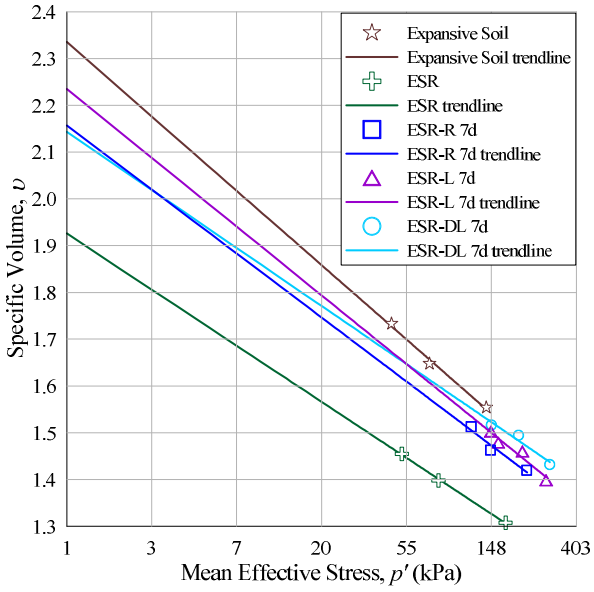

(b)

Figure 5.27 CSL of expansive soil, ESR (Dunham-Friel 2009) and ESR-fly ash specimens cured for 7 days in (a) *p′-q* space and (b) *p′-v* space.

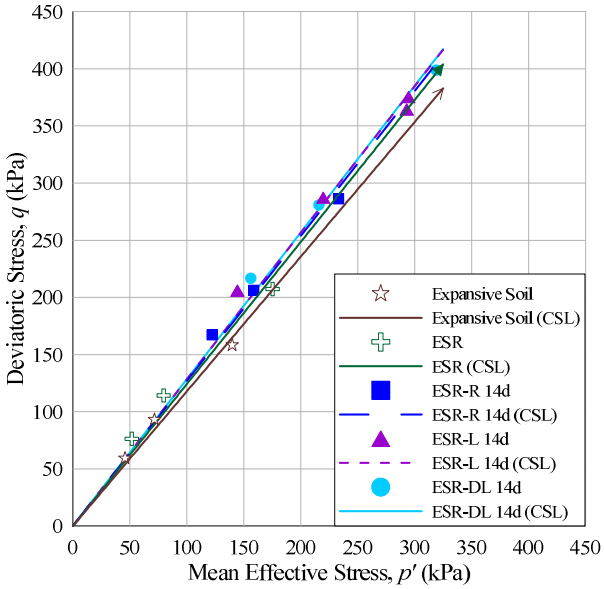

(a)

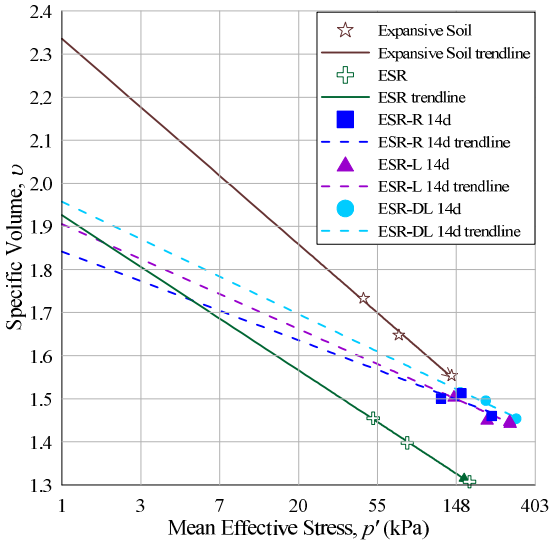

(b)

Figure 5.28 CSL of expansive soil, ESR (Dunham-Friel 2009) and ESR-fly ash specimens cured for 14 days in (a) *p′-q* space and (b) *p′-v* space.

5.7.2. Effect of Curing Time

To evaluate the effect of curing time on the undrained triaxial response of the specimens, the variation of the deviatoric stress, excess pore water pressure and the Skempton's pore pressure parameter *A* with axial strain are shown in Figures 5.29 through 5.31 for specimens cured for 7 and 14 days for mean effective stresses equal to 50, 100 and 200 kPa. Stress paths are shown in Figures 5.32 through 5.34 for specimens cured for 7 and 14 days. Similar as in Section 5.7.1, Figures 5.35 through 5.37 shows the CSL, in *p´-q* space and *p´-v* space, of ESR-fly ash specimens cured for 7 and 14 days, respectively.

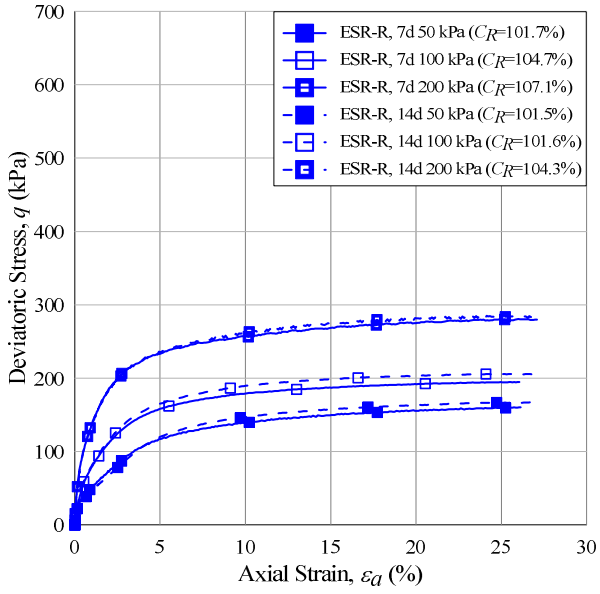

(a)

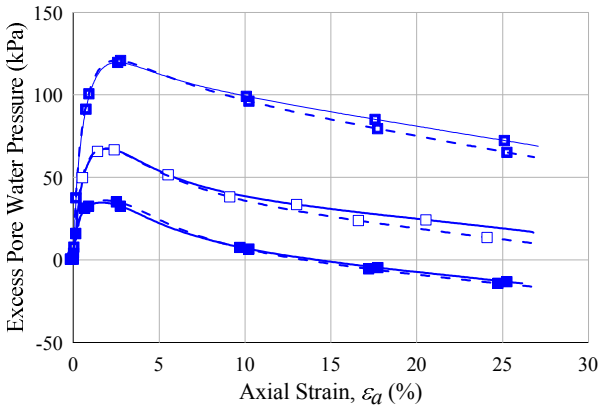

(b)

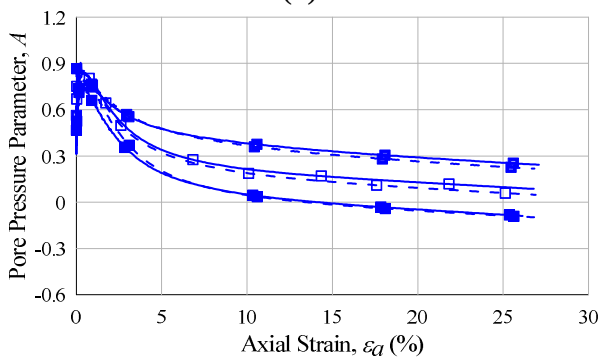

(c)

Figure 5.29 CIU response at mean effective stresses of 50, 100 and 200 kPa of ESR-R specimens cured for 7 and 14 days: (a) deviatoric stress, (b) excess pore water pressure, and (c) pore water pressure parameter *A* versus axial strain.

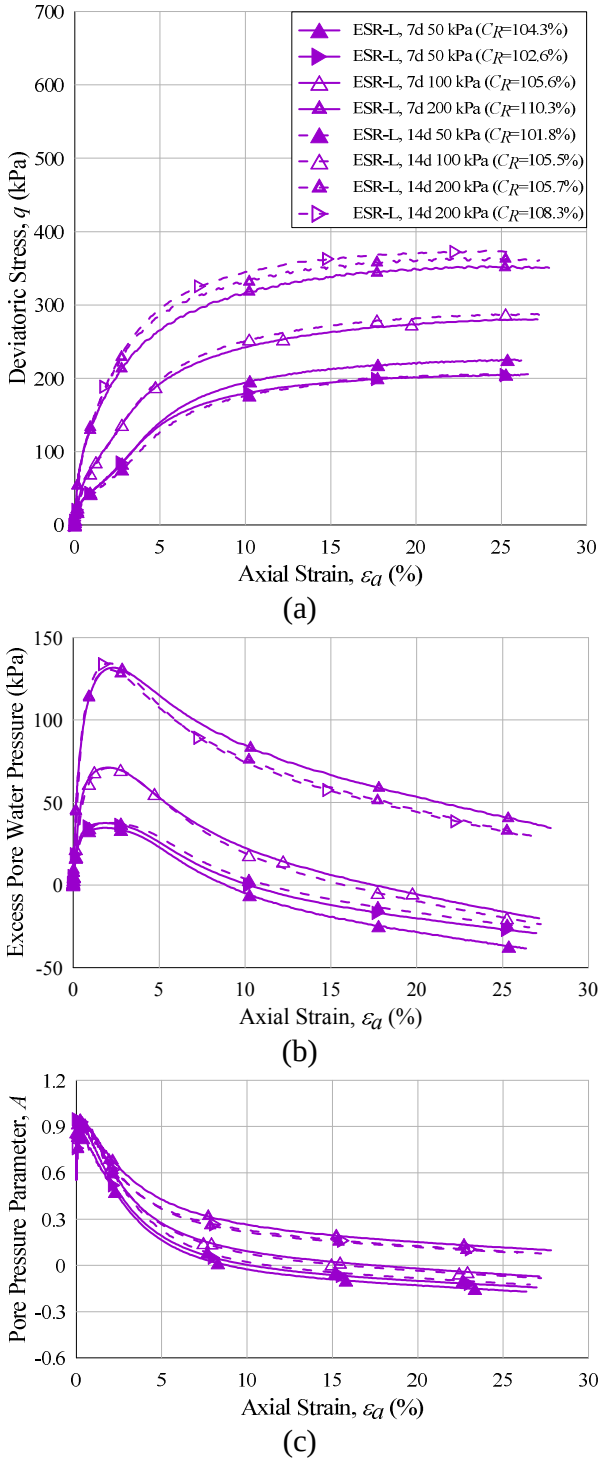

Figure 5.30 CIU response at mean effective stresses of 50, 100 and 200 kPa of ESR-L specimens cured for 7 and 14 days: (a) deviatoric stress, (b) excess pore water pressure, and (c) pore water pressure parameter A versus axial strain.

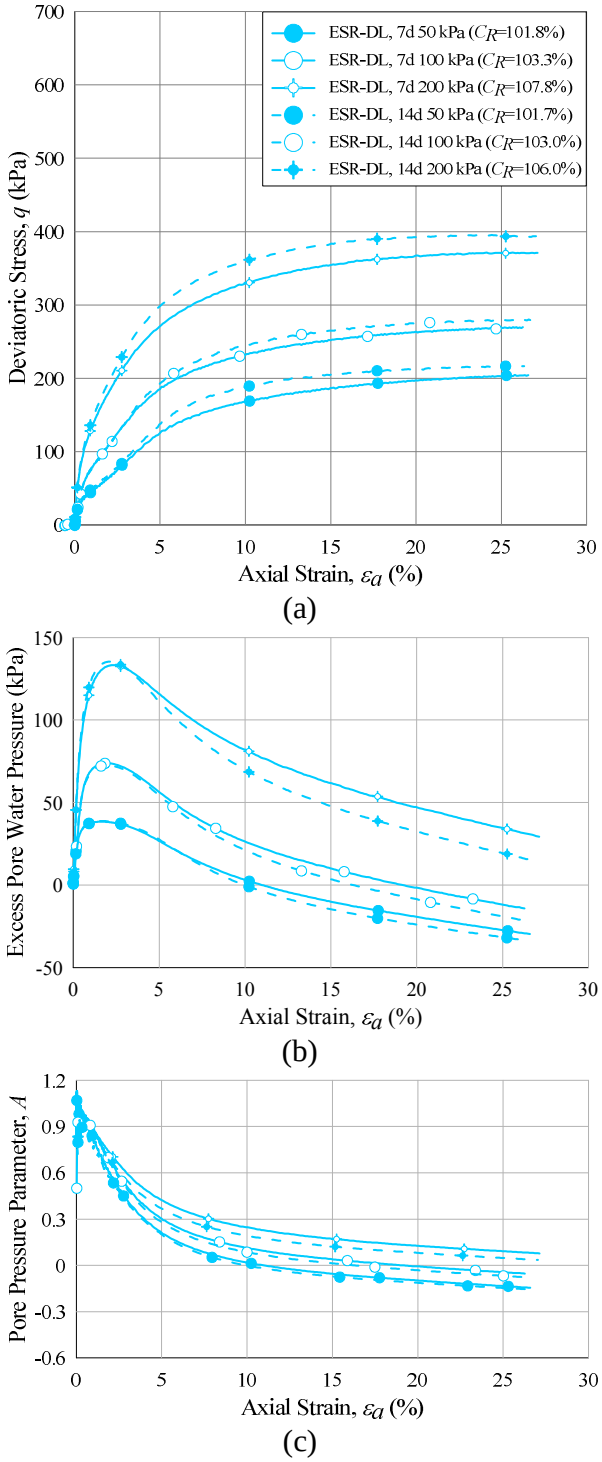

Figure 5.31 CIU response at mean effective stresses of 50, 100 and 200 kPa of ESR-DL specimens cured for 7 and 14 days: (a) deviatoric stress, (b) excess pore water pressure, and (c) pore water pressure parameter A versus axial strain.

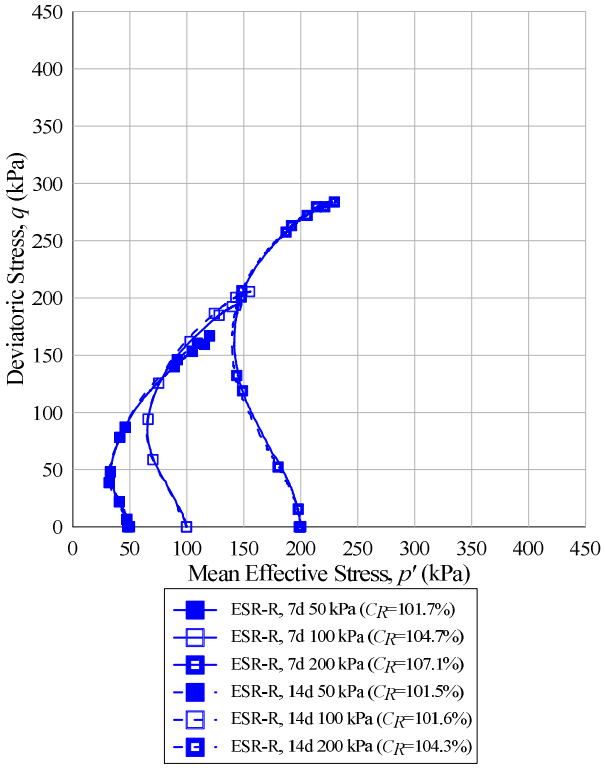

Figure 5.32 Stress path (p'-q space) ESR-R specimens cured for 7 and 14 days.

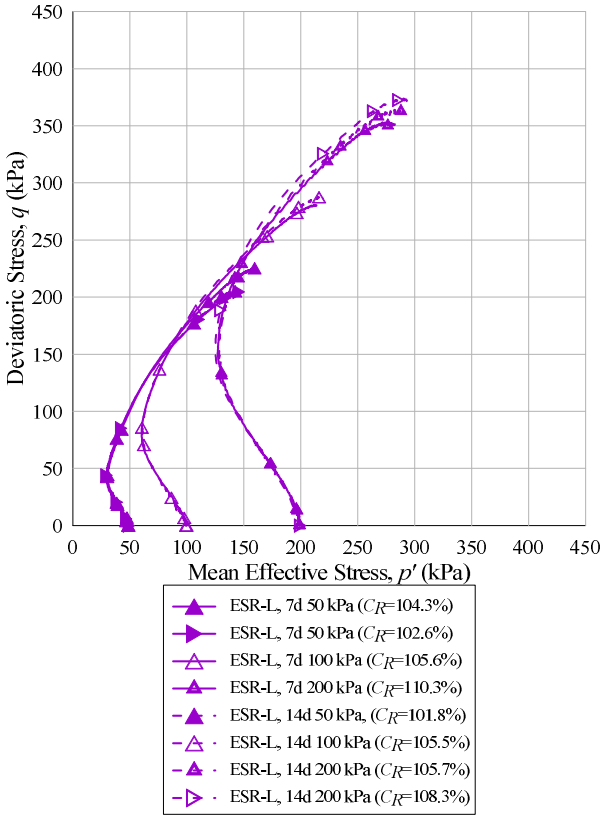

Figure 5.33 Stress path (p'-q space) ESR-L specimens cured for 7 and 14 days.

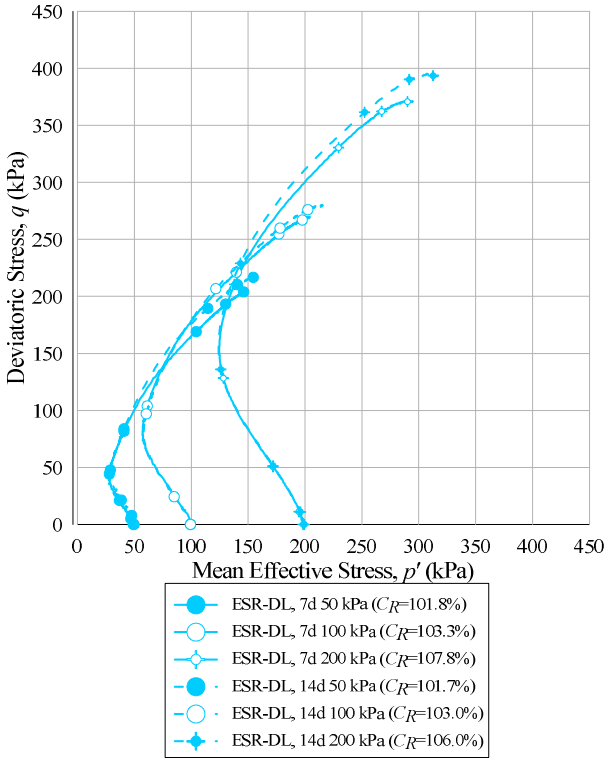

Figure 5.34 Stress path (p'-q space) ESR-DL specimens cured for 7 and 14 days.

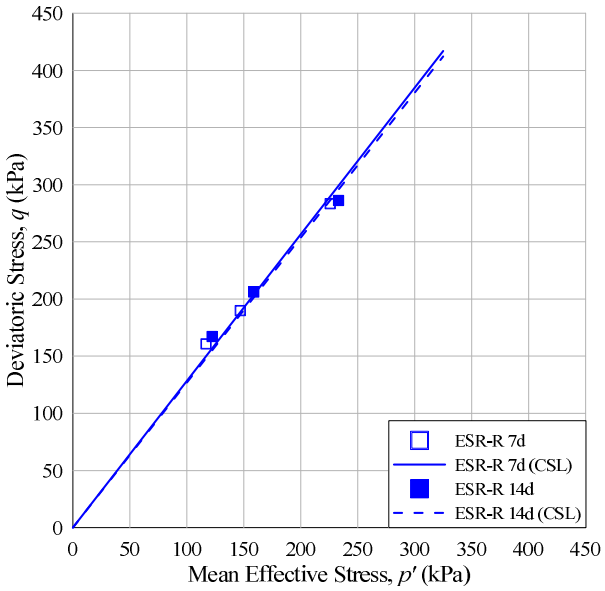

(a)

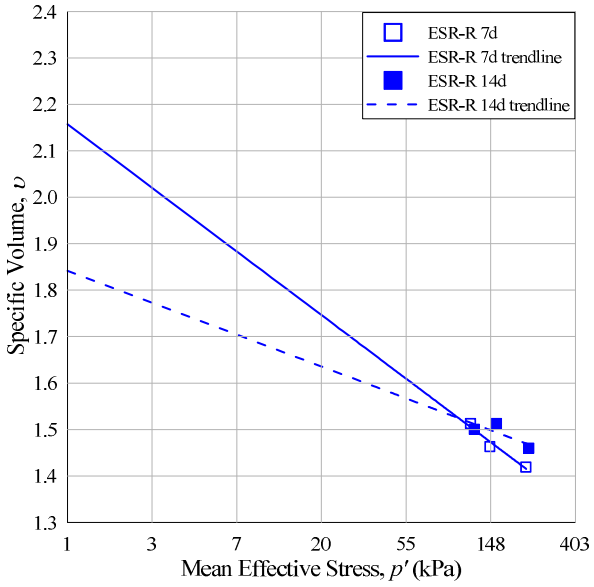

(a)

Figure 5.35 CSL of ESR-R specimens cured for 7 and 14 days in: (a) *p′-q* space and (b) *p′-v* space.

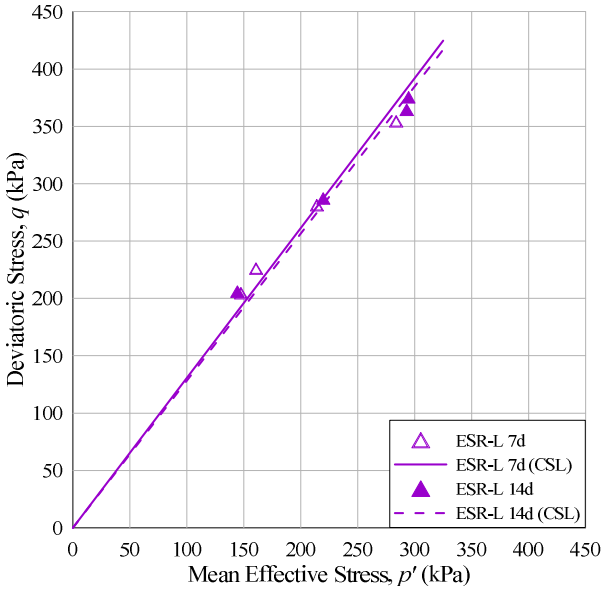

(a)

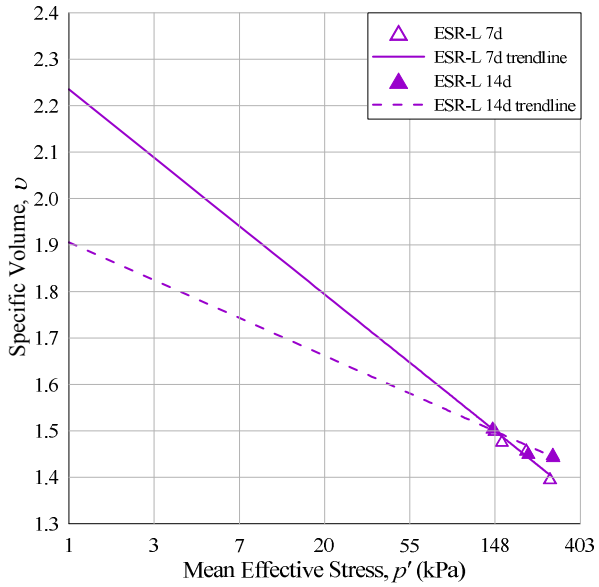

(b)

Figure 5.36 CSL of ESR-L specimens cured for 7 and 14 days in: (a) p'-q space and (b) p'-v space.

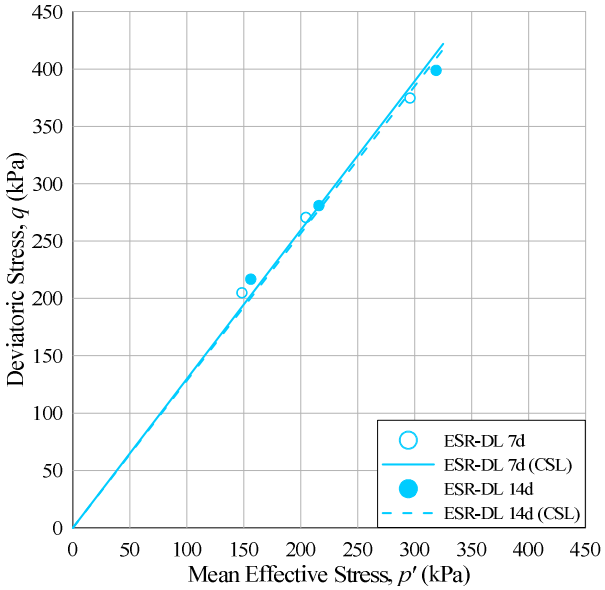

(a)

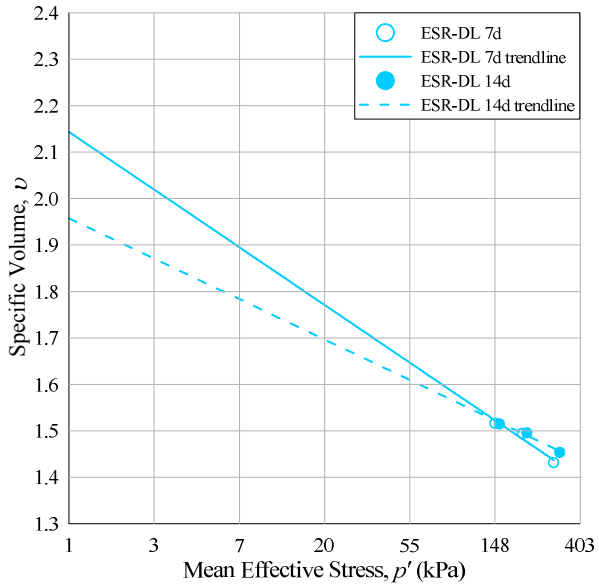

(b)

Figure 5.37 CSL of ESR-DL specimens cured for 7 and 14 days in: (a) *p´-q* space and (b) *p´-v* space.

5.8. Stiffness

5.8.1. Effect of Fly Ash

The stiffness of ESR-R, ESR-L and ESR-DL specimens, cured for 7 and 14 days were evaluated both at large and very small strains. Large-strain stiffness was evaluated using external transducers during undrained triaxial compression. The stiffness at very small strains was evaluated at each isotropic consolidation stage by measuring the shear wave velocity of the specimens using bender elements. The results of the very small-strain stiffness are summarized below in Table 5.9. Figures 5.38 through 5.40 show stiffness results in the very small-strain and large-strain ranges for specimens cured for 7 days. Likewise, Figures 5.41 through 5.43 show stiffness for specimens cured for 14 days. Figure 5.44 summarizes the very small-strain stiffness as a function of mean effective stress.

Table 5.9 Summary of very small strain stiffness of ESR (Dunham-Friel 2009) and ESR-fly ash specimens cured for 7 and 14 days.

Material	Curing Time	Target Mean Effective Stress, p'	Shear Wave Velocity, V_s	Shear Modulus, G_o
	(day)	(kPa)	m/s	MPa
ESR		30	84.4	13.5
ESR		50	98.0	18.3
ESR		100	124.2	30.2
ESR		200	153.4	47.2
ESR-R	7	30	132.4	32.0
ESR-R	7	50	155.0	44.0
ESR-R	7	100	190.1	66.2
ESR-R	7	200	218.2	87.1
ESR-R	14	30	161.3	46.5
ESR-R	14	50	167.7	50.4
ESR-R	14	100	206.0	76.1
ESR-R	14	200	234.5	98.6
ESR-L	7	30	126.3	29.4
ESR-L	7	50	157.9	46.1
ESR-L	7	100	198.5	72.9
ESR-L	7	200	236.0	102.9
ESR-L	14	30	164.3	48.0
ESR-L	14	50	172.6	53.1
ESR-L	14	100	206.4	76.0
ESR-L	14	200	252.4	113.6
ESR-DL	7	30	130.4	30.7
ESR-DL	7	50	153.9	42.9
ESR-DL	7	100	193.4	67.7
ESR-DL	7	200	237.1	101.7
ESR-DL	14	30	143.6	36.9
ESR-DL	14	50	172.4	53.3
ESR-DL	14	100	205.4	75.7
ESR-DL	14	200	243.9	106.7

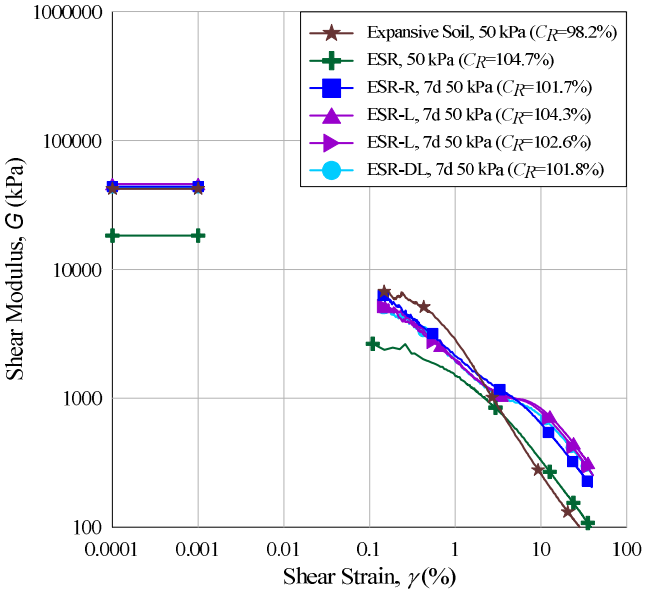

Figure 5.38 Stiffness degradation response of expansive soil, ESR (Dunham-Friel 2009), and ESR-fly ash specimens cured for 7 days at a mean effective stress of p'=50 kPa.

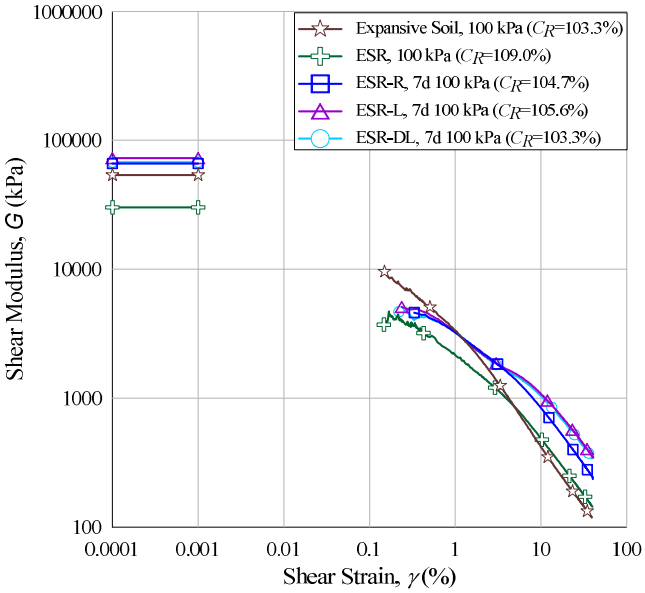

Figure 5.39 Stiffness degradation response of expansive soil, ESR (Dunham-Friel 2009), and ESR-fly ash specimens cured for 7 days at a mean effective stress of p'=100 kPa.

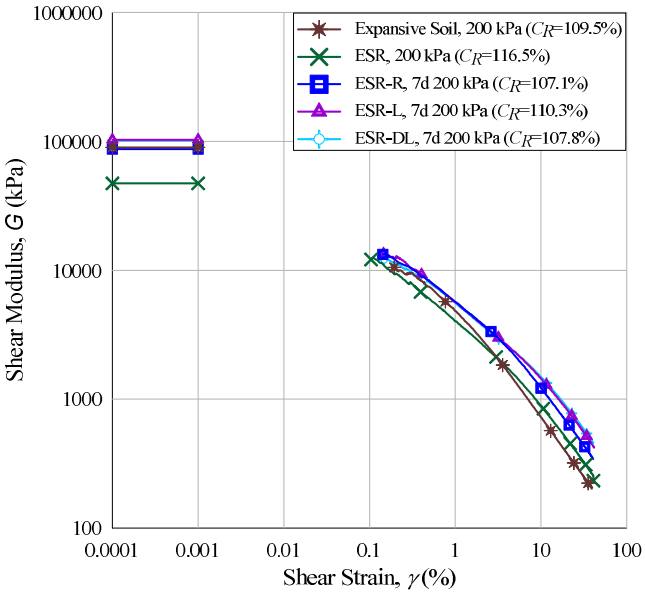

Figure 5.40 Stiffness degradation response of expansive soil, ESR (Dunham-Friel 2009), and ESR-fly ash specimens cured for 7 days at a mean effective stress of p'=200 kPa.

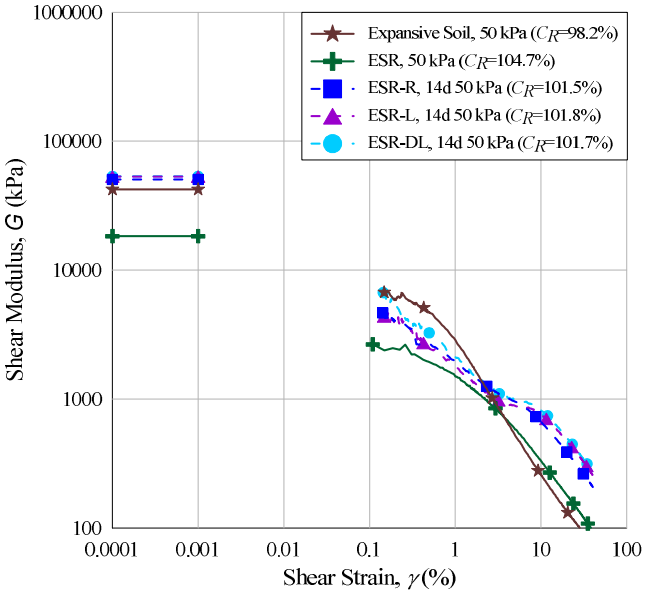

Figure 5.41 Stiffness degradation response of expansive soil, ESR (Dunham-Friel 2009), and ESR-fly ash specimens cured for 14 days at a mean effective stress of p'=50 kPa.

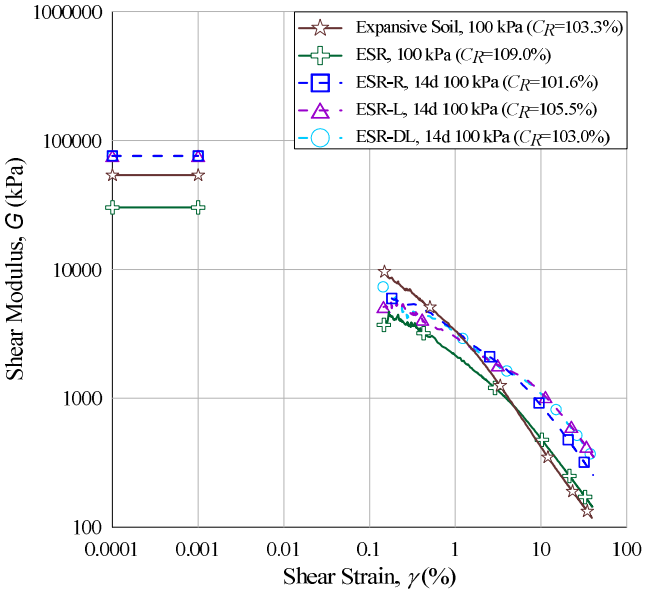

Figure 5.42 Stiffness degradation response of expansive soil, ESR (Dunham-Friel 2009), and ESR-fly ash specimens cured for 14 days at a mean effective stress of p'=100 kPa.

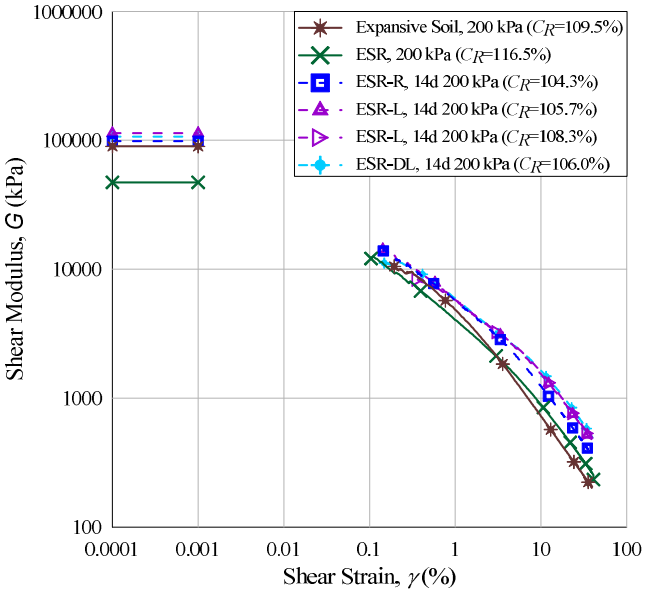

Figure 5.43 Stiffness degradation response of expansive soil, ESR (Dunham-Friel 2009), and ESR-fly ash specimens cured for 14 days at a mean effective stress of p'=200 kPa.

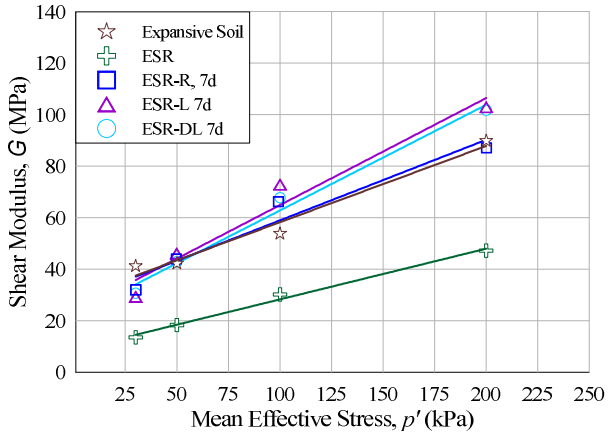

(a)

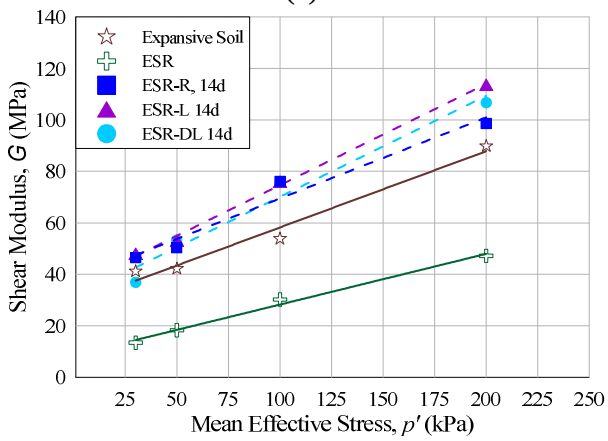

(b)

Figure 5.44 Variation of maximum shear modulus with mean effective stress for expansive soil, ESR (Dunham-Friel 2009) and ESR-fly ash specimens: (a) cured for 7 days and (b) cured for 14 days.

5.8.2. Effect of Curing Time

The variation of very small- and large-strain stiffness as a function of axial strain is shown in Figures 5.45 through 5.47 for ESR-R, ESR-L and ESR-DL specimens, respectively. Results are presented for each ESR-fly ash to illustrate differences between 7 and 14 days of curing. Figures 5.48 through 5.50 show the variation of very small-strain stiffness of ESR-R, ESR-L, and ESR-DL specimens with mean effective stress.

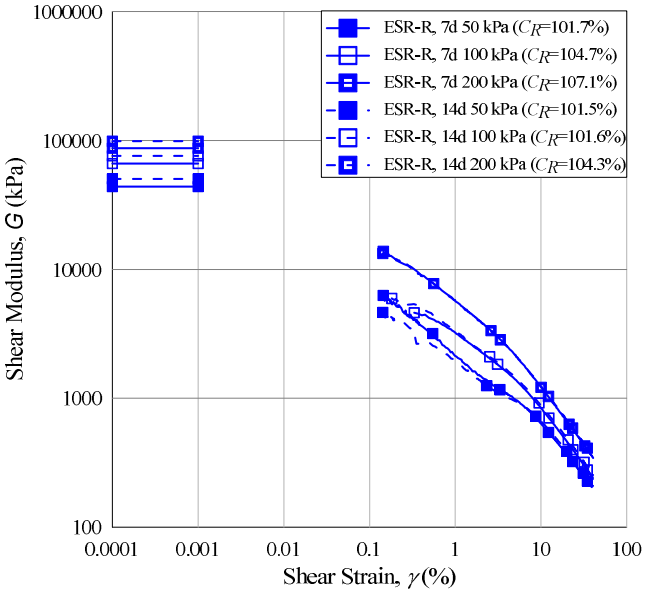

Figure 5.45 Stiffness degradation response of ESR-R specimens cured for 7 and 14 days.

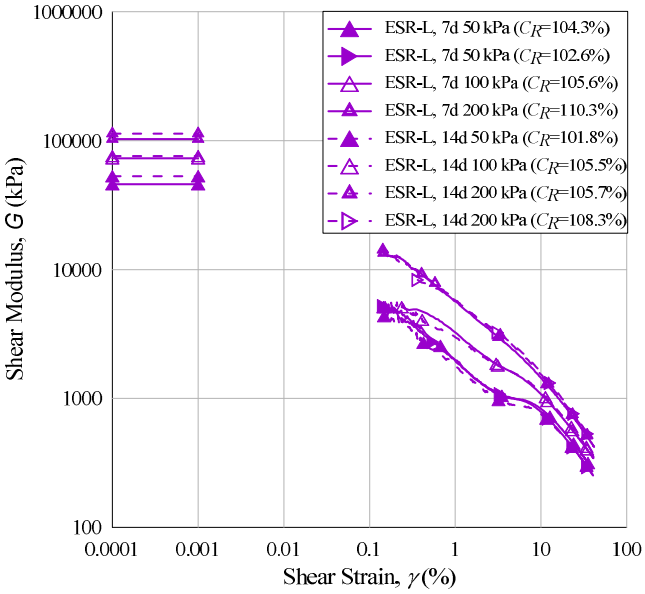

Figure 5.46 Stiffness degradation response of ESR-L specimens cured for 7 and 14 days.

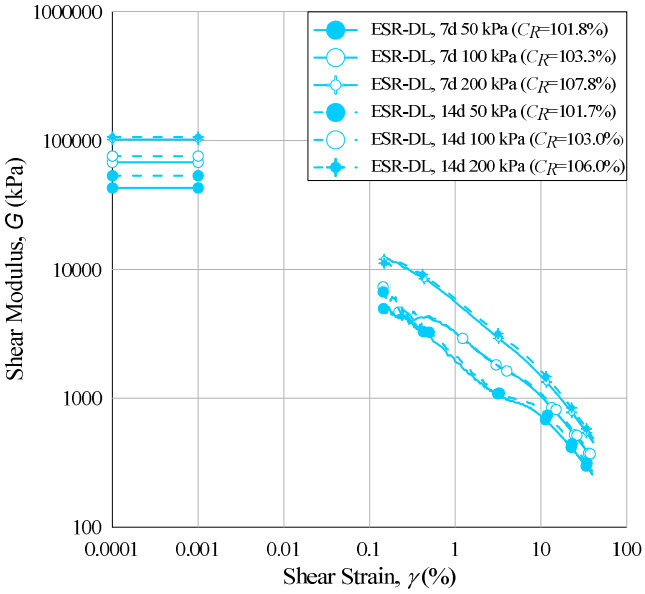

Figure 5.47 Stiffness degradation response of ESR-DL specimens cured for 7 and 14 days.

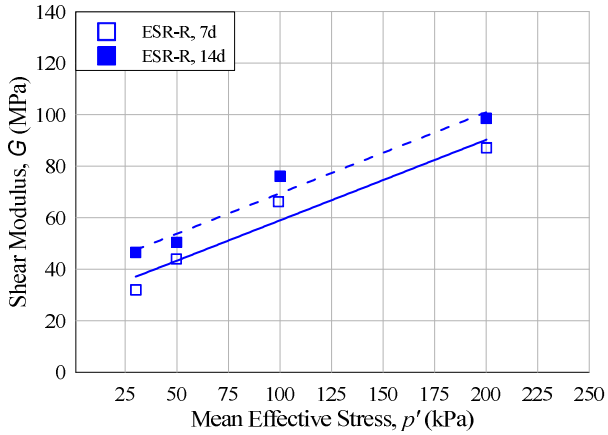

Figure 5.48 Variation of maximum shear modulus with mean effective stress for ESR-R specimens cured for 7 and 14 days.

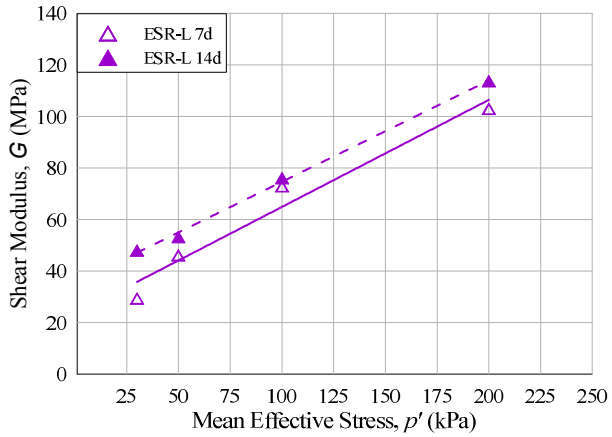

Figure 5.49 Variation of maximum shear modulus with mean effective stress for ESR-L specimens cured for 7 and 14 days.

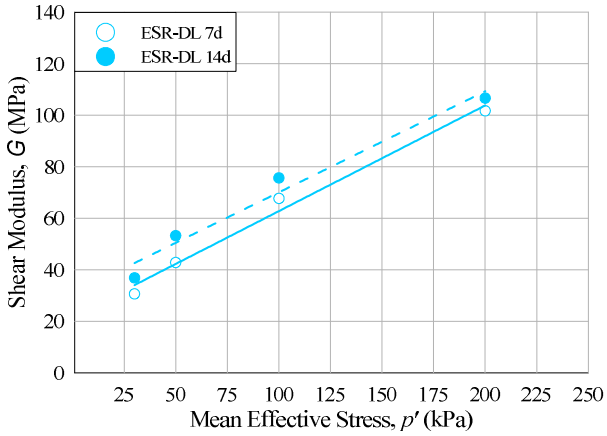

.

Figure 5.50 Variation of maximum shear modulus with mean effective stress for ESR-DL specimens cured for 7 and 14 days.

CHAPTER 6: ANALYSIS OF RESULTS

6.1. Mixture Design

Figure 5.1 shows the variation of the liquid and plastic limits of expansive soil and R-fly ash mixtures aged for 1 h as a function of the *FAC* content of the mixture. The results indicate a continuous increase in the liquid and plastic limits of the mixtures with increasing *FAC*. Lime fixation of the expansive soil-R fly ash mixture, cured for 1 h, was not clearly defined following this approach.

Since the lime fixation point of the expansive soil R-fly ash mixture cured for 1 h was not observed, this laboratory investigation was altered to determine the effect of curing time on the liquid and plastic limits of the mixtures. A mixture of the expansive soil with R-fly ash at a constant *FAC* of 10.7% was subjected to various aging times before proceeding with the Atterberg limit testing (Figure 5.2). These new results showed an initial increase in both the liquid and plastic limits between 0 h and 24 h. Relatively minor changes in the liquid and the plastic limits were further observed between 24 h and 168 h (7 days) of aging. The limited changes observed in the liquid and plastic limits after 24 h of aging suggest 24 h is necessary for the most prominent changes in liquid limit and plastic limit to develop.

Liquid and plastic limit tests were also performed on the expansive soil-L fly ash mixture for 1 h and 24 h of aging time (Figure 5.3). Results shown in Figure 5.3 suggest the 24-h aging period provides a clearer, more systematic approach to identify the lime fixation point of the mixtures, in accordance with data from Figure 5.2.

The 24-h aging time results show the liquid limit of the mixtures initially increase to a *FAC* of about 14 to 16%. Above this threshold *FAC*, the liquid limit of the mixtures stays fairly constant up to the maximum *FAC* tested (30%). A similar trend in the plastic limit of the mixtures can be observed for the tests completed at 1-h aging. The plastic limit tends to increase up to a *FAC* of approximately 14% and then remains relatively constant until the maximum *FAC* tested is reached.

According to Hilt and Davidson (1960), the plastic limit is indicative of the amount of lime required to satisfy the soil's affinity for lime. Thus, a *FAC* of 14% was deemed to satisfy the lime fixation of the expansive soil L-fly ash mixture. This *FAC* (equal to 14%) was used for the R, L and DL-fly ash blends for the remaining laboratory testing. This selected *FAC* is believed to be the minimum *FAC* required to develop pozzolanic reactions in the expansive soil L-fly ash mixture and thus was kept constant for all other expansive soil-fly ash mixtures. For the selected *FAC* of 14%, the amount of (MgO + CaO) in the R, L, and DL-fly ashes is approximately 4.9, 4.8, and 3.7%, respectively.

6.2. Compaction Parameters

The addition of fly ash to the ESR mixtures, when compacted with standard effort, lowered the standard Proctor maximum dry unit weight a maximum of 0.4 kN/m^3. The difference between the standard Proctor optimum water contents of the ESR and the ESR-R, ESR-L and ESR-DL mixtures was -0.7, -0.1, and +0.4%, respectively.

Fly ash addition to the ESR mixture, under modified Proctor effort, appears to have little effect on the maximum dry unit weight, with a maximum absolute difference 0.2 kN/m^3 or less. The addition of fly ash to the ESR mixtures has a more substantial effect on the modified Proctor optimum water content. The addition of R-fly ash, L-fly ash, and DL-fly ash to the ESR mixture changed the ESR modified Proctor optimum water content by -1.7, -1.8, and -2.0%, respectively.

6.3. Unconfined Compression Testing

Unconfined compression (ASTM Specification D 2166) testing of ESR and ESR-fly ash mixtures was performed as part of the experimental program. As pointed out previously in Section 4.5, the only purpose of these unconfined compression tests was to confirm that the *FAC* selected was sufficient to promote pozzolanic reactions within the ESR mixtures stabilized with fly ash. The potential development of pozzolanic reactions in the ESR-fly ash mixtures was assessed by comparison of the peak axial stress measured in unconfined compression for all of the ESR and ESR-fly ash mixtures tested. Unconfined compression testing results were neither used nor intended to assess the shear strength parameters (i.e. ϕ_c or s_u) of the materials tested. This is because the unconfined

compression specimens were not saturated prior to shearing and both the initial soil suction in the specimens and the pore pressures during unconfined compression were not measured. Without an accurate measurement of the initial stress state of the specimens (induced by soil suction), it would be conceptually wrong to expect unconfined compression test results can correlate to the actual shear strength parameters of the materials tested. Any discussion on the actual shear strength parameters of the materials tested in this study is carried out at a later section based on the results of triaxial tests performed on fully-saturated specimens subjected to well known states of stress and density.

6.3.1. Effect of Fly Ash

Unconfined compression testing results completed after 7 and 14 days are summarized in Table 5.2 and are shown in Figure 5.6 and Figure 5.7.

Results of the specimens cured for 7 days indicate the unconfined compressive strength (equal to the maximum axial stress applied to the specimen) of the ESR was improved with the addition of all three fly ashes. On average, the maximum stress exhibited by the ESR-R and the ESR-L was 134 kPa (191% of the maximum axial stress exhibited by the ESR). The maximum axial stress of the ESR-DL was 157 kPa (224% of ESR). The states of the specimens were all within -0.4 to +0.8% of their respective standard Proctor optimum water contents and within 94.1 to 96.1% of their corresponding standard Proctor maximum unit weight (these are shown in Table 5.1). The coefficient of variation determined for the peak axial stress ranged from 3 to 7%.

The ESR-R, ESR-L and ESR-DL specimens subjected to unconfined compression after 14 days of curing, exhibited maximum axial stresses of 175 (250% of the ESR), 166 (237% of the ESR) and 167 kPa (239% of the ESR), respectively. The states of the specimens were within -1.0 to +0.8% of their respective standard Proctor optimum water contents and 94.1 to 96.3% of their corresponding standard Proctor maximum dry unit weight. The coefficient of variation determined for the peak axial stress ranged from 5 to 8%.

The unconfined compression test results suggest that pozzolanic reactions developed both in 7 days and in 14 days in all of the ESR mixtures stabilized with fly ash, regardless of the type of fly ash used. The largest improvements after 7 days and 14 days of curing were observed in specimens stabilized with DL and R-fly ashes, respectively. At 7 and 14 days of curing, the unconfined compressive strength of specimens stabilized with off-specification fly ash was equal to or exceeded the unconfined compressive strength attained by the specimens stabilized with the standard Class C fly ash (L-fly ash).

6.3.2. Effect of Curing Time

To evaluate the effect of curing time on the development of pozzolanic reactions, ESR specimens stabilized with R, L, and DL-fly ashes were subjected to unconfined compression after 7 and 14 days of curing. The results are summarized in Table 5.2 and shown in Figures 5.8 through 5.10 for ESR-R, ESR-L, ESR-DL specimens, respectively.

The variation of the maximum axial stress exhibited stabilized specimens as a function of curing time is shown in Figure 5.11.

Results suggest improvements are attained with the additional curing of 7 days (i.e. from 7 days to 14 days) time for all stabilized specimens. The maximum axial stress exhibited after 14 days of curing was approximately 131%, 124% and 106% of the unconfined compressive strength exhibited after 7 days curing for the ESR-R, ESR-L and ESR-DL specimens, respectively. The largest improvements were observed for the specimens stabilized with L-fly ash and R-fly ash. This is likely due to the higher amounts of (CaO+MgO) in the R and L-fly ashes (the (CaO+MgO) content of the R and L fly ashes is approximately 132 and 128% of the amount in the DL-fly ash, respectively).

6.4. Triaxial Specimen Preparation

Table 5.3 indicates the initial soil state of each triaxial specimen. The initial C_R values were within 95.1 to 96.7% and water contents were with -0.7 to +0.4% of standard Proctor optimum water contents. The coefficient of variation determined for the C_R was <0.5%.

6.5. Isotropic Swell

Isotropic swell testing was initially conducted on each specimen subjected to triaxial testing as discussed in Section 4.6.3. Results of the isotropic swell testing are summarized in Table 5.3. None of the specimens subjected to isotropic swell testing exhibited swell.

For comparison, an expansive soil specimen exhibited 2.3% swell (Seda et al. 2007) and an ESR specimen exhibited 6.5% swell (Dunham-Friel 2009). The initial state of the expansive soil was near 100% of the standard Proctor maximum dry unit weight and at optimum water content. The initial state of the ESR specimen was near 95% of standard Proctor maximum dry density and on the dry side of optimum water content. The expansive soil specimen was inundated with water under a vertical stress of 6 kPa. The ESR specimen was inundated with water under an isotropic stress of 10 kPa.

Due to the differences in the initial soil states of the expansive soil, ESR, and ESR-fly ash specimens, the effect the addition of fly ash to the ESR has on swell is difficult to quantify. However, some likely conclusions about the swell exhibited by the specimens can be made.

Some basic factors used to characterize soils include soil mineralogy, soil water chemistry, soil suction, fabric, and soil state. Soil mineralogy is typically referred to in terms of three basic minerals: clay kaolinite (very low expansion), illite and vermiculite (low to moderately expansive). The crystal structure of the layered minerals is typically negatively charged on the surfaces and positively charged on the edges forming a diffuse double layer (DDL). Overlapping of the DDL's of the mineral generate repulsive forces between the clay particles (Nelson & Miller, 1992). The resulting repulsive forces of the DDL's layers are macroscopically the "swell pressure" of the soil. These repulsive forces are balanced by the current stress state of the soil which can be characterized in terms of

pore water pressure (u_w) and pore air pressure (u_a) in unsaturated soils. Effective stresses in the soil are identified by either $(\sigma - u_a)$ or $(\sigma - u_w)$. When u_a is greater than u_w, soil suction exists within the soil matrix (Nelson & Miller 1992):

$$\mu = (u_a - u_w) \qquad \text{(Equation 23)}$$

where μ is the matric suction. The soil's tendency to swell is a result of its natural attempt to equalize its unbalanced internal stresses such that μ approaches zero once the soil becomes saturated. Thus, by adding water initially to the soil, the soil can satisfy its affinity for water by adsorbing polar water molecules cations thus reduce the soil suction. During specimen preparation, this was likely accomplished by compacting specimens near standard Proctor optimum water content and allowing a minimum period of 16 h for the material to soak prior to compaction.

The second possible reason to the negligible swell could be attributed to the addition of fly ash to the expansive soil. As indicated in Section 2.7, the swell of expansive soil can potentially be reduced by the addition of fly ash. This potential swell reduction is due to two factors. The first relates to the development of particle bonding which reduces/restricts relative movement of the soil particles within the soil matrix (American Coal Ash Association 2003). The second factor is due to cation exchange with Ca^{2+} and Mg^{2+} replacing water molecules needed to satisfy the DDL of the soil.

6.6. Isotropic Consolidation

6.6.1. Effect of Fly Ash

The change in specific volume as a function of the mean effective stress (natural log scale) is summarized in Table 5.4 for expansive soil and ESR (Dunham-Friel 2009) and in Table 5.5 for ESR-R, ESR-L and ESR-DL specimens cured for 7 and 14 days. Those results are shown in and Figure 5.12 for specimens cured for 7 days and in Figure 5.13 for specimens cured for 14 days.

The slope of the trend line, in lnp'-v space, and the v intercept at p'=1 are summarized in Table 5.5. In isotropic compression, the slope and intercept of the trendline are expressed λ and v_n for normally consolidated (OCR=1) soils κ and v_k and for overconsolidated (OCR>1) soils, respectively (Schoefield & Wroth 1968). Since the specimens contained 6.7-mm granulated rubber, it is necessary to over compact the specimens in the mold during the compaction process for any expansion that occurs when the load applied to the last layer is removed. As a result, the actual stress history of the specimens is unknown since only total stresses are controlled during compaction. However, based on the A_f values shown in Figures 5.15 through 5.20, most of the ESR-fly ash specimens are overconsolidated. Hence, the slope is identified as κ and the intercept as v_k. The trendline slope in lnp'-v space is associated with the material stiffness and is indicative of the potential compressibility of the mixture upon a certain increment in mean effective stress. Specimens cured for 7 and 14 days exhibit similar isotropic compression responses.

The ESR-fly ash specimens exhibited a compression slope of approximately 27 to 33% of the expansive soil and approximately 33 to 46% of the ESR. These results suggest that the addition of fly ash to the ESR increases the stiffness in isotropic compression of ESR mixtures and thus reducing their compressibility.

As indicated in Section 4.6.5, the consolidation coefficient (c_{vi}) and the coefficient of volume compressibility (m_{vi}) were determined during isotropic consolidation (Table 5.6). Similar parameters were for K_o boundary conditions and the hydraulic conductivity (k) were estimated following the procedures outlined in Section 4.6.5. These results are summarized in Table 5.6.

In isotropic conditions, results from Table 5.6 indicate that ESR-L and ESR-DL specimens generally exhibited a lower average c_{vi} and a higher average m_{vi} than the ESR-R specimens. The average k of the ESR-R, ESR-L and ESR-DL specimens was similar at a mean effective stress of 50 kPa, 100 kPa and 200 kPa. The k decreased in all ESR-fly ash specimens with increases in mean effective stress.

6.6.2. Effect of Curing Time

The variation in specific volume (v) with the natural log of mean effective stress (p') is summarized in Table 5.5 and shown in Figure 5.14. The slopes of the trendlines clearly reduce from 7 days of curing to 14 days of curing. This suggests that the compressibility of the mixtures is reduced with curing time for the curing times used in this study as

stiffness increased due to cementation. Largest improvements in stiffness were observed in specimens stabilized with R and L-fly ashes.

6.7. Triaxial Compression

The results of the isotropically consolidated undrained triaxial compression (CIU) tests are discussed in this section. Discussion of the CIU test results focus on the analysis of effective stress paths (p', q) stress-strain response, and the variation of excess pore pressure (Δu) with axial strain (ε_a) during undrained compression.

6.7.1. Effect of Fly Ash

The variation of deviatoric stress (q), excess pore pressure (Δu), and Skempton's pore pressure parameter A with ε_a for ESR-fly mixtures, at mean effective stress levels of 50, 100 and 200 kPa, are shown in Figures 5.15 through 5.17, respectively, for specimens cured for 7 days and in Figures 5.18 through 5.20 for specimens cured for 14 days.

The stress-strain response (ε_a, q) of ESR-L and ESR-DL is relatively similar at all levels of mean effective stress. The ESR-R specimens exhibited lower deviatoric stress than the ESR-L and ESR-DL specimens. At relatively small axial strains (<3.0%), the excess pore pressures exhibited by ESR-L and ESR-DL specimens were systematically higher than the ESR-R specimens in all cases. This trend was even more pronounced at higher levels of mean effective stress. In all specimens, the excess pore water pressure reaches a peak and then reduces with further strains. In all cases, the ESR-L and ESR-DL specimens exhibit the most negative excess pore pressures generation at large strains.

None of the ESR-fly ash specimens reached a "true" critical state, defined by no changes in excess pore pressure with additional axial strains at the end of the tests (with ε_a approximately equal to 27%).

The initial positive excess pore pressure generation is due to the initial tendency of the specimens to contract which is also observed in ESR specimens (Dunham-Friel 2009). Once the maximum positive excess pore pressure is mobilized, the specimens underwent a slight phase transformation after which the excess pore pressures are reduced and may even become negative due to tendency of the specimens to dilate upon further deformation. The largest reductions in excess pore pressures were observed for the ESR-L and ESR-DL specimens, followed by the ESR-R. In all cases, the excess pore pressures at large strains were much more negative than those observed for the ESR. Since the ESR and ESR-fly ash specimens all contained the same *RC*, the additional tendency towards dilation during undrained loading may be explained due to the development of pozzolanic bonds within the ESR-fly ash matrix.

The slope of the stress-strain response (q versus ε_a) of ESR-fly ash specimens, subjected to CIU testing at mean effective stress of 50 kPa changes abruptly for axial strains equal to approximately 2 to 3%. This change in stiffness is related to the yield of the material and depends on p'. At axial strain levels <2% the cemented structure is relatively intact and the stiffness is large. At about 2% axial strain, the pozzolanic bonds start to deteriorate and the shear resistance becomes increasingly dependent on particle friction and rearrangement. This sudden stiffness change is also observed at a mean effective

stress of 100 kPa, although not as pronounced as in the 50-kPa case. Yield is not observed at a mean effective stress of 200 kPa. This behavior is typical of the yield stress behavior reported for cemented soils. Large isotropic consolidation stresses tend to break particle cementation during isotropic compression so no clear yield stress is observed during subsequent undrained triaxial compression (Leroueil & Vaughan 1990, Rinaldi & Capdevila 2006).

The pore water pressure parameter (*A*) is directly related to the development of excess pore pressure during undrained loading. Thus, the pore pressure parameter *A* follows the same trend as the excess pore pressure development previously discussed. The pore pressure parameter *A* at failure (A_f), determined at the largest axial strain, varied between 0.1 to -0.2 for all ESR-fly ash specimens. According to Skempton (1954), A_f values between 0.0 to -0.5, would be typical of slightly to heavily over-consolidated clay.

In accordance with the critical state framework, a critical state line (CSL) was fitted to the p', q failure states of each mixture with p', q at failure defined as the point of maximum axial strain for each test. Average results for the CSL stress ratio (*M*) and corresponding critical state friction angle (ϕ_c) for each mixture are summarized in Table 5.8. Results indicate that ϕ_c is nearly the same for ESR-L and ESR-DL, which are slightly higher than the ESR-R specimens. Figure 5.27 and Figure 5.28 illustrate the CSL for each of the ESR-fly ash mixtures. These plots also show the CSL for the expansive soil and the ESR tested by Dunham-Friel (2009). The CSL line of the ESR-fly ash mixtures is steeper than the CSL's of the ESR and expansive soil for specimens cured for

7 and 14 days. The ESR-fly ash specimens exhibited a ϕ_c of approximately 107 to 110% of the ϕ_c of the expansive soil, and approximately 102 to 105% of the ESR's ϕ_c. The shear strength, defined by the M or ϕ_c, of the ESR mixture was improved by the addition of fly ash. This improvement was observed regardless of the type of (Class C or off-specification) fly ash used.

6.7.2. Effect of Curing Time

Figure 5.29 through Figure 5.31 show the variation of deviatoric stress (q), excess pore water pressure (Δu) and Skempton's pore pressure parameter (A) as a function of axial strain (ε_a) for the ESR-R, ESR-L, and ESR-DL specimens, respectively. The stress paths for each of the ESR-R, ESR-L and ESR-DL specimens cured for 7 and 14 days are shown in Figures 5.32 through 5.34, respectively. Likewise, the CSLs are shown in Figures 5.35 through 5.37.

The typical effect of curing time is as follows: an increase in curing time increases q and induces generation of less positive (or more negative) Δu at large strains for specimens tested at similar initial states.

As discussed in Section 6.7.1, the ESR-fly specimens exhibited phase transformation. After phase transformation, with the exception of the ESR-L specimen at p'=50 kPa, all of the ESR-fly ash specimens exhibited lower excess pore pressures generation at 14 days of curing than at 7 days of curing. This suggests the specimens show a greater tendency towards dilatency with increasing in curing time, likely resulting from the development

of additional pozzolanic bonds among particles in the mixtures. This same trend can also be observed in terms of the Skempton's pore pressure coefficient *A*.

Observation of the CSLs in p' versus q space indicates that in all ESR-fly ash specimens, a slightly higher CSL slope (or higher ϕ_c) was observed for specimens cured for 7 days than specimens cured for 14 days. This reduction in ϕ_c is of the order of about 0.4˚ for curing times varying from 7 to 14 days (Table 5.8). In general, and as noted previously, none of the ESR-fly ash specimens truly reached a constant level of excess pore pressure at large axial strains.

6.8. Stiffness

Large-strain stiffness of ESR-fly specimens cured for 7 and 14 days were measured during triaxial compression using external displacement and force transducers. Stiffness at very small strains was evaluated by measurement of the shear wave velocity (V_s) of the specimens after they were saturated (B value greater than 0.99 was obtained for all specimens) and isotropically consolidated to mean effective stress levels of 30, 50, 100 and 200 kPa. After V_s was measured, the very small-strain stiffness was determined according to Equation 9, as described in Section 4.6.1.

6.8.1. Effect of Fly Ash

The stiffness degradation response of ESR-fly ash specimens is shown in Figures 5.38 through 5.40 and Figures 5.41 through 5.43 for specimens cured for 7 and 14 days,

respectively. A plot of the very small-strain stiffness as a function of mean effective stress and curing time is shown in Figure 5.44.

At all levels of mean effective stress and curing times, the stiffness at both very small strains and large strains of ESR-fly ash stabilized specimens was greater than the stiffness exhibited by the ESR specimens without fly ash.

The improvement of stiffness at very small strains imparted by the addition of fly ash to ESR specimens (Table 5.9) was greatest at low mean effective stress and lowest at the largest mean effective stress. On average, at mean effective stress levels of 30, 50, 100 and 200 kPa the very small-strain stiffness of ESR-fly ash specimens was approximately 284, 269, 244 and 222% greater than the stiffness of the ESR, respectively.

Large-strain stiffness of ESR-fly ash specimens was greater than the ESR's in all cases and all levels of mean effective stress. At shear strains of approximately 4%, the slope of the stiffness degradation curve presents a breakpoint and appears to "flatten" with increasing shear strains up to about 8%. This breakpoint and "flattening" are due to the breakage (yield) of the pozzolanic bonds within the ESR-fly ash matrix after which both the shear strength and stiffness are gradually controlled by the frictional characteristics of the mixtures. As seen before in the q versus ε_a plots, this phenomenon is much more prominent at a mean effective stress of 50 kPa.

At very small strains, the stiffness of the ESR-fly ash specimens is similar to or greater than the stiffness of the expansive soil. At large strains, the ESR-fly ash specimens exhibited similar or slightly higher stiffness than the expansive soil.

6.8.2. Effect of Curing Time

The degradation of stiffness of ESR-R, ESR-L and ESR-DL specimens cured for 7 and 14 days is shown in Figures 5.45 through 5.47. The variation of stiffness at very small strains with mean effective stress is shown in Figures 5.48 through 5.50.

At mean effective stress levels of 30, 50, 100 and 200 kPa the very small-strain stiffness of ESR-fly ash specimens cured for an 14 days was on average approximately 143, 118, 110, and 109% greater than the stiffness of the ESR-fly ash specimens cured for 7 days, respectively. At large strains, no discernable trend/difference was observed between specimens cured for 7 or 14 days.

The stiffness improvement observed at very small strains is due to the pozzolanic bonds in the ESR-fly ash matrix. At large shear strains, most of the pozzolanic bonds are broken during shearing, and thus the stiffness is governed by the frictional characteristics of the matrix. Thus, at large strains, additional stiffness improvement was not expected to develop as a result of additional curing.

CHAPTER 7: CONCLUSIONS

The first objective of this research was to determine if a conventional Class C fly ash could be used to improve the stiffness and shear strength of an ESR mixture. Secondly, determine if off-specification fly ashes could be used in lieu of conventional Class C fly ash. Thirdly, to determine a *FAC* necessary to promote pozzolanic development in the ESR-fly ash specimens and to assess the impact of various types of fly ashes on the soil's index properties (liquid limit and plastic limit). The main findings related to the results presented in this paper are summarized below.

7.1. Mixture Design

The minimum *FAC* required to promote pozzolanic reactions with the soil was determined by evaluation of the plastic limit of the expansive soil and fly ash. The minimum time necessary for aging the R-fly ash with the expansive soil prior to plastic limit evaluations was determined to be 24 h. Evaluation of the plastic limit, based on the concept of the "lime fixation point" (Hilt & Davidson, 1960), suggested a minimum *FAC* of 14% should be used in the ESR-L mixture. Unconfined compression test results suggest the *FAC* selected for the ESR-L mixture promoted the development of pozzolanic reactions within 7 days with further improvement at 14 days for all other ESR-fly ash mixtures.

7.2. Isotropic Compression

The isotropic compression response of the ESR-fly ash specimens was evaluated based on the slope of the isotropic compression lines in lnp'-v space which was significantly less than the slope observed for the ESR mixture. At 7 days of curing, the slope of the isotropic compression lines of ESR-fly ash specimens was approximately 42% of the slope of the ESR. After 14 days of curing, the compression slope was approximately 37% of the ESR.

7.3. Shear Strength

Addition of fly ash to the ESR improved the critical state strength of the ESR mixtures. For specimens stabilized with fly ash, the critical state friction angle (ϕ_c) was improved from 31.0 degrees (for the ESR) to between 31.6 to 32.4 degrees for the ESR-fly cured for 7 and 14 days.

7.4. Stiffness

ESR-fly ash specimens cured for 7 and 14 days exhibited higher stiffness than the ESR mixture. At very small strains, stabilization of the ESR mixtures with fly ash significantly increased the stiffness of the ESR mix. At very small strains, the stiffness was approximately, 222 to 284% greater than the ESR's stiffness. The greatest improvement in stiffness was observed at lower mean effective stresses, and after 14 days of curing.

7.5. Off-Specification Fly Ash

Improvements imparted by the addition of the off-specification fly ashes to the ESR mixture were similar to or greater than the improvements imparted by the standard Class C fly ash. Those improvements include peak stress during unconfined compression, stiffness through isotropic compression and critical state friction angle. The very small-strain stiffness was improved most with the standard Class C fly ash, followed by the high-carbon, and high-sulfur off-specification fly ashes.

7.6. Suggestions for Future Work

Based on the results of this study, suggestions for future work may involve:

1) Evaluation of potential ettringite formation in mixtures of expansive soil and ESR stabilized with high sulfur content off-specification fly ashes.
2) Evaluation of the effectiveness of off-specification fly ash in stabilizing non-expansive soils and/or aggregate base.
3) Evaluation of the environmental impact of soils stabilized with off-specification fly ashes.
4) Performance evaluation of expansive soil or ESR stabilized with conventional and/or off-specification fly ashes in civil engineering applications.
5) Evaluation of regional availability and life-cycle cost analysis using off-specification fly ashes and ESR-fly ash mixtures in civil engineering applications.

CHAPTER 8: REFERENCES

AASHTO T 307. *Determining the Resilient Modulus of Soils and Aggregate Materials.* AASHTO.

Abshire, M. S. (2002). *Differential Moisture Migration and Heave Beneath Slabs over Dipping Expansive Shale.* Fort Collins, Colorado: Colorado State University.

Ahmed, I., & Lovell, C. W. (1993). Rubber Soils as Lightweight Geomaterials. *Transportation Research Record 1422* .

American Coal Ash Association Educational Foundation. (2008). *Soil Stabilization and Pavement Recycling with Self-Cementing Coal Fly Ash.* Aurora, Colorado: American Coal Ash Association.

American Coal Ash Association. (2003). *Fly Ash Facts for Highway Engineers.* Washington: Federal Highway Administration.

ASTM C 117. *Standard Test Method for Materials Finer than 75-μm (No. 200) Sieve in Mineral Aggregates by Washing.* ASTM International.

ASTM C 136. *Standard Test Method for Sieve Analysis of Fine and Coarse Aggregates.* ASTM International.

ASTM C 618. *Standard Specification for Coal Fly Ash and Raw or Calcined Natural Pozzolan for Use in Concrete.* ASTM International.

ASTM D 1557. *Standard Test Methods for Laboratory Compaction Characteristics of Soil Using Modified Effort.* ASTM International.

ASTM D 2166. *Standard Test Method for Unconfined Compressive Strength of Cohesive Soil.* ASTM International.

ASTM D 4318. *Standard Test Method for Liquid Limit, Plastic Limit, and Plasticity Index of Soils.* ASTM International.

ASTM D 4767. *Standard Test Method for Undrained Triaxial Compression Test of Cohesive Soils.* ASTM International.

ASTM D 698. *Standard Test Methods for Laboratory Compaction Characteristics of Soil Using Standard Effort.* ASTM International.

ASTM D 854. *Standard Test Methods for Specific Gravity of Soil Solids by Water Pycnometer.* ASTM International.

Atkinson, J. H. (2000). Non-linear Soil Stiffness in Routine Design. *Geotechnique 50,* 487-508.

Atkinson, J. (1993). *The Mechanics of Soils and Foundations.* England: McGraw-Hill.

Baldi, G., Hight, D. W., & Thomas, G. E. (1988). A re-evaluation of conventional triaxial test methods. In ASTM, *Advanced Triaxial Testing of Soil and Rock* (pp. 219-263).

Braddock, W. A., Wohlford, D. D., & O'Connor, J. T. (1989). *Geologic Map of the Horsetooth Reservoir Quadrangle, Larimer County, Colorado: U.S. Geological Survey Map GQ-1625.* U.S. Geological Survey .

Center for Transportation Research and Education. (2005). *Fly Ash Stabilization for Non-Uniform Subgrade Soils, Volume I: Engineering Properties and Construction Guidelines.* Ames, Iowa: Iowa State University.

Cetin, H., Fener, M., & Gunaydin, O. (2006). Geotechnical Properties of Tire-cohesive Clayey Soil Mixtures as a Fill Material. *Engineering Geology 88* , 110-120.

Cokca, E. (2001). Use of Class C Fly Ashes for the Stabilization of an Expansive Soil. *Journal of Geotechnical and Geoenvironmental Engineering*, 568-573.

Colorado Department of Public Health and Environment. (2009). *Fifth Annual Report to the Transportation Legislation Review Committee on the Status of Waste Tire Recycling in Colorado for Calendar Year 2008.* Denver, Colorado.

Dunham-Friel, J. (2009). *Shear Strength and Stiffness of Expansive Soil and Rubber (ESR) Mixtures in Undrained Axisymmetric Compression.* Fort Collins, Colorado: Colorado State University.

Dyvik, R., & Madshus, C. (1985). Laboratory Measurements of Gmax using Bender Elements. *ASCE Convention: Advances in the Art of Testing Soils Under Cyclic Conditions.* Detroit, Michigan.

Edil, T. B., Acosta, H. A., & Benson, C. H. (2006). Stabilizing Soft Fine-Grained Soils with Fly Ash. *Journal of Materials in Civil Engineering*, 283-294.

Head, K. H. (1986). *Manual of Soil Laboratory Testing.* London: Pentech Press Limited.

Henkel, D. J. (1956). The Effect of Overconsolidation on the Behaviour of Clays During Shear. *Geotechnique*, 139-150.

Hilt, G. H., & Davidson, D. T. (1960). Lime Fixation in Clayey Soils. *Highway Research Board*.

Humphrey, D. N., Sandford, T. C., Cribbs, M. M., & William, P. M. (1993). Shear Strength and Compressibility of Tire Chips for Use as Retaining Wall Backfill. *Transportation Research Record 1422*, 29-35.

Jardine, R. J., Symes, M. J., & Burland, J. B. (1984). The Measurement of Soil Stiffness in the Triaxial Apparatus. *Geotechnique 34, No. 3*, 323-340.

Jovicic, V., Coop, M. R., & Simic, M. (1996). Objective Criteria for Determining Gmax from Bender Element Tests. *Geotechnique 46*, 357-362.

Kim, H. K., & Santamarina, J. C. (2008). Sand-rubber Mixtures (Large Rubber Chips). *Can. Geotech*, 1457-1466.

Lee, J. H., Salgado, R., Bernal, A., & Lovell, C. W. (1999). Shredded Tires and Rubber-Sand as Lightweight Backfill. *Journal of Geotechnical and Geoenvironmental Engineering*, 132-141.

Lee, J.-S., Dodds, J., & Santamarina, J. C. (2007). Behavior of Rigid-Soft Particle Mixtures. *Journal of Materials in Civil Engineering*, 179-184.

Leroueil, S., & Vaughan, P. R. (1990). The General and Congruent Effects of Structure in Natural Soils and Weak Rocks. *Geotechnique 40, No. 3*, 467-488.

Misra, A. (1998). Stabilization Characteristics of Clays Using Class C Fly Ash. *Transportation Research Record*, 46-54.

Muir-Wood, D. (2004). *Geotechnical Modeling.* New York, New York: Spon Press.

Nelson, J. D., & Miller, D. J. (1992). *Expansive Soil Problems and Practice in Foundation and Pavement Engineering.* New York: John Wiley & Sons, Inc.

Ozkul, Z. H., & Baykal, G. (2001). Shear Behavior of Compacted Rubber Fiber-Clay Composite in Drained and Undrained Loading. *Journal of Geotechnical and Geoenvironmental Engineering*, 767-781.

Rinaldi, V., & Capdevila, J. A. (2006). Effect of Cement and Saturation on the Stress-Strain Behavior of a Silty Clay. *ASCE*, 1157-1168.

Rubber Manufacturers Association. (2009, May). *Scrap Tire Markets in the United States.* Retrieved from http://www.rma.org/scrap_tires

Salgado, R. (2006). *The Engineering of Foundations.* McGraw-Hill.

Schoefield, A., & Wroth, P. (1968). *Critical State Soil Mechanics.* London: Cambridge University Press.

Seda, J. H., Joon, L. C., & Carraro, J. A. (2007). Beneficial Use of Waste Tire Rubber for Swelling Potential Mitigation in Expansive Soils. *Geotechnical Special Publication 172.* Denver, Colorado: American Society of Civil Engineers.

Shirley, D. J., & Hampton, D. L. (1977). *Shear-wave Measurements in Laboratory Sediments.* Austin: The University of Texas at Austin.

Skempton, A. W. (1954). The Pore Pressure Coefficients A and B. *Geotechnique,* 143-147.

Sourcewatch.org. (n.d.). *Existing_coal_plants_in_Colorado*. Retrieved May 2010, from Source Watch: http://www.sourcewatch.org

Transportation Research Board. (1987). *Lime Stabilization: Reactions, Properties, Design, and Considerations.* Washington, D.C.: Transportation Research Board.

U.S. Environmental Protection Agency. (2010, January 26). *CCP Applications*. Retrieved March 19, 2010, from Coal Combustion Products Partnership: http:/www.epa.gov/waste/partnershipes/c2p2/use/index.htm

U.S. Environmental Protection Agency. (2008). *High-Volume Use of High-Carbon Fly Ash for Highway Construction, Case Study 21*. U.S. Environmental Protection Agency.

U.S. EPA. (2006). *Scrap Tire Cleanup Guidebook.* U.S. EPA.

U.S. Environmental Protection Agency. (2005). *Using Coal Ash in Highway Construction: A Guide to Benefits and Impacts.* EPA.

Viggiani, G., & Atkinson, J. H. (1995). Interpretation of Bender Element Tests. *Geotechnique 45*, 149-154.

Viggiani, G., & Atkinson, J. H. (1995). Stiffness of Fine-grained Soil at Very Small Strains. *Geotechnique 45*, 249-265.

Youwai, S., & Bergado, D. (2003). Strength and Deformation Characteristics of Shredded Rubber Tire-Sand Mixtures. *Can. Geotech*, 254-264.